IMPERIAL COLLEGE LONDON
DEPARTMENT OF ELECTRICAL AND ELECTRONIC ENGINEERING

Transceiver Optimisation for MIMO High-Speed Downlink Packet Access (HSDPA) System

Irina Chi Wai Ma

June 2014

A thesis submitted in fulfillment of the requirements for the degree
of Doctor of Philosophy and the Diploma of Imperial College London

Declaration of Originality

I hereby declare that the work presented in this thesis is my own and that all else is appropriately referenced.

Copyright Declaration

The copyright of this thesis rests with the author and is made available under a Creative Commons Attribution Non-Commercial No Derivatives licence. Researchers are free to copy, distribute or transmit the thesis on the condition that they attribute it, that they do not use it for commercial purposes and that they do not alter, transform or build upon it. For any reuse or redistribution, researchers must make clear to others the licence terms of this work

Abstract

In recent years, the growth of smart phone industry drives its users to demand better quality multimedia services while achieving faster internet speeds. With a higher number of subscribers and more data hungry applications, there is a need to improve the current 3G HSDPA data rate until the 4G network is fully implemented globally. Therefore, the aim of this thesis is to improve the downlink data rate of the HSDPA system throughput through both transmitter and receiver optimisations while balancing the complexities of the optimisation algorithms.

Initially, improving system throughput through power allocation strategies is investigated in this thesis. Current schemes proposed in the literature that use Equal SINR Equal Rate (ESER) allocation can improve the system throughput for single rate allocation but require a rather high complexity. In this thesis, a *System Value* (SV) criterion is proposed to decrease the traditional ESER allocation method while achieving similar system throughput performance.

To further increase the system throughput, a Successive Interference Cancellation (SIC) receiver is proposed which not only improves the data rate but also has a reduced complexity. The proposed SIC receiver can be used in conjunction with both ESER allocation schemes as well as equal energy allocation schemes.

Another transmitter optimisation strategy is to improve the signature sequences. A signature sequence design that minimises correlations between the sequences while reducing the Inter-Symbol Interference (ISI) and noise is proposed. To reduce the amount of channel state information required, a signature sequence selection method which removes the signature sequences that are heavily affected by interference is also proposed.

The proposed optimisation strategies have been verified through MATLAB simulations. Moreover, practical measurements using the National Instruments (NI)-PXIe testbed have been carried out for the proposed SIC algorithm which further confirm its effectiveness in a real world environment.

Acknowledgements

Firstly, I would like to express my gratitude to my former supervisor, Dr. Mustafa Gurcan, for his excellent guidance and encouragement ever since I was an undergraduate student and throughout my PhD studies. The time he has invested in me has made it possible to complete my PhD thesis and writing good publications.

I would also like to thank my current supervisor, Prof. Athanassios Manikas, for his lectures have inspired me to learn more about the wireless communications area; and for his advice and support for my final stage of my PhD studies.

I would like to thank my former research team members, Anusorn Chungtragarn, Hamdi Joudeh and Qinxin Liu for their emotional support and technical discussions we shared. I truly enjoyed the time we have spent together and treasure the friendship we have made. I would also like to thank my new group members including Zexi Fang, Ren He, Thibaud Gabillard, Akinbiyi Akindoyin, Vidhya Sridhar and Evangelos Venieris for providing a friendly environment and support. I am also very privileged to have made many friends and met helpful staff from different research groups during my studies at Imperial College.

Last but not least, I would like to express my gratitude towards my parents Iao Iao Ma and Karen Hooi, who have raised me up in a loving environment, providing me with good education and being always there for me. I am also thankful to have my husband Jeffrey Chan who always stands by my side.

Contents

Abstract **7**

Acknowledgements **9**

Contents **9**

List of Figures **15**

List of Tables **17**

Abbreviations **19**

Notation **21**

1 Introduction **23**
1.1 Evolution of Telecommunications 23
1.2 Wireless Channel with Multipath Propagation 24
1.3 Frequency Selective MIMO Channel Model 26
1.4 Challenges of the HSDPA System 28
1.5 Thesis Outline 30

2 Constraint Optimisation and "System Value" Approach **33**
2.1 Link Throughput Maximisation 33
2.2 The MIMO HSDPA Transceiver Model 35
2.2.1 The HSDPA Transmitter Architecture 37
2.2.2 The HSDPA Receiver Architecture 39
2.2.3 Channelisation Codes for the HSDPA System 41
2.2.4 PCI Codebook for Two Transmit Antennas 42
2.2.5 Energy and SNR Definitions 43
2.3 The Constraint Optimisation Problem 45
2.4 Equal Rate Allocation 47
2.4.1 EEER Allocation 48
2.4.2 Equal SINR Equal Rate Allocation 48
2.5 Rate Adaptive Two-Group Optimisation 50
2.5.1 Equal SINR Two-Group Allocation 50
2.5.2 Equal Energy Two-Group Allocation Algorithm 52
2.5.3 Complexity of ESER & ESTG using Constraint Optimisation . . 53
2.6 The System Value Approach 54
2.7 Evaluation of ES & EE with System Value Approach 57

2.8 Summary . . . 63

3 A Novel SIC-based "System Value" Receiver 65
3.1 Interference Cancellation Receivers Overview . . . 66
3.2 The System Model for the SIC receiver . . . 67
3.3 SV Approach with the SIC Receiver . . . 69
3.4 Simplification of Covariance Matrix Inversion for SIC . . . 71
3.5 EEER Approach with the Simplified SIC Receiver . . . 73
3.6 ES Approaches with the Simplified SIC Receiver . . . 73
3.6.1 Iterative Energy Calculation for SIC . . . 74
3.7 Complexity Analysis of the Proposed SIC Schemes . . . 76
3.8 The Performance of SIC Schemes . . . 77
3.9 Experimental Results . . . 80
3.9.1 NI-PXIe Based Experimental Setup . . . 81
3.9.2 Comparison between Measurements and Simulations . . . 82
3.10 Summary . . . 87

4 Signature Sequence Optimisation and Feedback Analysis 89
4.1 Signature Sequence Optimisation . . . 90
4.2 Optimised Signature Sequence . . . 91
4.3 Evaluation of Different Signature Sequences . . . 92
4.4 Feedback and Channel Removal . . . 94
4.5 Selecting the Optimum Signature Sequence Set . . . 96
4.5.1 Signature Sequence Selection for Each $\widetilde{K}$ . . . 96
4.5.2 Signature Sequence Selection for ES and EE Allocations . . . 99
4.6 Complexity of Signature Sequence Selection . . . 101
4.7 Performance of Signature Sequence Selection . . . 102
4.8 Obtaining Channel State Information at Transmitter . . . 106
4.9 Analysis of Link Adaptation Feedback . . . 108
4.10 Multiplexing & Array gains in MIMO FDD Systems . . . 110
4.10.1 Evaluation of Partial CSIT in MIMO FDD Systems . . . 112
4.11 Summary . . . 119

5 Summary, Conclusions and Future Work 121
5.1 Summary and Conclusions . . . 121
5.2 List of Contributions . . . 123
5.3 Future Work . . . 124
5.3.1 Channel model with correlations and Doppler effects . . . 124
5.3.2 Extend the work to minimise inter-cell interference . . . 124
5.3.3 Codebook design with more codewords . . . 125

Publications Arising from This Work 127

Appendices 129

A The Proof of $\mathbf{D}_k^{-1}$ and $\mathbf{C}_k^{-1}$ (Chapter 3) 129
A.1 The formation of $\mathbf{D}_k^{-1}$ . . . 130
A.2 The formation of $\mathbf{C}_k^{-1}$ . . . 131

B The Chip Level SIC receiver (Chapter 3) 133
B.1 Channel 135
B.2 Receiver 136
B.2.1 MMSE Filter 137
B.2.2 Estimation and Detection 138

C Supplementary Material for the Testbedding System (Chapter 3) 139
C.1 Overview of Testbeds and Prototypes 139
C.2 Further Details on the NI-PXIe Testbed 140
C.3 Further Measurement Results over the EVA Channels 143

D PCI Codebooks (Chapter 4) 145
D.1 PCI Codebook for Three Transmit Antennas 145
D.2 PCI Codebook for Four Transmit Antennas 146

References 149

List of Figures

2.1 HSDPA System Model with Transmitter and MMSE Receiver 36
2.2 ESER Algorithm using Constraint Optimisation 49
2.3 ESTG Algorithm using Constraint Optimisation 52
2.4 ESER Algorithm using System Value Approach 56
2.5 ESTG Algorithm using System Value Approach 57
2.6 Comparison of Different Energy Allocation Schemes (Pedestrian-A) . . . 60
2.7 Comparison of Different Energy Allocation Schemes over (Pedestrian-B) 60
2.8 Energy Difference Ratio of ESER and ESTG (Pedestrian-A) 62

3.1 SIC Receiver for the HSDPA System 67
3.2 System Value SIC Algorithm 75
3.3 Comparison of SIC and Non-SIC Schemes (Pedestrian-A) 78
3.4 Comparison of SIC and Non-SIC Schemes (Pedestrian-B) 78
3.5 Comparison of Different SIC Receivers 79
3.6 Simulations & Experiments Comparisons over Pedestrian-A (non-SIC) . 84
3.7 Simulations & Experiments Comparisons over Pedestrian-A (SIC) 84
3.8 Comparison of Different Schemes over the Testbed (Pedestrian-A) 86
3.9 Different Schemes over Testbed for (Pedestrian-B) 86
3.10 Comparison of Different Schemes over Testbed for (EVA) 87

4.1 Comparisons of Different Signature Sequences (Pedestrian-A) 93
4.2 Comparisons of Different Signature Sequences (Pedestrian-B) 94
4.3 ESTG Schemes with K and $K^\star$ Spreading Sequences (Pedestrian-A) . . 102
4.4 ESTG Schemes with K and $K^\star$ Spreading Sequences (Pedestrian-B) . . 103
4.5 EETG Schemes with K and $K^\star$ Spreading Sequences (Pedestrian-A) . . 104
4.6 EETG Schemes with K and $K^\star$ Spreading Sequences (Pedestrian-B) . . 104
4.7 Comparison of Improved EETG against ESTG (Pedestrian-A) 105
4.8 Comparison of Improved EETG against ESTG (Pedestrian-B) 106
4.9 SV Sum Rate with 2 Transmit Antennas (Pedestrian-A) 112
4.10 SV Sum Rate with 2 Transmit Antennas over (Pedestrian-B) 113
4.11 MIMO with non-SIC schemes for Pedestrian-A channel 115
4.12 MIMO with SIC schemes for Pedestrian-B channel 115
4.13 MIMO with non-SIC schemes for Pedestrian-A channel 116
4.14 MIMO with SIC schemes for Pedestrian-B channel 117
4.15 $2 \times 3, 2 \times 4, 3 \times 4$ non-SIC v.s. $3 \times 2, 4 \times 2, 4 \times 3$ SIC (Pedestrian-A) . . 118
4.16 $2 \times 3, 2 \times 4, 3 \times 4$ non-SIC v.s. $3 \times 2, 4 \times 2, 4 \times 3$ SIC (Pedestrian-B) . . 119

C.1 Software & Hardware Processing Unit of the Rapid Prototyping System 141

C.2 NI PXIe Hardware Platform 142
C.3 Simulations and Experiments Comparisons over EVA (MMSE) 143
C.4 Simulations and Experiments Comparisons over EVA (SIC) 144

List of Tables

2.1 PCI for Two Transmit antennas 43
2.2 Energies and SNR definitions 44
2.3 Set of Discrete Rates b_p, Target SINRs & SVs 58
2.4 Pedestrian-A Power Delay Profile 58
2.5 Pedestrian-B Power Delay Profile 58
2.6 Computational Complexity for Different Schemes 62

3.1 Computational Complexity for Different Schemes 76
3.2 Specifications for NI 5791 RF Transceiver Adapter Module 82
3.3 Specifications for NI 7966R FPGA 82
3.4 Specifications for the Channel Emulator 82
3.5 Extended Vehicular-A Power Delay Profile 83

4.1 CQI Table Corresponding to TS25.214 v.11.6.0 7Ib 108
4.2 Link Adaptation Feedback for Different Optimisation Schemes 110

D.1 PCI Codebook for Three Transmit Antennas 146
D.2 LTE System with Four Transmit Antennas 147

Abbreviations

ADC	Analogue to Digital Converter
AMC	Adaptive Modulation and Coding
ARQ	Automatic Repeat Request
CQI	Channel Quality Indicator
CSI	Channel State Information
CSIT	Channel State Information at the Transmitter
DAC	Digital to Analogue Converter
DDC	Digital Down Converter
DUC	Digital Up Converter
EDGE	Enhanced Data rate for Global Evolution
EE	Equal Energy
EEER	Equal Energy Equal Rate
EETG	Equal Energy Two-Group
ER	Equal Rate
ES	Equal SINR
ESER	Equal SINR Equal Rate
ESTG	Equal SINR Two-Group
EVA	Extended Vehicular A
FDD	Frequency Division Duplex
FPGA	Field-Programmable Gate Array
GPRS	General Packet Radio Service
GSM	Global System for Mobile communications
HSDPA	High-Speed Downlink Packet Access
ICI	Inter-Code Interference
IF	Intermediate Frequency
ISI	Inter-Symbol Interference
LTE	Long Term Evolution
MIMO	Multiple-Input Multiple-Output
ML	Maximum Likelihood
MMSE	Minimum Mean Square Error
MSE	Mean Square Error
NI	National Instruments
OFDM	Orthogonal Frequency Division Multiplexing

OVSF	Orthogonal Variable Spreading Factor
OSTBC	Orthogonal Space-Time Block Codes
PA	Pedestrian A
PB	Pedestrian B
PC	Personal Computer
PCI	Precoding Control Indicator
PDP	Power Delay Profile
PIC	Parallel Interference Cancellation
QAM	Quadrature Amplitude Modulation
RF	Radio Frequency
SIC	Successive Interference Cancellation
SINR	Signal-to-Interference-plus-Noise Ratio
SISO	Single-Input Single-Output
SR	Sum Rate
STTC	Space-Time Trellis Codes
SV	System Values
TDD	Time Division Duplex
TG	Two-Group
TTI	Transmission Time Interval
UE	User Equipment
WCDMA	Wide Code Division Multiple Access
WiMAX	Worldwide Interoperability for Microwave Access
ZF	Zero-Forcing

Notation

$\mathbb{C}^{N\times M}$	Set of complex numbers of matrix dimension $N \times M$
$\mathbb{R}^{N\times M}$	Set of real numbers of matrix dimension $N \times M$
$\mathbb{N}^{N\times M}$	Set of natural numbers of matrix dimension $N \times M$
x	Scalar
$\underline{x}$	Column vector
$\mathbf{X}$	Matrix
$(\cdot)^H$	Complex conjugate (Hermitian) transpose of a vector or a matrix
$(\cdot)^T$	Transpose of a vector or a matrix
$(\cdot)^*$	Complex conjugate of a vector or a matrix
$(\cdot)^{-1}$	Inverse of a matrix
$\text{diag}(\underline{x})$	Diagonal matrix whose diagonal elements are elements of $\underline{x}$
$\text{diag}(\mathbf{X})$	Vector containing the diagonal elements of matrix $\mathbf{X}$
$[\underline{x}]_i$	The i^{th} element of vector $\underline{x}$
$E(\cdot)$	Expectation
$\underline{0}_N$	Zero vector of length N
$\mathbf{0}_{N\times M}$	Zero matrix of dimension $N \times M$
$\mathbf{I}_N$	Identity matrix of dimension $N \times N$
$\mathbf{J}_N$	Shift matrix of dimension $N \times N$
$\otimes$	Kronecker product
$\odot$	Hadamard product
$\text{Re}(\cdot)$	Real part of a complex number/vector

Chapter 1

Introduction

Due to the emergence of smart phones and tablets with its data-hungry applications, telecommunications has been one of the fastest growing industries [1] where service providers have to meet the ever-growing demand on data speeds. The fourth generation (4G) Long Term Evolution (LTE) system has recently been introduced worldwide to meet the demand but requires service providers to upgrade their base stations and change the network architectures [2]. However, a more economic alternative is proposed in this thesis aiming at improving the current third generation (3G) HSDPA system by optimising the transceiver design such that it can achieve a sum rate close to the LTE equivalent (under the same bandwidth and channel conditions). This implies that the existing base stations and network architectures can still be used while providing faster Internet speed to the end users.

1.1 Evolution of Telecommunications

Wireless communications was initially developed for voice transmission which then evolved to support simple text messaging and mobile Internet. The first integrated voice and mobile service came in the 3G system [3]. It employed Wide Code Division Multiple Access (WCDMA) which supports parallel transmissions for multiple users through the use of spreading codes. However, the initial release of WCDMA Release

99 has a peak data rate of only 2Mbps and only achieves 384kbps in practice [4] which can only cater for the low-end data applications.

The introduction of HSDPA which is a packet based service, further enhances the peak data rate to 14Mbps. This scheme allows all the spreading codes to be assigned to a single user and supports Adaptive Modulation and Coding (AMC) and fast scheduling which further optimises the downlink throughput compared to WCDMA [5]. The AMC allows the use of more discrete rates by choosing a combination of modulation techniques, transport block sizes and coding scheme that are best suited for the current channel condition [6].

With the continuous growth in the smart phone and tablet industry and its data hungry applications, there needs to be further enhancements in Internet speeds [7]. The use of multiple antennas is an attractive way to further increase system throughput without requiring additional bandwidth by exploiting a new dimension - space [8–11]. Therefore, the Multiple-Input Multiple-Output (MIMO) schemes have been introduced to the HSDPA system in release 7 for the two-transmit-antenna system [12] which further pushes the peak data rate to 28Mbps for the downlink while the four-transmit-antenna scheme has been recently incorporated in release 11 [13].

1.2 Wireless Channel with Multipath Propagation

Contrary to the traditional communications systems with fixed lines, wireless communications systems can transfer information between two or more points without being connected by electrical conductors. This enhances users' experience by supporting mobility so that users can call and surf the Internet while on the go. However, radio wave propagation in the wireless channel is more dynamic and unpredictable. The presence of certain objects such as buildings, mountains and water bodies causes physical phenomena during radio propagation including reflections, diffractions and scattering [14, 15]. Therefore, in addition to Additive White Gaussian Noise (AWGN), the performance of wireless communications systems is highly affected by the channel environment [16].

Channel fading occurs when the signal amplitude varies over time and frequency. A wireless channel can experience two types of fading: large-scale fading and small-scale fading. Large-scale fading occurs when the mobile handset moves over a large distance. It is caused by path loss of a signal or shadowing of large objects. In contrast, small-scale fading is the rapid fluctuations of the signal levels from constructive and destructive interference of multiple signal paths (multipath) and varies over small distances.

The effect of frequency selective multipath propagation strongly affects the achievable data rate of a wireless system. In [17–19], practical measurements have been produced and evaluated which showed that the achievable data rate is much lower than the channel capacity, especially in environments with significant time dispersion including heavily populated urban environments [19]. Although the spreading codes of the HSDPA system are orthogonal to each other at the transmitter, the presence of multipath distorts the orthogonality between spreading codes when the signal arrives at the receiver and induces Inter-Code Interference (ICI). Furthermore, the received signals are also overlapping with each other, which causes Inter-Symbol Interference (ISI). The presence of such interferences together with estimation and Channel State Information (CSI) loss causes a degradation in performance of the HSDPA system. Hence, the difference between practical data rates and peak data rates is observed. The aim of this thesis is to maximise the data rate by minimising the ICI and ISI through various transmitter and receiver optimisation techniques.

The HSDPA downlink optimisation can be viewed as a two-part problem [6]: multi-user scheduling such as [20, 21] and single-user physical link throughput optimisation. The MIMO technology in the HSDPA system specified in release 7 only considers single-user MIMO and does not apply multi-user MIMO. Therefore, this thesis addresses the optimisation problem for single-user to maximise the system throughput while reducing the intra-cell interference. The MIMO frequency selective (multipath) channel model used throughout this thesis will be introduced next.

1.3 Frequency Selective MIMO Channel Model

A multipath fading model can be statistically characterised by its Power Delay Profile (PDP) and Doppler power spectrum. The PDP defines the time dispersion and frequency selectivity of a channel while the Doppler power spectrum defines the coherent time. The PDPs of different channels are normally given in the standards such as [22,23] for evaluation. As the channel is re-estimated for each block of data, a block fading channel model is assumed and therefore, Doppler effects are not considered throughout the thesis.

Defining T_c as the chip period, the symbol period is given by $\rho = NT_c$, where N is the spreading factor of the HSDPA system. For a radio channel with L resolvable paths, the PDP that is sampled at every chip period $P_{T_c}(n)$ is represented by:

$$P_{T_c}(n) = \sum_{l=0}^{L-1} P_{Tc,l}\delta(n-l) \tag{1.1}$$

where $P_{T_c,l}$ is the power of the l^{th} path, n is the sample number and δ is the Dirac function. After sampling, the power is normalised so that the PDP has a unity power gain. This produces the normalised square root of the PDP which can be represnted by the vector $\underline{h} = [h_0, \ldots, h_l, \ldots, h_{L-1}]^T$ where

$$h_l = \sqrt{\frac{P_{Tc,l}}{\sum_{j=0}^{L-1} P_{T_c,j}}} \text{ for } l = 0, ..., L-1. \tag{1.2}$$

In this thesis, a MIMO channel model is used having N_T transmit antennas and N_R receive antennas. The MIMO paths between each pair of transmit and receive antennas (say n_t and n_r) can be represented by the normalised channel impulse response $\underline{h}^{(n_r,n_t)} = [h_0^{(n_r,n_t)}, ..., h_{L-1}^{(n_r,n_t)}]^T \in \mathbb{C}^{L\times 1}$ with Rayleigh distribution generated from the normalised square root PDP.

It is assumed that the channel conditions between each pair of antennas (n_r, n_t) have the same PDP (but different and uncorrelated channel impulse response), which can be represented by the channel convolutional matrix between each pair of antennas as:

$$\mathbf{H}^{(n_r,n_t)} = \begin{bmatrix} h_0^{(n_r,n_t)}, & 0 & \cdots & 0 \\ h_1^{(n_r,n_t)}, & h_0^{(n_r,n_t)}, & \ddots & 0 \\ \vdots & \vdots & \ddots & \vdots \\ h_{L-1}^{(n_r,n_t)}, & h_{L-2}^{(n_r,n_t)}, & \ddots & 0 \\ 0 & h_{L-1}^{(n_r,n_t)}, & \ddots & 0 \\ 0 & 0 & \ddots & 0 \\ \vdots & \vdots & \ddots & \vdots \\ 0 & 0 & \ddots & 0 \\ 0 & 0 & \ddots & h_0^{(n_r,n_t)} \\ 0 & 0 & \ddots & h_1^{(n_r,n_t)} \\ \vdots & \vdots & \ddots & \vdots \\ 0 & 0 & \cdots & h_{L-1}^{(n_r,n_t)} \end{bmatrix} \in \mathbb{C}^{(N+L-1)\times N}, \tag{1.3}$$

while the overall MIMO channel matrix is represented as:

$$\mathbf{H} = \begin{bmatrix} \mathbf{H}^{(1,1)}, & \cdots, & \mathbf{H}^{(1,N_T)} \\ \vdots & \ddots & \vdots \\ \mathbf{H}^{(N_R,1)}, & \cdots, & \mathbf{H}^{(N_R,N_T)} \end{bmatrix} \in \mathbb{C}^{N_R(N+L-1)\times N_T N}. \tag{1.4}$$

Due to the presence of multipath, some of the information in the received signal will be spilled over to the previous and next symbol period and causes ISI. To compensate for the ISI, the received signal of the previous and next symbol period will need to be considered. The MIMO channel of the previous symbol block and the next symbol block are represented by $\mathbf{H}_1$ and $\mathbf{H}_2$ respectively, and are defined as follows:

$$\mathbf{H}_1 = \left(\mathbf{I}_{N_R} \otimes \left(\mathbf{J}_{N+L-1}^T\right)^N\right)\mathbf{H} \in \mathbb{C}^{N_R(N+L-1)\times N_T N} \tag{1.5}$$

$$\mathbf{H}_2 = \left(\mathbf{I}_{N_R} \otimes \mathbf{J}_{N+L-1}^N\right)\mathbf{H} \in \mathbb{C}^{N_R(N+L-1)\times N_T N} \tag{1.6}$$

where $\mathbf{J}$ is the shift matrix and the lower script defines its dimension. In this case the dimension is $(N+L-1)\times(N+L-1)$ and the shift matrix is formed as follows:

$$\mathbf{J}_{N+L-1}=\begin{bmatrix} \underline{0}^T_{N+L-1}, & 0 \\ \mathbf{I}_{N+L-1}, & \underline{0}_{N+L-1} \end{bmatrix} \in \mathbb{C}^{(N+L-1)\times(N+L-1)} \tag{1.7}$$

When a matrix is multiplied by $\left(\mathbf{J}^T\right)^N$, the columns of the matrix will be shifted up by N chips (hence previous symbol block) while multiplying the matrix with $\mathbf{J}^T$ shifts the columns of the matrix down by N chips (next symbol block). The empty contents after shifting are filled with zeros. In the next section the challenges in the HSDPA systems to be addressed in this thesis are outlined.

1.4 Challenges of the HSDPA System

A number of research gaps that have not been addressed fully in the literature will be discussed in this thesis. These challenges are outlined below:

1. **Complexity of the constraint optimisation approach**: Due to the multipath propagation in the wireless channel, the received SINRs of each spread channel is different if equal energy allocation is used. When allocating equal rate to all the spread channels, the chosen rate has to satisfy the spread channel with the worst received SINR (lowest channel gain). Therefore, to maximise the system throughput, the SINRs of different spread channels have to be aligned. With a target (fixed) SINR, the SINRs of all spread channels can be equalised through iterative energy allocation. This is known as the Equal SINR Equal Rate (ESER) allocation scheme. However, the sum energy of this scheme is only known after the iterative energy adjustment process for each target SINR. Hence, the SINR that maximises the system throughput within the energy budget is not known until the iterative energy adjustment process is finished. Given a set of modulation and coding rates (also referred to as discrete bit rate in this thesis) available, as well as the relationship between bit rate and SINR, iterative energy allocation process is carried out for each discrete bit rate. The discrete bit rate that

maximises the system throughput without exceeding the total energy available will then be selected. This process involves two loops: the inner loop is for the iterative energy allocation (say $I_{\max} = 1000$ iterations) with matrix inversions, while the outer loop is for each target discrete bit rate/SINR (say P iterations). This method requires a minimum complexity of $PI_{\max}O(\alpha)$ where $O(\alpha)$ is the complexity of inverting $\alpha \times \alpha$ matrix. Therefore, even though the ESER allocation maximises the system throughput given an energy constraint for single rate allocation, it is not practical to implement due to its complexity. As a result, further simplification is required to reduce the iterative search of the maximum discrete bit rate to make the system more feasible to implement.

2. **Complexity of the SIC receiver**: Interference cancellation receivers are used to further maximise the system throughput by cancelling the detected signal in a spread channel by spread channel basis to reduce the overall interference. An SIC receiver was developed in [24] for the HSDPA system which can also be applied to the ES allocation. However, the complexity is very heavy as it requires one matrix inversion per spread channel in each energy allocation loop. Defining the total number of spread channels as K, the SIC with ES allocation will require K times more matrix inversion than the non-SIC receiver as described in point 1, making it even more difficult to implement into the hardware. Although the improvements in data rate of the SIC receiver is attractive, a lot of simplifications will be required to make it practically feasible to implement.

3. **Signature sequence optimisation**: Signature sequence optimisation is another way to further optimise the system throughput. This is because after transmitting through the frequency selective multipath channel, the simple Orthogonal Variable Spreading Factor (OVSF) codes which are orthogonal at the transmitter lose their orthogonality at the receiver and causes inter-code and inter-symbol interferences [1]. Therefore, the aim of signature sequence optimisation strategies in most literature is to ensure the signature sequences are orthogonal to each other when received. However, most of these strategies require large amount of Channel

[1] Except in the special case of frequency flat channels where the received signature sequences preserve their orthogonality.

State Information at the Transmitter (CSIT). In the Frequency Division Duplex (FDD) system, CSIT is obtained through feedback. Hence, it is important to optimise the signature sequences without requiring too much CSIT when FDD systems are used. On the other hand, the traditional water-filling algorithms removes those subchannels with low gains to increase the system capacity. Based on the water-filling channel removal method, the following questions have been raised:

(a) Will removing signature sequences with low SINR increase the system throughput for both EE and ES allocation?

(b) If so, can an algorithm that searches for the number of signature sequences to be removed to maximise the system throughput be developed without requiring too much CSIT?

1.5 Thesis Outline

Initially, in Chapter 2, the HSDPA system model to be used in Chapter 2 to 4 is described. Then, the constraint optimisation problem is explained and the new optimisation metric: *System Value* (SV) criterion is introduced. After that, the use of ESER approach is presented and compared to the simple EEER approach. Furthermore, the complexity of the ESER approach is also considered when used in conjunction with the constraint optimisation method which requires an inner loop for iterative energy adjustment and an outer loop that tests all discrete rates. Following that, the use of the SV criterion to eliminate the outer loop required in the ESER constraint optimisation approach is proposed [25].

In Chapter 3, the system throughput presented in Chapter 2 is further optimised by using the novel symbol-level SIC receiver that integrates equalisation and despreading to cancel spatial and temporal interference [25, 26]. Then, a simplified SIC algorithm is proposed which can be integrated with the SV criterion to reduce the complexity of the calculation of SVs as well as further reduces the complexity of the ESER scheme (in particular, the energy adjustment process). Finally, the proposed SIC algorithm

is further verified under practical measurements based on the National Instruments (NI)-PXIe testbed.

In Chapter 4, signature sequence optimisation techniques are explored. A signature sequence design that minimises correlations between codes while reducing inter-symbol interference and noise is proposed which requires full CSIT. When FDD system is implemented, only the receiver has full knowledge of CSI which means that CSIT is obtained through feedback. Therefore, a more practical signature sequence optimisation scheme is proposed without inducing too much CSI feedback. This method removes the signature sequences that have low received SINRs so that higher data rates can be allocated to the spread channels with high SINRs. This signature sequence selection method can be applied to both EE and ES allocation schemes with and without the proposed SIC receiver. Finally, the sum rate loss due to partial CSIT for different HSDPA MIMO systems with and without the proposed SIC receiver are evaluated.

Lastly, the thesis is concluded in Chapter 5. A list of the main contributions and recommendations for future work are also piy;omrf.

Chapter 2

Constraint Optimisation and "System Value" Approach

In this chapter, the use of power allocation (a transmitter optimisation strategy) with a symbol-level Minimum Mean Square Error (MMSE) equaliser is considered to maximise the system throughput for equal rate allocation subject to a power constraint. A novel *System Value* (SV) based optimisation criterion is proposed to provide a computationally efficient energy allocation method to maximise the system throughput with equal rate (or two rates) allocation. It is shown that the system throughput of the power allocation scheme with the proposed SV based maximisation criterion can achieve performance close to the system's sum rate with reduced complexity.

2.1 Link Throughput Maximisation

In the HSDPA system, a fixed set of orthogonal spreading codes known as the Orthogonal Variable Spreading Factor (OVSF) codes are used for the single-input single-output (SISO) system. In the case of multiple-input multiple-output (MIMO) systems, a larger set of signature sequence with double the length is required. Therefore, MIMO spreading codes are created by applying precoding to the OVSF codes. Note that these spreading codes are orthogonal at the transmitter, but this orthogonality is generally

lost at the receiver[1], creating inter-code interference (ICI) and inter-symbol interference (ISI) which degrades the system's performance [19]. In [27,28], it has been shown that the use of a linear MMSE receiver followed by a despreader can help to partially restore the orthogonality between codes. Therefore, an MMSE receiver is considered in this chapter.

Transmitter optimisation [29] includes signature sequence design which will be described in Chapter 3 and power allocation which is discussed in this chapter. The use of iterative energy adaptation for power allocation purposes has been explored in [30–32] which focuses on transceiver design optimisation while [33–37] focus on performing joint rate and power allocation at the transmitter. These power allocation strategies require iterative power adjustment to achieve a target optimisation criterion such as a target rate allocation or signal-to-noise-plus-interference ratio (SINR). There are two main objectives in joint rate and power adaptations. The first objective is to increase the power efficiency (or equivalently, reducing the amount of power required) to maintain the same quality of service or data rate such as [38–40]. This objective is mainly used for voice communications and ad-hoc network where reducing power usage is the priority. The second objective is to maximise the data rate subject to the total power available such as [30–33,35–37,39]. The focus of this chapter is to optimise the system throughput for single rate allocation through iterative power adjustment using a new optimisation metric, *System Value* (SV) criterion without being too computationally intensive. Before proceeding to the problem definition, a system model will be defined in the next section, together with the MMSE receiver, the spreading sequence formation as well as energy and SNR definitions. Following that, power allocation schemes including Equal Energy Equal Rate (EEER) and equal SINR equal rate allocation schemes will be discussed. This is then followed by a description of the Equal Energy Two-Group (EETG) and Equal SINR Two-Group (ESTG) schemes to further increase the system throughput. After that, the use of SV criterion to simplify the complexity of the ESER and ESTG schemes while maximising the system throughput will be introduced. Finally, results and conclusions are presented.

[1] The orthogonality between the spreading codes is lost after transmitting over the frequency selective multipath channel. However, the orthogonality is preserved if the channel is frequency flat.

2.2 The MIMO HSDPA Transceiver Model

A MIMO HSDPA system model is described in this section with a total number of transmit antennas N_T and receive antennas N_R. For a SISO system, $N_T = N_R = 1$. The HSDPA system uses OVSF codes as channelisation codes with a spreading factor of N. The use of precoding with OVSF codes forms a set of signature sequences for MIMO systems. The formation of spreading codes is given in Section 2.2.3. The total number of spread channels (signature sequences) that is used to transmit information is $K \leq \min(N_T, N_R)N$ for a MIMO system. The optimum number of spreading sequences is denoted as $K^\star \leq K$ and is used when signature sequence selection is performed in Chapter 4. When signature sequence selection is not performed (as in this chapter), $K^\star = K$.

The transceiver model is shown in Figure 2.1, which consists of transmitter, channel and receiver parts. Streams of bits are sent from the transmitter where they are encoded and mapped to symbols, spread and energy weighted to produce a transmit vector $\underline{z}_{n_t}$ for each transmit antenna before up-converting to the Radio Frequency (RF). The channel consists of multipaths and noise was presented in Section 1.3 of Chapter 1 (page 26). After down-converting from RF to baseband at the receiver, each antenna receives a signal $\underline{r}_{n_r}$ which contains the transmitted signal, together with interferences from multipath and noise. The received signals are then despread and demapped to binary bits. The next subsection will describe the transmitter.

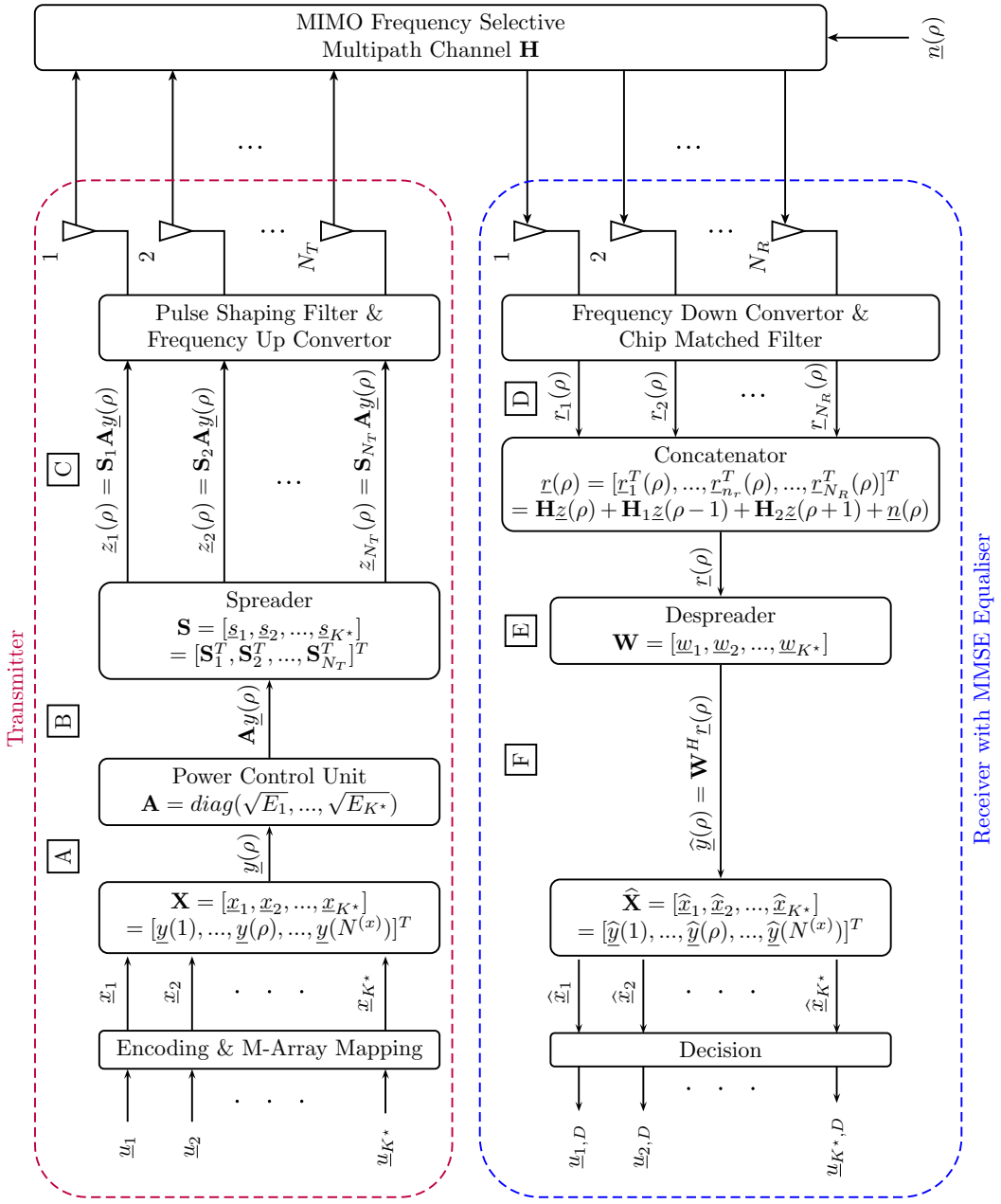


FIGURE 2.1: HSDPA System Model with Transmitter and MMSE Receiver

2.2.1 The HSDPA Transmitter Architecture

The first step of transmission is to generate binary data bit packets $\underline{u}_k$ for $k = 1, ..., K^\star$ spreading sequences. These data bits are then encoded and modulated using Quadrature Amplitude Modulation (QAM). The channel coding rate is defined as r_{code}, whilst the number of constellation points of QAM is represented by M which means each QAM symbol represents $b = \log_2 M$ bits. Hence, the effective bit rate after modulation and coding is $b_p = r_{code} \times \log_2 M$, while the effective bit rate carried over the k^{th} spread channel is represented by b_{p_k}. The coding rate and the modulation scheme are chosen according to Channel State Information (CSI) of the previous Transmission Time Interval (TTI), which is obtained through feedback from the receiver to the transmitter.

The symbols which are mapped from the encoded bits (at Point A, Figure 2.1) are represented by the symbol vector $\underline{x}_k \in \mathbb{C}^{N^{(x)} \times 1}$ for $k = 1, ..., K^\star$, where $N^{(x)} = \frac{TTI}{NT_c}$ is the number of symbols per packet over 1 TTI. It is assumed that the symbol vectors have unity norm, i.e. $\underline{x}_k^H \underline{x}_k = 1$. The symbols to be transmitted across all the $K^\star$ spread channels can be represented by an overall symbol matrix:

$$\mathbf{X} = [\underline{x}_1, ..., \underline{x}_{K^\star}] = \begin{bmatrix} \underline{y}(1)^T \\ \vdots \\ \underline{y}(\rho)^T \\ \vdots \\ \underline{y}(N^{(x)})^T \end{bmatrix} \in \mathbb{C}^{N^{(x)} \times K^\star} \tag{2.1}$$

where $\underline{y}(\rho)^T$ denotes the symbols across all spread channels at the ρ^{th} symbol period and $y(\rho)$ is given as follows:

$$\underline{y}(\rho) = [y_1(\rho), y_2(\rho), ..., y_{K^\star}(\rho)]^T \in \mathbb{C}^{K^\star \times 1} \tag{2.2}$$

with $\underline{y_k}(\rho)$ representing the symbol to be sent over the k^{th} spread channel at symbol period ρ.

Energies E_k for $k = 1, ..., K^\star$ are then allocated to each spreading sequence subject to an energy constraint:

$$\sum_{k=1}^{K^\star} E_k \leq E_T. \tag{2.3}$$

These energies across all the spreading sequences are represented by an amplitude matrix:

$$\mathbf{A} = \text{diag}\left[\sqrt{E_1}, \sqrt{E_2}, ..., \sqrt{E_{K^\star}}\right] \in \mathbb{R}^{K^\star \times K^\star}. \tag{2.4}$$

The energy weighted symbols are then spread by a set of spreading sequences (at Point B, Figure 2.1). Defining the set of OVSF channelisation codes as $\mathbf{S}_{OVSF} \in \mathbb{C}^{N \times N}$, and the precoding matrix as $\mathbf{F} \in \mathbb{C}^{N_T \times \min(N_T, N_R)}$, the MIMO signature sequence set is given by $\mathbf{S}_F = \mathbf{F} \otimes \mathbf{S}_{OVSF} \in \mathbb{C}^{(N_T N) \times \min(N_T, N_R) N}$, and a subset $K^\star$ spreading codes are selected for transmission:

$$\mathbf{S} = [\underline{s}_1, \underline{s}_2, ..., \underline{s}_{K^\star}] = \begin{bmatrix} \mathbf{S}_1 \\ \mathbf{S}_2 \\ \vdots \\ \mathbf{S}_{N_T} \end{bmatrix} \in \mathbb{C}^{(N_T N) \times K^\star} \tag{2.5}$$

where $|\underline{s}_k|^2 = 1$ and the spreading sequence matrix of the n_t^{th} antenna is represented by $\mathbf{S}_{n_t} \in \mathbb{C}^{N \times K^\star}$. The transmit vector for each antenna of each symbol period (see Point C, Figure 2.1) is therefore given by:

$$\underline{z}_{n_t}(\rho) = \mathbf{S}_{n_t} \mathbf{A} \underline{y}(\rho) \in \mathbb{C}^{N \times 1} \tag{2.6}$$

which are then fed to the pulse shaping filter at integer multiples of T_c before up converting to the desired carrier frequency. The transmit vector that contains signals from all antennas is represented by:

$$\underline{z}(\rho) = \begin{bmatrix} \underline{z}_1(\rho) \\ \underline{z}_2(\rho) \\ \vdots \\ \underline{z}_{N_T}(\rho) \end{bmatrix} = \mathbf{S}\mathbf{A}\underline{y}(\rho) \in \mathbb{C}^{(N_T N) \times 1} \tag{2.7}$$

while the transmit vectors for the previous and next symbol period can be formed as follows:

$$\underline{z}(\rho-1) = \mathbf{SA}\underline{y}(\rho-1) \in \mathbb{C}^{(N_T N)\times 1}, \tag{2.8}$$

$$\underline{z}(\rho+1) = \mathbf{SA}\underline{y}(\rho+1) \in \mathbb{C}^{(N_T N)\times 1}. \tag{2.9}$$

Note that when $\rho = 1$, $\underline{z}(\rho-1) = \underline{0}_{N_T N}$ and when $\rho = N^{(x)}$, $\underline{z}(\rho+1) = \underline{0}_{N_T N}$.

2.2.2 The HSDPA Receiver Architecture

After the signal is transmitted over the multipath channel as described in Section 1.3, the signal arrives at the receiver at radio frequency. The received signals are then down-converted to base band, the signals are sampled at integer multiples of T_c. The overall received signal after the chip matched filter at baseband of all receive antenna is represented by the vector:

$$\underline{r}(\rho) = \mathbf{H}\underline{z}(\rho)+\mathbf{H}_1\underline{z}(\rho-1)+\mathbf{H}_2\underline{z}(\rho+1)+\underline{n}(\rho) = \begin{bmatrix} \underline{r}_1(\rho) \\ \underline{r}_2(\rho) \\ \vdots \\ \underline{r}_{N_R}(\rho) \end{bmatrix} \in \mathbb{C}^{N_R(N+L-1)\times 1} \tag{2.10}$$

where $\underline{n}(\rho) \in \mathbb{C}^{N_R(N+L-1)\times 1}$ is the noise vector at the output of the receiver chip matched filter with properties $E\left\{\underline{n}(\rho)\underline{n}^H(\rho)\right\} = \sigma_n^2 \mathbf{I}_{N_R(N+L-1)}$. The received vector at each n_r^{th} received antenna is represented by $\underline{r}_{n_r}(\rho) \in \mathbb{C}^{(N+L-1)\times 1}$ (see Point D, Figure 2.1).

The received signature sequence of the current symbol period $\mathbf{Q}$, the previous symbol period $\mathbf{Q}_1$ and the next symbol period $\mathbf{Q}_2$ are defined as:

$$\mathbf{Q} = \mathbf{HS} = \left[\underline{q}_1, \underline{q}_2, ..., \underline{q}_{K^\star}\right] \in \mathbb{C}^{N_R(N+L-1)\times K^\star}, \tag{2.11}$$

$$\mathbf{Q}_1 = \mathbf{H}_1\mathbf{S} = \left[\underline{q}_{1,1}, ..., \underline{q}_{k,1}, ..., \underline{q}_{K^\star,1}\right] \in \mathbb{C}^{N_R(N+L-1)\times K^\star}, \tag{2.12}$$

$$\mathbf{Q}_2 = \mathbf{H}_2\mathbf{S} = \left[\underline{q}_{1,2}, ..., \underline{q}_{k,2}, ..., \underline{q}_{K^\star,2}\right] \in \mathbb{C}^{N_R(N+L-1)\times K^\star}. \tag{2.13}$$

From Equation (2.10) and Equation (2.11), it can be seen that the received signal per antenna and the signature sequences are $L-1$ chips longer than at the transmitter (see Equations (2.7) and (2.5) for comparisons). This shows that the received signals are affected by ISI and ICI after passing through the channel. To reduce ICI and ISI, the samples of the previous and next symbol period are taken into account in the despreading process by using Equation (2.12) and Equation (2.13) as shown in [41]. Furthermore, an MMSE equaliser will be used in this chapter to partially restore the orthogonality between codes. The MMSE equaliser architecture will be described next.

The MMSE Equaliser

Defining $\hat{y}_k(\rho)$ as the estimated symbol of the k^{th} spread channel at the symbol period ρ, the MMSE equaliser aims to minimise the Mean Square Error (MSE) between each transmitted symbol and estimated symbol: $\varepsilon_k = E\{|\hat{y}_k(\rho) - y_k(\rho)|\}$. The normalised MMSE linear despreading filter coefficients $\underline{w}_k$ can be formed using the following equation:

$$\underline{w}_k = \frac{\mathbf{C}^{-1}\underline{q}_k}{\underline{q}_k^H \mathbf{C}^{-1}\underline{q}_k} \in \mathbb{C}^{N_R(N+L-1)\times 1} \tag{2.14}$$

where $\mathbf{C}$ is the covariance matrix formed as follows:

$$\mathbf{C} = E\left\{\underline{r}(\rho)\underline{r}(\rho)^H\right\} \in \mathbb{C}^{N_R(N+L-1)\times N_R(N+L-1)} \tag{2.15}$$

$$= \mathbf{Q}\mathbf{A}^2\mathbf{Q}^H + \mathbf{Q}_1\mathbf{A}^2\mathbf{Q}_1^H + \mathbf{Q}_2\mathbf{A}^2\mathbf{Q}_2^H + \sigma_n^2\mathbf{I}_{N_R(N+L-1)}. \tag{2.16}$$

The despreading coefficients of all spread channels (see point E, Figure 2.1) can be represented by a matrix as follows:

$$\mathbf{W} = [\underline{w}_1, \underline{w}_2, ..., \underline{w}_{K^\star}] \in \mathbb{C}^{N_R(N+L-1)\times K^\star}. \tag{2.17}$$

The estimated symbol $\underline{\hat{y}}(\rho)$ of the transmitted symbol $\underline{y}(\rho)$ can be obtained after despreading (at point F, Figure 2.1) as below:

$$\underline{\hat{y}}(\rho) = [\hat{y}_1(\rho), \hat{y}_2(\rho), ..., \hat{y}_{K^\star}(\rho)]^T = \mathbf{W}^H\underline{r}(\rho) \in \mathbb{C}^{K^\star\times 1} \tag{2.18}$$

where

$$\hat{\mathbf{X}} = [\underline{\hat{x}}_1, \underline{\hat{x}}_2, ..., \underline{\hat{x}}_{K^\star}] = \begin{bmatrix} \underline{\hat{y}}(1)^T \\ \vdots \\ \underline{\hat{y}}(\rho)^T \\ \vdots \\ \underline{\hat{y}}(N^{(x)})^T \end{bmatrix} \in \mathbb{C}^{N^{(x)} \times K^\star}. \tag{2.19}$$

The SINR of the k^{th} spread channel is given as:

$$\gamma_k = \frac{E_k \left| \underline{w}_k^H \underline{q}_k \right|}{\underbrace{\sum_{\substack{j=1 \\ j \neq k}}^{K^\star} E_j \left| \underline{w}_k^H \underline{q}_j \right|}_{\text{interference from other codes}} + \underbrace{\sum_{j=1}^{K^\star} E_j \left| \underline{w}_k^H \underline{q}_{j,1} \right|}_{\text{ISI from } \rho-1} + \underbrace{\sum_{j=1}^{K^\star} E_j \left| \underline{w}_k^H \underline{q}_{j,2} \right|}_{\text{ISI from } \rho+1} + \underbrace{\sigma_n^2 \underline{w}_k^H \underline{w}_k}_{\text{noise}}}. \tag{2.20}$$

When MSE ε_k of each k^{th} spread channel is minimised at the output of the MMSE despreader, the SINR of the k^{th} spread channel can be rewritten by substituting Equation (2.14) into Equation (2.20) as follows:

$$\gamma_k = \frac{E_k \underline{q}_k^H \mathbf{C}^{-1} \underline{q}_k}{1 - E_k \underline{q}_k^H \mathbf{C}^{-1} \underline{q}_k} \tag{2.21}$$

and there is relationship between system value λ_k, ε_k and γ_k as given below:

$$\lambda_k = 1 - \varepsilon_k = \frac{\gamma_k}{1 + \gamma_k} = E_k \underline{q}_k^H \mathbf{C}^{-1} \underline{q}_k. \tag{2.22}$$

Next, the formation of signature sequences for the HSDPA system will be described.

2.2.3 Channelisation Codes for the HSDPA System

The channelisation codes (or signature sequences for SISO case) used in the HSDPA system are the OVSF codes with a spreading factor of $N = 16$, as specified in the HSDPA standard in [42]. The OVSF codes are formed in a recursive manner from $j = 0$ to $j = \log_2(N)$ where $n = 1, ..., N$. By initiating $\mathbf{S}_0 = 1$, the recursive OVSF

codes $\mathbf{S}_j$ can be formed as follows:

$$\mathbf{S}_j = \begin{bmatrix} \mathbf{S}_{j-1}, & \mathbf{S}_{j-1} \\ \mathbf{S}_{j-1}, & -\mathbf{S}_{j-1} \end{bmatrix} \in \mathbb{C}^{2^j \times 2^j}. \tag{2.23}$$

As an example, the steps of forming OVSF codes with $N = 4$ (i.e. $\mathbf{S}_j$ for $j = 0, 1, 2$) is given below:

1. Initiate $\mathbf{S}_0 = 1$.
2. Form $\mathbf{S}_1 = \begin{bmatrix} \mathbf{S}_0, & \mathbf{S}_0 \\ \mathbf{S}_0, & -\mathbf{S}_0 \end{bmatrix} = \begin{bmatrix} 1, & 1 \\ 1, & -1 \end{bmatrix}$.
3. Form $\mathbf{S}_2 = \begin{bmatrix} \mathbf{S}_1, & \mathbf{S}_1 \\ \mathbf{S}_1, & -\mathbf{S}_1 \end{bmatrix} = \begin{bmatrix} 1, & 1, & 1, & 1 \\ 1, & -1, & 1, & -1 \\ 1, & 1, & -1, & -1 \\ 1, & -1, & -1, & 1 \end{bmatrix}$.

Hence, the final OVSF codes represented by $\mathbf{S}_{OVSF}$ for $N = 4$ is $\mathbf{S}_{OVSF} = \mathbf{S}_2$. Using the same method, the OVSF codes for the HSDPA with $N = 16$ can be formed such that $\mathbf{S}_{OVSF} = \mathbf{S}_4$. As this chapter concentrates on the 2×2 MIMO spatial multiplexing system, a precoding codebook needs to be defined to form a set of signature sequences for the MIMO system with 2 transmit antennas.

2.2.4 PCI Codebook for Two Transmit Antennas

The precoding matrix $\mathbf{F}$ for the HSDPA with two transmit antennas is given in [43] which is formed as follows:

$$\mathbf{F} = \begin{bmatrix} F_1, & F_1 \\ F_2, & -F_2 \end{bmatrix} \in \mathbb{C}^{2\times 2} \tag{2.24}$$

with the precoding weights given as follows:

$$F_1 = \frac{1}{\sqrt{2}}, \tag{2.25}$$

$$F_2 \in \left\{\frac{1+j}{2}, \frac{1-j}{2}, \frac{-1+j}{2}, \frac{-1-j}{2}\right\}. \tag{2.26}$$

Defining $\mathbf{F}^n$ to represent different codebooks, where n is the index of the codebooks, the PCI table for two transmit antennas is given in Table 2.1. The precoding matrix $\mathbf{F}^{n^\star}$ that can achieve the highest sum rate is selected to be used for transmission, so that $\mathbf{F} = \mathbf{F}^{n^\star}$.

TABLE 2.1: PCI for Two Transmit antennas

Codebook	1 stream	2 streams
$\mathbf{F}^0$	$\begin{bmatrix} \frac{1}{\sqrt{2}} \\ \frac{1+j}{2} \end{bmatrix}$	$\begin{bmatrix} \frac{1}{\sqrt{2}} & \frac{1}{\sqrt{2}} \\ \frac{1+j}{2} & \frac{-1-j}{2} \end{bmatrix}$
$\mathbf{F}^1$	$\begin{bmatrix} \frac{1}{\sqrt{2}} \\ \frac{1-j}{2} \end{bmatrix}$	$\begin{bmatrix} \frac{1}{\sqrt{2}} & \frac{1}{\sqrt{2}} \\ \frac{1-j}{2} & \frac{-1+j}{2} \end{bmatrix}$
$\mathbf{F}^2$	$\begin{bmatrix} \frac{1}{\sqrt{2}} \\ \frac{-1+j}{2} \end{bmatrix}$	$\begin{bmatrix} \frac{1}{\sqrt{2}} & \frac{1}{\sqrt{2}} \\ \frac{-1+j}{2} & \frac{1-j}{2} \end{bmatrix}$
$\mathbf{F}^3$	$\begin{bmatrix} \frac{1}{\sqrt{2}} \\ \frac{-1-j}{2} \end{bmatrix}$	$\begin{bmatrix} \frac{1}{\sqrt{2}} & \frac{1}{\sqrt{2}} \\ \frac{-1-j}{2} & \frac{1+j}{2} \end{bmatrix}$

With the channelisation codes and the precoding matrix as described above, the full set of signature sequences for the MIMO system can be formed using the following equation:

$$\mathbf{S}_F = \mathbf{F} \otimes \mathbf{S}_{OVSF} \in \mathbb{C}^{(N_T N)\times(N_T N)} \tag{2.27}$$

2.2.5 Energy and SNR Definitions

The aim of this chapter is to maximise the total data rate for a given amount of total energy E_T where it is defined as the total energy per symbol period. The energy assigned to each spreading code for each symbol period is given as E_k for $k = 1, ..., K^\star$

where

$$\sum_{k=1}^{K^\star} E_k \leq E_T. \tag{2.28}$$

With the chip period defined as T_c as shown in the previous chapter, the relation to the symbol period is given as $\rho = NT_c$ where N is the spreading factor (processing gain). This also implies that the total chip energy in a chip period has the energy E_c with the relationship of $E_T = NE_c$.

In QAM system, the average chip SNR per receive antenna is given as $\frac{E_c}{N_0}$ where N_0 is the single sided power spectral density. This relation holds if the PDP of the channel is normalised (as defined in Chapter 1). This means that the average power gain of the channel impulse response vector between each pair of antennas is normalised, i.e. $E\left\{(\underline{h}^{n_r,n_t})^H \underline{h}^{n_r,n_t}\right\} = 1$. When the mean square error (MSE) is between the transmit and received symbols are minimised at the output of the receiver (point F of Figure 2.1), the SINR at the output of the despreading unit of the k^{th} spreading sequence (also referred to as received SINR of the k^{th} spread channel), γ_k can be calculated as:

$$\gamma_k = \frac{E_k \underline{q}_k^H \mathbf{C}^{-1} \underline{q}_k}{1 - E_k \underline{q}_k^H \mathbf{C}^{-1} \underline{q}_k}. \tag{2.29}$$

The above parameters are also illustrated in Table 2.2.

TABLE 2.2: Energies and SNR definitions

Symbol	Definition
E_T	Total energy in a symbol period
E_k	Energy of a spread channel
E_c	Total energy in a chip period
T_c	Chip period
NT_c	Symbol period
σ_n^2	AWGN power per dimension
$N_0/2$	Double sided power spectral density of AWGN
E_c/N_0	Chip SNR per receive antenna
γ_k	SINR at the output of despreader for the k^{th} spreading sequence
N	Spreading factor

In the next section, the constraint optimisation problem formulation will be defined. After that, the equal rate allocation for the simple equal energy distribution as well as the more optimised equal SINR scheme is described.

2.3 The Constraint Optimisation Problem

The aim of this chapter is to maximise the total rate $R_T = \sum_{k=1}^{K^\star} b_{p_k}$ where b_{p_k} is the discrete bit allocated to each spreading sequence subject to the total energy available $E_T = \sum_{k=1}^{K^\star} E_k$. This optimisation can be done by varying energy allocation and can be formulated as a mathematical expression as follows:

$$\max R_T = \sum_{k-1}^{K^\star} b_{p_k} \tag{2.30}$$

$$\text{s.t.} \begin{cases} \displaystyle\sum_{k=1}^{K^\star} E_k \leq E_T & \text{(2.31a)} \\ \displaystyle E_k = \frac{\Gamma(2^{b_{p_k}} - 1)}{\left(1 + \Gamma(2^{b_{p_k}} - 1)\right) \underline{q}_k^H \mathbf{C}^{-1} \underline{q}_k} & \text{(2.31b)} \\ \text{and } b_{p_k} = b_p \in \{b_1, \ldots, b_P\} \text{ for } k = 1, \ldots, K^\star & \text{(2.31c)} \end{cases}$$

where $\mathbf{C}$ is a function of $E_1, \ldots, E_{K^\star}$ and Γ is the gap value (a constant).

Similar problems of optimising the total rate have been explored in literature in terms of maximising the minimum weighted SINR [44], minimising MSE [45–47] or maximising the weighted sum rate [48].

Given that the MMSE receiver is used (as shown in the system model in Section 2.2), the problem stated in Equation (2.30) can be tackled through addressing a closely related problem: the sum MSE minimisation problem. It has been shown in [49, 50] that minimising the sum MSE is equivalent to maximising a lower bound of the sum rate. With the aim of maximising the total rate, the SV optimisation metric proposed in this chapter is closely related to MSE through the following equation:

$$\varepsilon_k = 1 - \lambda_k \text{ for } k = 1, ..., K^\star \tag{2.32}$$

where ε_k is the MSE of the k^{th} spread channel and λ_k is the SV of the k^{th} spread channel. Therefore, minimising sum MSE is related to maximising sum SV as shown

in the following equation:

$$\sum_{k=1}^{K^\star} \varepsilon_k = K^\star - \sum_{k=1}^{K^\star} \lambda_k \text{ for } k = 1, ..., K^\star \tag{2.33}$$

given that $K^\star$ is a constant and λ_k for $k = 1, ..., K^\star$ are positive numbers.

When optimising the total rate in Equation (2.30), both E_k and the covariance matrix $\mathbf{C}$ are functions of each other which require energy to be iteratively updated using Equation (2.31b) for each spreading sequence and for a given target discrete rate $b_{p_k} = b_p$. This implies that the matrix inverse $\mathbf{C}^{-1}$ is recalculated according to the energies E_k for $k = 1, ..., K^\star$ at each energy iteration. This process continues until all energies converge to fixed values.

The above iterative energy calculation process is repeated for different rate combinations: $b_p \in \{b_1, ..., b_P\}$ until a given rate combination maximises the total rate while satisfying the energy constraint. This energy constraint optimisation approach is discussed later on in Sections 2.4.2 and 2.5.1.

Apart from maximising the total rate, another optimisation objective is to have a feasible practical implementation by reducing the number of energy iterations using the proposed SV to approximate the maximum b_p within the energy constraint. Using the Shannon's capacity equation, the sum rate of the system can be written as:

$$C_T = \sum_{k=1}^{K^\star} \log_2 \left(1 + \frac{\gamma_k}{\Gamma}\right) \tag{2.34}$$

With the system value λ_k and SINR γ_k and MSE relation as given in Equation (2.22) the system value sum rate can be written as:

$$C_T = \sum_{k=1}^{K^\star} \log_2 \left(1 + \frac{\lambda_k}{\Gamma(1-\lambda_k)}\right) \tag{2.35}$$

The objective is to find $\lambda_k \geq \lambda_{k,tar}$ where $\lambda_{k,tar} = \frac{\Gamma(b_{p_k}-1)}{1+(\Gamma(b_{p_k}-1))}$ within the energy constraint so as to achieve R_T close to C_T but without requiring to repeat energy iteration for each discrete rate combinations. The SV optimisation method is discussed

in Section 2.6. The next section will describe the equal rate allocation approaches using equal energy allocation and equal SINR allocation.

2.4 Equal Rate Allocation

Equal rate allocation means the same rate b_p is transmitted over all the spread channels. Given a set of achievable discrete rates $\{b_p\}_{p=1}^{P}$ in a practical system, the relationship between the target SINR γ_{tar} and the discrete bit rate is related as follows:

$$\gamma_{tar}(b_p) = \Gamma\left(2^{b_p} - 1\right) = \frac{\lambda_{tar}}{1 - \lambda_{tar}} \tag{2.36}$$

where λ_{tar} is the target system value. The relationship between the SINR at the output of the despreading unit as a function of energy, multipath channel and channelisation codes are given as follows:

$$\gamma_k = \frac{E_k \underline{q}_k^H \mathbf{C}^{-1} \underline{q}_k}{1 - E_k \underline{q}_k^H \mathbf{C}^{-1} \underline{q}_k} = \frac{\lambda_k}{1 - \lambda_k} \tag{2.37}$$

where λ_k is the system value of the k^{th} spread channel defined as follows:

$$\lambda_k = E_k \underline{q}_k^H \mathbf{C}^{-1} \underline{q}_k. \tag{2.38}$$

In this chapter, two different ways of allocating equal rates to all spreading codes are described. The simplest way is called the equal energy equal rate (EEER) allocation, where the total energy E_T is divided equally amongst the spreading sequences. In a multipath channel environment, the use of equal energy allocation yields different SINR γ_k at the output of the despreader for each k^{th} spreading codes. To guarantee the transmitted data can be correctly received, the data rate corresponding to the spread channel with the worst condition (i.e. lowest SINR or lowest channel gain) will be used. This means that the available energy is not efficiently used to transmit data. Therefore, to maximise the total data rate when allocating the same rates to all spreading codes, the SINR levels of all spread channels have to be equal and maximised within the

energy constraint. This is known as equal SINR equal rate (ESER) allocation. In the next two subsections, the EEER and ESER allocation are presented.

2.4.1 EEER Allocation

Finding the rate of EEER allocation is very straight forward. This is done by allocating all spread channels with the same energy and finding their corresponding SINR. Then, select the SINR of the worse spread channel and find the corresponding bit rate using the relation:

$$b_t = \log_2\left(\frac{\gamma_{\min}}{\Gamma} + 1\right) \tag{2.39}$$

where $\gamma_{\min}$ is the minimum value of $\{\gamma_1, \ldots, \gamma_k, \ldots, \gamma_{K^\star}\}$. Finally, quantise the bit rate so it satisfies $b_p < b_t \leq b_{p+1}$. The total rate is $R_T = K^\star b_p$. The steps can be summarised as follows:

Algorithm 1 Equal Energy and Equal Rate Allocation

1: Allocate energy equally to all spreading codes $E_k = \frac{E_T}{K^\star}$ for $k = 1, ..., K^\star$
2: Calculate $\mathbf{Q}, \mathbf{Q}_1, \mathbf{Q}_2$ from Equation (2.11) and $\mathbf{C}$ from Equation (2.16)
3: Find the SINR γ_k using Equation (2.37) for $k = 1, ..., K^\star$. Store them in $\{\underline{\gamma}\}_k$
4: Select the minimum SINR $\gamma_{\min}$ from $\{\gamma_1, \ldots, \gamma_k, \ldots, \gamma_{K^\star}\}$.
5: Map the SINR to the unquantised bit rate using $b_t = \log_2\left(\frac{\gamma_{\min}}{\Gamma} + 1\right)$
6: Quantise b_t such that $b_p < b_t \leq b_{p+1}$

Although simple, energy is not efficiently used in the EEER approach, as there are many other spread channels with higher SINRs are able to load higher data rates. This effect is more severe in channel environments that are heavily affected by multiple paths. In the next section, the use of ESER which equalises the SINR across all spread channels to maximise the total sum rate will be introduced.

2.4.2 Equal SINR Equal Rate Allocation

As described previously, to increase the total rate when allocating the same b_p to all spreading codes, the SINRs at the output of all despreading units have to be equalised and maximised. For a given target SINR level $\gamma_{tar}(b_p)$, the iterative energy calculation can be used to align the SINRs at the output of all despreading units to be equal to

the target SINR. The energy allocation of each spreading code E_k and therefore the summed energy $\sum_{k=1}^{K^\star} E_k$ for the target SINR level can only be determined after the whole iterative energy adjustment process. Hence, to find the maximum b_p that can be loaded within the energy constraint, iterative energy calculations have to be performed for every b_p value, until it satisfies the following inequality:

$$\sum_{k=1}^{K^\star} E_k(b_p) \leq E_T < \sum_{k=1}^{K^\star} E_k(b_{p+1}). \tag{2.40}$$

The total rate for the ESER allocation scheme is $R_T = K^\star b_p$. The whole process of ESER allocation is illustrated in Figure 2.2. The iterative energy adjustment process is described in the next part.

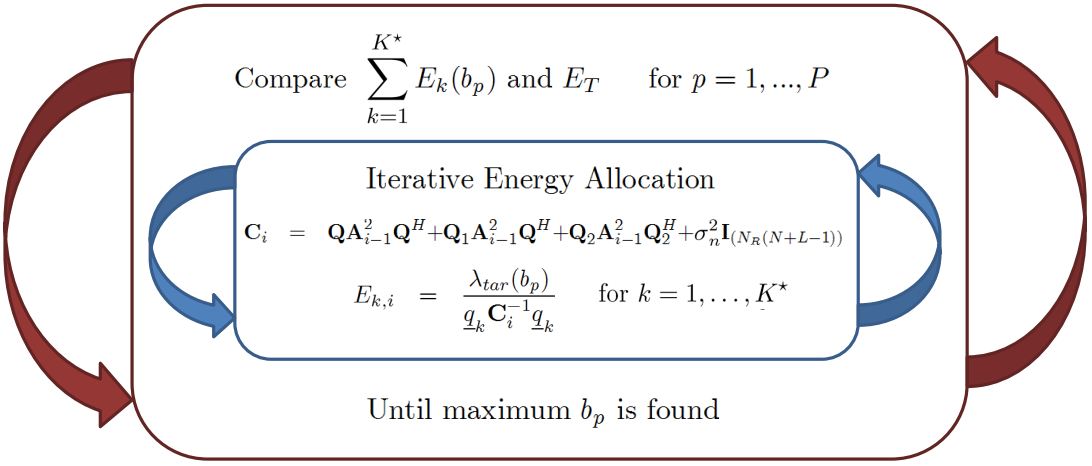


FIGURE 2.2: ESER Algorithm using Constraint Optimisation

The SINR alignment is an iterative process because whenever the energy of a spreading code, say k is updated, the SINR of other despreading units are affected. Therefore, it constantly requires iterative adjustments until a threshold is satisfied. For a given target SINR $\gamma_{tar}(b_p) = \Gamma\left(2^{b_p} - 1\right)$, and the system value $\lambda_{tar}(b_p) = \frac{\gamma_{tar}(b_p)}{1+\gamma_{tar}(b_p)}$, the iterative energy allocation process can be implemented as in Algorithm 2.

When the energies for all spreading sequences settle, the SINR at the output of all despreading units are the same and the summed energy $\sum_{k=1}^{K^\star} E_k(b_p)$ can then be compared to the total energy E_T until the inequality in Equation (2.40) is satisfied. Since the SINRs are aligned after the energy allocation process, this system is referred

Algorithm 2 Iterative Energy Allocation Process for ESER Scheme

Initialisation:
Calculate the target SINRs $\gamma_{tar}(b_p) = \Gamma\left(2^{b_p} - 1\right)$
Calculate its system values
$\lambda_{tar}(b_p) = \frac{\gamma_{tar}(b_p)}{1+\gamma_{tar}(b_p)}$
Assign energies $E_k = \frac{E_T}{K^\star}$ to all $k = 1, ..., K^\star$ signature sequences
Form the amplitude matrix $\mathbf{A}_0$ as in Equation (2.4)
Set iteration index $i = 1$ and error $\varepsilon = 1$
for $i < I_{\max}$ or $\varepsilon = \left|\sum_{k=1}^{K^\star}\left(E_{k,i} - E_{k,i-1}\right)\right| < 0.01\%$ **do**
    Update the covariance matrix:
    $\mathbf{C}_i = \mathbf{Q}\mathbf{A}_{i-1}^2\mathbf{Q}^H + \mathbf{Q}_1\mathbf{A}_{i-1}^2\mathbf{Q}_1^H + \mathbf{Q}_2\mathbf{A}_{i-1}^2\mathbf{Q}_2^H + N_0\mathbf{I}_{N_R(N+L-1)}$
    Revise the energy calculation $E_{k,i} = \frac{\lambda_{tar}(b_p)}{\underline{q}_k\mathbf{C}_i^{-1}\underline{q}_k}$ for $k = 1, ..., K^\star$
    Update $\mathbf{A}_i$.

to as Equal SINR Equal Rate (ESER) scheme. The Two-Group (TG) allocation which can further improve the system throughput of both the ESER and EEER schemes, known as ESTG and EETG respectively will be described in the next section.

2.5 Rate Adaptive Two-Group Optimisation

So far, rate allocation is carried out such that one single rate is used to allocate to all spreading sequences. In this section, the two-group allocation is described, where a group of spreading sequences are allocated with rate b_p while a second group that is of better channel conditions are allocated with rate b_{p+1}. The equal SINR two-group allocation which further maximises the system throughput will be described next.

2.5.1 Equal SINR Two-Group Allocation

Given the energy constraint, the way to maximise the sum rate when the single rate allocation is carried out was shown in the previous section. Although the sum rate is maximised for the single rate allocation, there exists unused (residual) energy in the system given by:

$$E_{res} = E_T - \sum_{k=1}^{K^\star} E_k. \tag{2.41}$$

This energy is not used because it cannot support a higher transmission rate for all spreading sequences. However, this remaining energy can support up to m signature

sequences to transmit at rate b_{p+1}. Therefore, the rate adaptive two-group optimisation [51, 52] can be used to further optimise the total rate by loading the first $(K - m)$ channels with rate b_p and m channels with rate b_{p+1}. Hence, the total rate becomes:

$$R_T = (K^\star - m)b_p + mb_{p+1}. \tag{2.42}$$

To perform ESTG optimisation, ESER allocation in the previous section has to be performed first to find the optimum b_p value. Knowing the b_p value, the number of spreading sequences, m, that can be loaded with b_{p+1} can be found through iterative energy allocation. Starting from $m = 1$, the iterative energy calculation is performed until the following inequalities are satisfied:

$$\sum_{k=1}^{K^\star-m} E_k(b_p) + \sum_{k=K^\star-m+1}^{K^\star} E_k(b_{p+1}) \leq E_T < \sum_{k=1}^{K^\star-m+1} E_k(b_p) + \sum_{k=K^\star-m+2}^{K^\star} E_k(b_{p+1}). \tag{2.43}$$

To find the optimum m, the energy iteration has to be modified to accommodate two different rates. The modified energy allocation process is summarised as shown in Algorithm 3.

Algorithm 3 Iterative Energy Allocation Process for ESTG Scheme

Initialisation
Calculate the target SINRs $\gamma_{tar}(b_p) = \Gamma\left(2^{b_p} - 1\right)$ and $\gamma_{tar}(b_{p+1}) = \Gamma\left(2^{b_{p+1}} - 1\right)$
Calculate its system values
$\lambda_{tar}(b_p) = \frac{\gamma_{tar}(b_p)}{1+\gamma_{tar}(b_p)}$ and $\lambda_{tar}(b_{p+1}) = \frac{\gamma_{tar}(b_{p+1})}{1+\gamma_{tar}(b_{p+1})}$
Assign energies of all k spread channels as $E_k = \frac{E_T}{K^\star}$
Form the amplitude matrix $\mathbf{A}_0$ as in Equation (2.4).
Set iteration index $i = 1$ and error $\varepsilon = 1$
for $i < I_{\max}$ or $\varepsilon = \left|\sum_{k=1}^{K^\star} (E_{k,i} - E_{k,i-1})\right| < 0.01\%$ **do**
    Update the covariance matrix:
    $\mathbf{C}_i = \mathbf{Q}\mathbf{A}_{i-1}^2\mathbf{Q}^H + \mathbf{Q}_1\mathbf{A}_{i-1}^2\mathbf{Q}_1^H + \mathbf{Q}_2\mathbf{A}_{i-1}^2\mathbf{Q}_2^H + N_0\mathbf{I}_{(N_R(N+L-1))}$
    Revise the energy calculation:
    $E_{k,i} = \frac{\lambda_{tar}(b_p)}{\underline{q}_k\mathbf{C}_i^{-1}\underline{q}_k}$ for $k = 1, ..., (K^\star - m)$
    $E_{k,i} = \frac{\lambda_{tar}(b_{p+1})}{\underline{q}_k\mathbf{C}_i^{-1}\underline{q}_k}$ for $k = (K^\star - m + 1), ..., K^\star$
    Update $\mathbf{A}_i$.

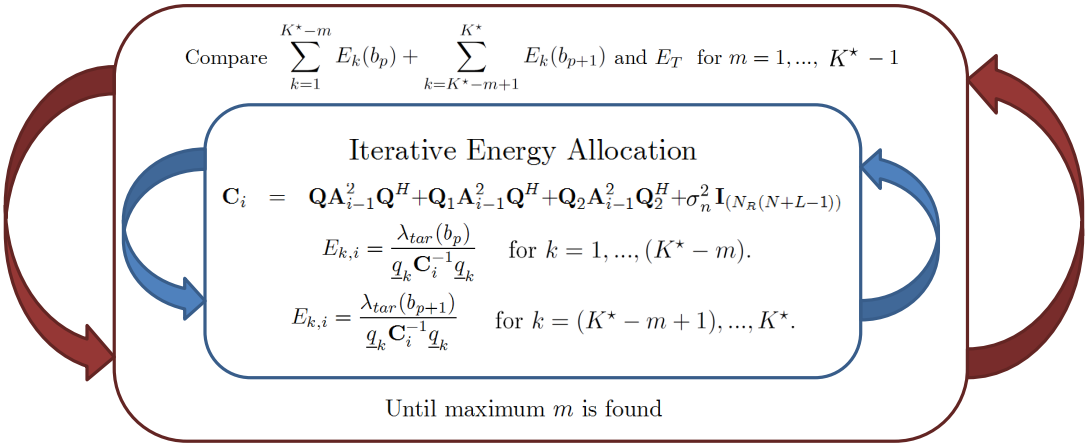


FIGURE 2.3: ESTG Algorithm using Constraint Optimisation

2.5.2 Equal Energy Two-Group Allocation Algorithm

Therefore, in addition to performing ESER to find the optimum b_p value as illustrated in Figure 2.2, a further iterative search for m value together with iterative energy allocation needs to be performed which is summarised and illustrated in Figure 2.3.

The ESTG allocation in the previous subsection can further improve the system throughput of the ESER scheme. Similar to the use of two-group scheme in ES allocation, the use of two data rates for the EE allocation to observe its improvement is also explored in this subsection. The idea of Equal Energy Two-Group (EETG) is to load the spread channels that has the SINR $\gamma_k \geq \gamma_{b_{p+1}}$ with rate b_{p+1}. So that the total rate becomes

$$R_T = (K^\star - m)\, b_p + m\lambda_{opt}(b_{p+1}). \tag{2.44}$$

The procedure for the EETG can be summarised as follows:

Algorithm 4 EETG Allocation Algorithm

1: Allocate energy equally to all spread channels $E_k = \frac{E_T}{K^\star}$ for $k = 1, ..., K^\star$
2: Calculate $\mathbf{Q}, \mathbf{Q}_1, \mathbf{Q}_2$ from Equation (2.11) and $\mathbf{C}$ from Equation (2.16)
3: Find the SINR γ_k using Equation (2.37) for $k = 1, ..., K^\star$
4: Select the minimum SINR $\gamma_{\min}$ from $\{\gamma_1, \ldots, \gamma_k, \ldots, \gamma_{K^\star}\}$
5: Find b_p such that $\gamma(b_p) \leq \gamma_{min}$
6: Load the k^{th} spread channel with b_p if γ_k satisfy $\gamma(b_p) \leq \gamma_k < \gamma(b_{p+1})$ for $k = 1, \ldots, K^\star$
7: Load the k^{th} spread channel with b_{p+1} if $\gamma_k \geq \gamma(b_{p+1})$ for $k = 1, \ldots, K^\star$

2.5.3 Complexity of ESER & ESTG using Constraint Optimisation

Although the use of ESER and ESTG approaches optimises the sum rate, the complexity of such systems needs to be considered and analysed. As shown in Figure 2.2, the ESER allocation process requires $I_{\max}$ energy iterations for each target rate (inner loop). However, the iterative energy process needs to be computed for each discrete rate until the maximum rate that satisfies the energy constraint is found. Considering that there are usually $P = 16$ different modulations and coding rates in the HSDPA standards [43], and that $I_{\max}$ is set to 1000 in this thesis[2], the ESER algorithm requries a total of 16000 energy iterations. Considering each energy iteration involves a matrix inversion $\mathbf{C}^{-1}$ of dimension $N_R(N+L-1) \times N_R(N+L-1)$ where $N = 16$ as defined in the standard, the minimum value of N_R and L is 1, the complexity of each energy iteration is at least $O(16^3)$. For this thesis, a 2×2 MIMO system is assumed. Hence, the complexity of $\mathbf{C}^{-1}$ becomes $O(32^3)$. Therefore, the ESER scheme requires 16000 of $O(32^3)$ which is very complex.

When ESTG scheme is used, a further $(K^\star - 1)I_{\max}$ energy iterations are required to find m. Therefore, ESTG requires a total of $(P + K^\star - 1)I_{\max}$ energy iterations (where the maximum number of spread channels for the 2×2 MIMO system is 32), the ESTG requires 47000 of $O(32^3)$ operations which is even more complex.

To make ESER and ESTG practical, there is a need to decrease their complexities. Therefore, the use of SV approach [26] is proposed in this chapter, which can approximate the discrete rate b_p before the energy calculations and hence, the SV approach eliminates the need of the outer loop in the constraint optimisation. In other words, the number of iterative energy calculations and matrix inversions is reduced to $I_{\max}$ for both systems or equivalently 1000 of $O(32^3)$ operations are required. The system value approach will be described in the next section.

[2] $I_{\max}$ is set to 1000 because even if the algorithms have not converged yet, the received SINR of the different spread channels are roughly equal (accuracy of 3 decimal places) for the received SNR rage used in this thesis.

2.6 The System Value Approach

As shown in the previous section, the use of ESER allocation scheme maximises the total rate for single group allocation and ESTG allocation scheme can further minimise the wasted energy due to discrete loss. On the other hand, the use of constraint optimisation is very computationally intensive. In this section, the use of system value approximation to reduce the complexity of searching for the optimum b_p and hence λ_{tar} without going through the expensive iterative search is proposed. This approach reduces the overall complexity and decreases the total number of energy updates from $PI_{\max}$ and $(P+K-1)\,I_{\max}$ for ESER and ESTG respectively to $I_{\max}$.

When ESER allocation scheme is performed, the system values of all spread channels are equalised[3]. The aim in this section is to find λ_k for $k = 1, \ldots, K^\star$ and hence, λ_{tar} and b_p within the energy constraint but without carrying iterative energy calculation for each discrete rate combination. This can be represented in a mathematical expression as follows:

$$\text{Find } \lambda_k = \sum_{k=1}^{K^\star} E_k \underline{q}_k^H \mathbf{C}^{-1} \underline{q}_k \geq \lambda_{tar}(b_p) \text{ for } k = 1, \ldots, K^\star \tag{2.45}$$

$$\text{s.t.} \begin{cases} \lambda_1 = \ldots = \lambda_k = \ldots = \lambda_{K^\star} & \text{and} \quad (2.46a) \\ \sum_{k=1}^{K^\star} E_k \leq E_T & (2.46b) \end{cases}$$

This would normally require unequal energy allocation for frequency selective channels as shown in the ESER and ESTG schemes in the previous sections. To eliminate the computational complexity required to find λ_{tar} and b_p as shown in Section 2.4.2, an approximation is used based on the SV criterion. Defining the total system value as:

$$\lambda_T = \sum_{k=1}^{K^\star} \lambda_k = \sum_{k=1}^{K^\star} E_k \underline{q}_k^H \mathbf{C}^{-1} \underline{q}_k, \tag{2.47}$$

it has been observed that the total system value is not very much affected by energy allocation, given the total energy $E_T = \sum_{k=1}^{K^\star} E_k$ remains the same. Therefore, for

[3]This is because the received SINR of all spread channels are equalised and the relationship between system values and SINRs is $\lambda_k = \frac{\gamma_k}{1+\gamma_k}$ for $k = 1, \ldots, K^\star$.

ESER scheme where the aim is to achieve equal SINR and hence, equal system values, λ_k for such schemes can be approximated using the following equation:

$$\lambda_k \simeq \frac{\lambda_{T,EE}}{K^\star} = \lambda_{mean} \text{ for } k = 1, \ldots, K^\star \tag{2.48}$$

where λ_{mean} is the mean system value and $\lambda_{T,EE}$ is the total system value for equal energy allocation defined as:

$$\lambda_{T,EE} = \sum_{k=1}^{K^\star} \lambda_{k,EE} = \frac{E_T}{K^\star} \sum_{k=1}^{K^\star} \underline{q}_k^H \mathbf{C}^{-1} \underline{q}_k. \tag{2.49}$$

Thus, λ_{mean} can be used to find the target system value $\lambda_{tar}(b_p)$, the target SINR $\gamma_{tar}(b_p)$ and the optimum b_p for ES allocation by using the following the criterion:

$$\lambda_{tar}(b_p) \leq \lambda_{mean} < \lambda_{tar}\left(b_{p+1}\right). \tag{2.50}$$

Furthermore, the number of spread channels m that can be loaded with rate b_{p+1} can also be found with λ_{mean} by satisfying the following inequality:

$$(K^\star - m)\lambda_{tar}\left(b_p\right) + m\lambda_{tar}\left(b_{p+1}\right) \leq \lambda_{mean} < (K^\star - m - 1)\lambda_{tar}\left(b_p\right) + (m+1)\,\lambda_{tar}\left(b_{p+1}\right). \tag{2.51}$$

Therefore, the total rate for

- ESER allocation scheme: $R_T = K^\star b_p$ and
- ESTG allocation scheme: $R_T = (K^\star - m)b_p + mb_{p+1}$

can be found prior to energy allocation involving only one matrix inversion by using λ_{mean} in Equation (2.48). Then, using the target system value λ_{tar}, the iterative energy allocation is done as before in Section 2.4.2 (page 48) for ESER allocation scheme or Section 2.5.1 (page 50) for ESTG allocation scheme.

In summary, by using the system value approximation in Equation (2.48) to obtain λ_{mean},

- the target system value λ_{tar} and hence

- rates b_p, b_{p+1} and m

can be found before energy calculations. This method decreases the number of matrix inversions required for finding rates and energy allocation from:

- $PI_{\max}$ to $I_{\max}$ for the ESER allocation schemes and
- $(P + K^\star - 1)I_{\max}$ to $I_{\max}$ for the ESTG allocation schemes.

The ESER and ESTG allocations using the system value approach are illustrated in Figures 2.4 and 2.5. It can also be seen that the outer loop of Figures 2.2 (page 49) and 2.3 (page 52) has been eliminated.

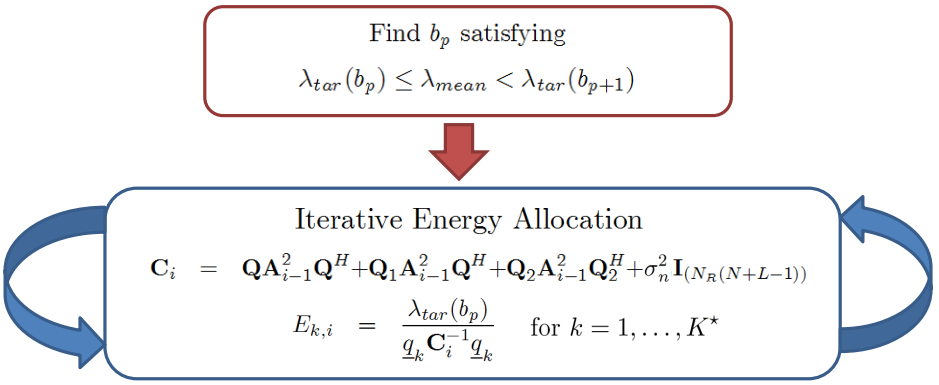


FIGURE 2.4: ESER Algorithm using System Value Approach

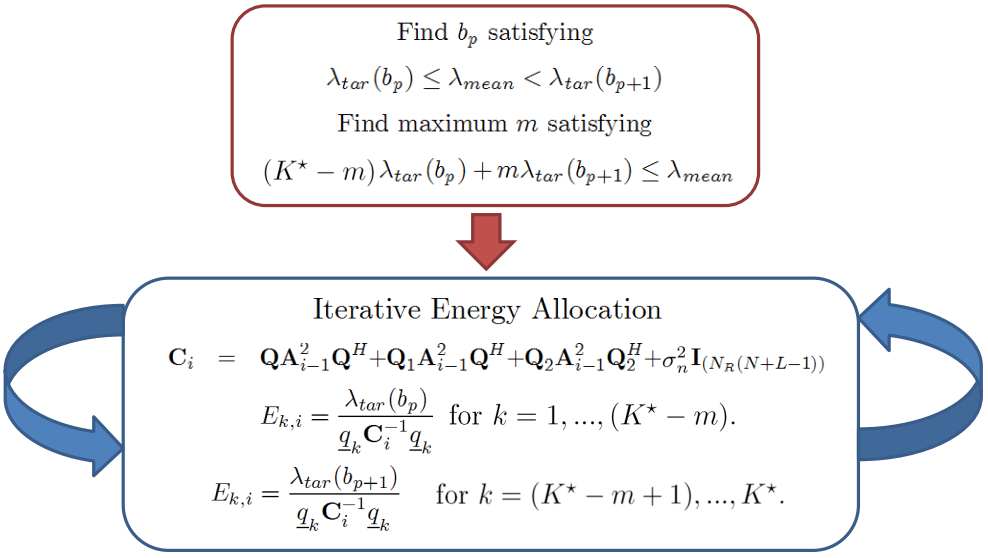


FIGURE 2.5: ESTG Algorithm using System Value Approach

2.7 Evaluation of ES & EE with System Value Approach

The results for this thesis are simulated with the set of discrete rate b_p as shown in Table 2.3, a chip rate of $T_c = 260$ns as defined in the standard and $\Gamma = 0$dB[4]. Additive white Gaussian noise with noise power $\sigma_n^2 = 0.01$ is assumed[5]. The full number of channelisation codes used per MIMO stream is 16, as $K \leq N$ and $N = 16$ as defined in the standard, while the OVSF codes with precoding in [43] are used. Hence, the 2×2 MIMO scheme such as this chapter will have $2N = 32$ available spreading codes. The total rate in bits per second (bps) when sum rate and system throughput are considered is calculated as $\frac{R_T}{T_c N}$ where R_T is the total rate in symbols per second.

The Pedestrian-A and Pedestrian-B channels are used for result evaluations in this thesis. The power delay profile (PDP) of the Pedestrian-A and Pedestrian-B channels are given in [22] at irregular intervals as shown in Table 2.4 and Table 2.5. The channel covariance matrix formulation described in Section 1.3 requires the channel impulse responses at regular sample period (in this case, at period intervals of T_c is used). The steps to convert the PDP from irregular sample periods to chip period intervals are shown in [26] and can be summarised as follows:

[4]In theory, the gap value should be 0dB, however, in practice the $\Gamma \geq 0dB$

[5]As the SNR per received antenna is used as a measurement metric while E_T varies, σ_n^2 can be an arbitrary constant

TABLE 2.3: Set of Discrete Rates b_p, Target SINRs & SVs

b_p	$\gamma^*(b_p)$	$\lambda^*(b_p)$
0.0	0.00	0.0000
0.5	0.41	0.2929
1.0	1.00	0.5000
1.5	1.83	0.6464
2.0	3.00	0.7500
2.5	4.656	0.8232
3.0	7.00	0.8750
3.5	10.31	0.9116
4.0	15.00	0.9375
4.5	21.63	0.9558
5.0	31.00	0.9688
5.5	44.25	0.9779
6.0	63.00	0.9844

TABLE 2.4: Pedestrian-A Power Delay Profile

Excess tap delay (ns)	Relative power (dB)
0	0
110	−9.7
190	−19.2
410	−22.8

TABLE 2.5: Pedestrian-B Power Delay Profile

Excess tap delay (ns)	Relative power (dB)
0	0
20	−0.9
800	−4.9
1200	−8.0
2300	−7.8
3700	−23.9

Steps to Find Normalised PDP in Regular Sampling Period

1. The PDP in Table 2.4 and Table 2.5 can be written as $P(t) = \sum_i P_i \delta(t - \tau_i)$ where P_i is the linear power at delay τi

2. The power of the l^{th} tap $P_{Tc,l}$ is given as the sum of all power in $P(t)$ between time intervals of $t = lT_c - \frac{T_c}{2}$ and $t = lT_c + \frac{T_c}{2}$:
   $P_{Tc,l} = \sum_i P_i$ for $l = \left\lfloor \frac{\tau_i}{T_c} + 0.5 \right\rfloor$.

3. The sample PDP can be written as $P_{T_c}(n) = \sum_{l=0}^{L-1} P_{Tc,l} \delta(n - l)$.

4. The power is then normalised so that the PDP has a unity power gain such that $h_l = \sqrt{\frac{P_{Tc,l}}{\sum_{j=0}^{L-1} P_{T_c,j}}}$ for $l = 0, ..., L-1$.

5. The normalised square root PDP is given as $\underline{h} = [h_0, ..., h_l, ..., h_{L-1}]^T$.

The square root of the sampled PDP for the Pedestrian-A and Pedestrian-B used in this thesis are given as:

- $\underline{h}_{PA} = [0.9923, 0.1034, 0.0683]^T$
- $\underline{h}_{PB} = [0.6369, 0.5742, 0, 0.3623, 0, 0.253, 0, 0, 0, 0.2595, 0, 0, 0, 0, 0.047]^T$

The comparison of EEER (green solid lines), EETG (green dotted lines), ESER (lilac solid lines) and ESTG schemes (purple dotted lines) are shown in Figures 2.6 and 2.7 in terms of system throughput and the system value sum rate (black dotted lines) in Mbps is plotted against the chip SNR per receive antenna as defined in Section 2.2.5. The two-group (TG) allocations are represented by the dotted lines while the equal rate (ER) allocations are represented by normal lines. It is shown that for both Pedestrian-A and Pedestrian-B channels, a total data rate close to its system value sum rate can be achieved through the use of ESTG schemes while the EEER scheme achieve the worst system throughput. For the Pedestrian-A channel as shown in Figure 2.6, the improvement of using ESER scheme over EEER scheme is about 7Mbps at SNR of 20dB, and similar improvements are observed between ESTG scheme and EETG scheme. The total enhancement for EEER scheme to ESTG scheme is about 9Mbps at SNR of 20dB. The use of ESTG scheme is better than ESER scheme by 2 to 3Mbps in

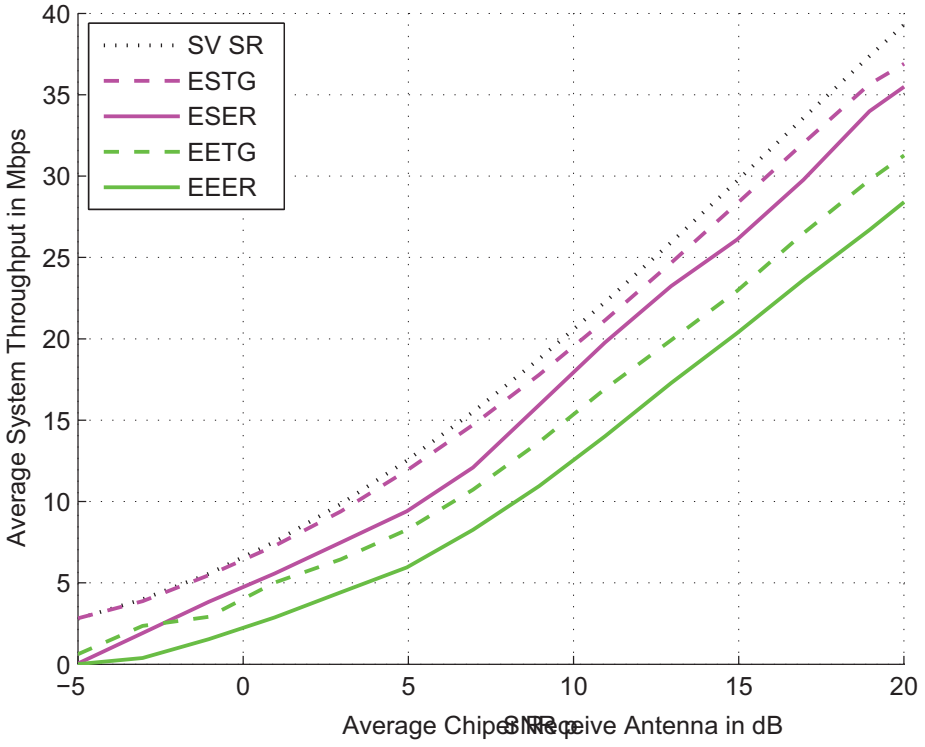


FIGURE 2.6: Comparison of Different Energy Allocation Schemes (Pedestrian-A)

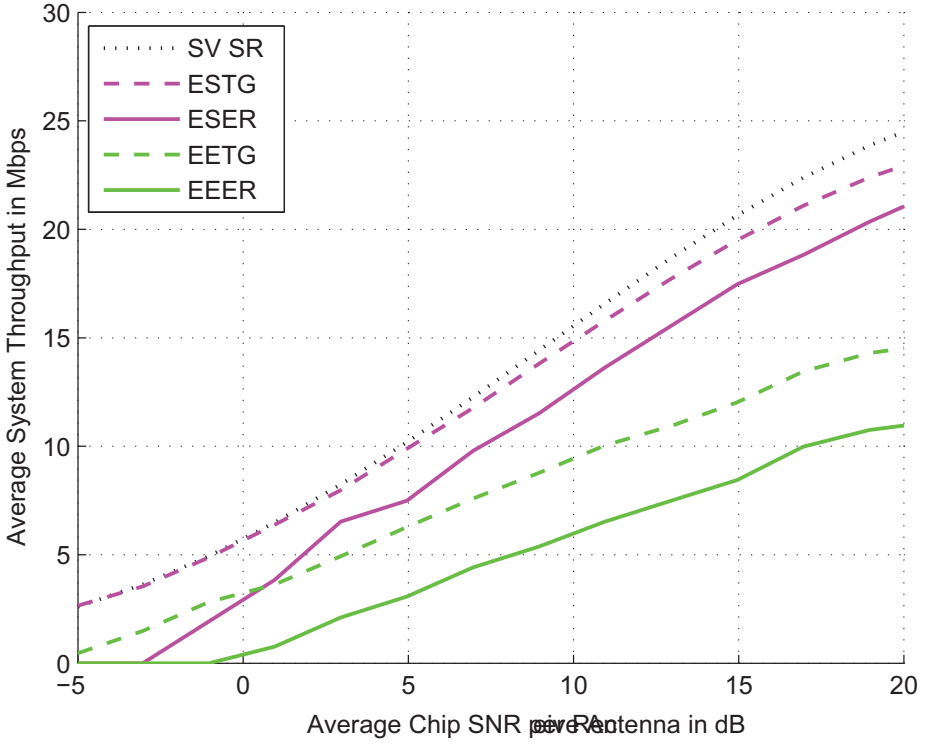


FIGURE 2.7: Comparison of Different Energy Allocation Schemes over (Pedestrian-B)

most SNR regions while a 3Mbps improvement is observed when using EETG scheme instead of EEER scheme. The different allocation schemes for the Pedestrian-B channel are illustrated in Figure 2.7. The use of ES allocations has a much higher system throughput compared to EE allocations where the system throughput seems to saturate at high SNR values. The EEER scheme and EETG scheme curves saturate to 11Mbps and 15Mbps at receive SNR of 20dB respectively; while the ESER scheme and ESTG scheme achieve around 21 and 23Mbps respectively at receive SNR of 20dB. For the Pedestrian-B channel, the improvement from using ESTG scheme compared to ESER scheme is about 3.5Mbps, and a 6 to 7 Mbps enhancement is observed when using EETG scheme instead of EEER scheme for most SNR regions. This shows that the use of EETG scheme instead of EEER scheme can bring much improvement in channels with a long power delay profile without too much complexity.

To justify if the system value approach is a good approximation to find b_p and m, the energy difference is compared in Figure 2.8. The energy difference ratio is calculated as:

$$E_{ratio} = \frac{E_T - \sum_{k=1}^{K^\star} E_k}{E_T}. \tag{2.52}$$

Ideally, the energy difference should be 0 because we would like to use up all available energy to increase the system throughput. From Figure 2.8, it can be seen that the ESER allocation using SV approach will not exceed the total amount of energy, while the energy difference ratio of ESTG allocation fluctuates around the zero line. The reason why energy difference ratio is 1 at SNR=$-$5dB for ESER approach is because there were not enough energy to load any data (even the lowest data rate) into all the spreading codes. Therefore, the sum energy is zero. This shows that the use of system value is a very good approximation to finding the b_p and m without incurring the extra computational complexity in the constraint optimisation approach.

Finally, Table 2.6 shows the comparison of computational complexity in terms of number of matrix inversions for different optimisation schemes including the traditional ESER and ESTG constraint optimisation, the simplified system value ESER and ESTG, as well as the EEER and EETG approaches. The least computational intensive approaches are EEER and EETG approach, while the constraint optimisation

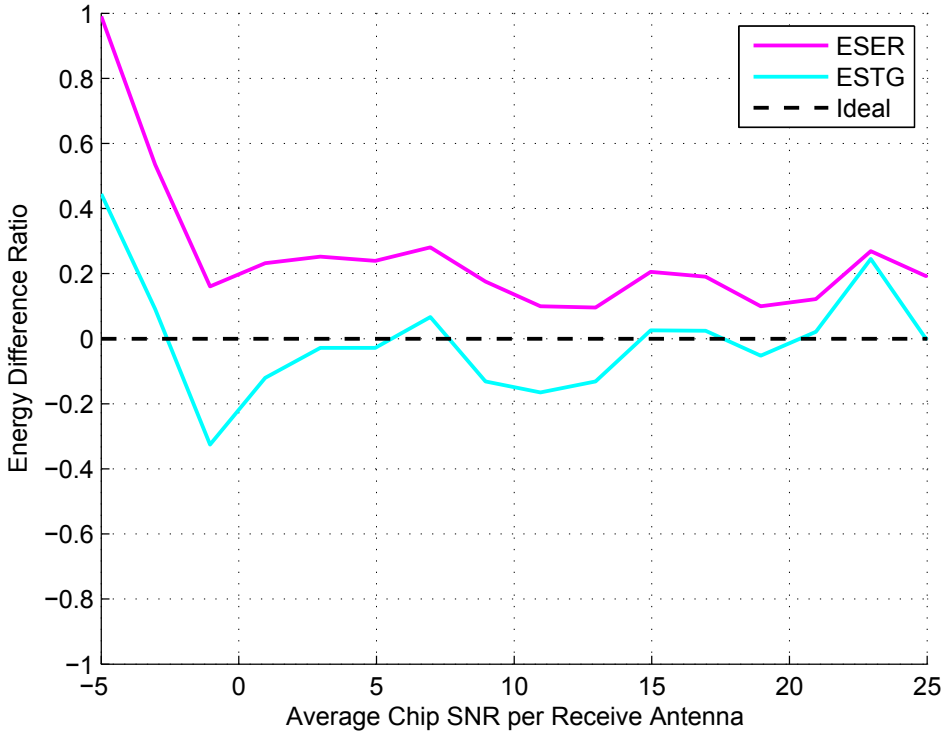


FIGURE 2.8: Energy Difference Ratio of ESER and ESTG (Pedestrian-A)

approach for the ESER and especially ESTG are too computationally expensive for it to be practical. The development of system value approach reduces number of matrix inversions required by roughly P or $P + K^\star - 1$ times, making the ESER and ESTG approach more implementable in practice.

TABLE 2.6: Computational Complexity for Different Schemes

Optimisation	no. of $\mathbf{C}^{-1}$ to find rates	no. of $\mathbf{C}^{-1}$ to find rates and energy
Traditional ESER	$PI_{\max}$	$PI_{\max}$
Traditional ESTG	$(P + K^\star - 1)I_{\max}$	$(P + K^\star - 1)I_{\max}$
SV ES	1	$I_{\max} + 1$
SV TG	1	$I_{\max} + 1$
EEER	1	1
EETG	1	1

2.8 Summary

In this chapter, the traditional way to maximise the total data rate with the specified signature sequence set and the MMSE receiver by using the ESER and ESTG approach is shown. The system throughputs for the ESER, ESTG and EEER, EETG are analysed. It is shown that the system throughput of ESTG scheme achieves close to the system value sum rate and that ES schemes have a much higher throughput than the EE schemes. However, the search for the rate b_p and energy allocation is rather computationally expensive, requiring a total of:

- $PI_{\max}$ matrix inversions for the ESER allocation scheme and
- $(P + K^{\star} - 1)\, I_{\max}$ matrix inversions for ESTG allocation scheme.

Hence, the *system value* (SV) approach was proposed to simplify the constraint optimisation approach by finding the rate b_p and m prior to energy allocation. By using the SV approach, the b_p, b_{p+1} and m can be found with only 1 covariance matrix inversion, and a further $I_{\max}$ matrix inversion for finding energy allocation for both SV based ERES and ESTG allocation. In other words, the proposed method reduces the number of matrix inversions by P and $(P + K^{\star} - 1)$ times compared to the constraint optimisation approach.

So far, the use of power allocation, a transmitter optimisation strategy to increase the system throughput has been discussed in this chapter. In the next chapter, ways to further increase the system throughput using a more optimised receiver will be introduced.

Chapter 3

A Novel SIC-based "System Value" Receiver

In the previous chapter, the use of energy allocation with the *System Value* (SV) optimisation criterion was proposed to improve the system throughput while keeping the system practical for implementation. This optimisation was carried using the symbol-level MMSE receiver which partially restores the orthogonality between the received spreading codes. In this chapter, an MMSE based Successive Interference Cancellation (SIC) receiver formation is proposed and is integrated with the system value approach for the ES and EE allocation schemes. This receiver is simpler than the equivalent receiver proposed in [24] and provide a complexity reduction during the iterative energy allocation process and furthermore, enhances the sum rate and system throughput. Moreover, the proposed SIC algorithms are tested in both MATLAB simulations and experimental measurements using the National Instruments (NI)-PXIe testbed system. It is shown that both simulations and experimental results agree and that the use of SIC receiver has significant improvements in terms of system throughput and sum rate. Additionally, it is observed that the integration of the SIC receiver in the HSDPA system achieves a sum rate close to the more ISI resilient LTE scheme [53] with an MMSE receiver.

3.1 Interference Cancellation Receivers Overview

The aim of interference cancellation receivers is to use the detected data streams to cancel the interference in the received signal so as to reduce the overall interference and increase the system throughput. There are two main types of interference cancellation receivers: SIC and Parallel Interference Cancellation (PIC). Normally, SIC cancels interference in an ordered and successive manner across the MIMO streams or spreading codes, starting from the streams or codes that have higher SINRs to reduce error propagation in detection [54]. On the other hand, PIC receivers such as [55–57] simultaneously process all signals and perform cancellation after all the signals are decoded independently which introduce less delays compared to SIC receivers [58,59]. In [59], the complexity of PIC has been analysed. Denoting n_p as the number of cancellation stages required for PIC, it has been analysed that the PIC is n_p times the complexity of the SIC. Since this thesis is concered with reducing complexity, the SIC receiver is considered in this chapter.

The SIC can be combined with different receivers such as the RAKE receiver in [60,61] and MMSE [62]. Receivers in [58,62] perform interference cancellation with MMSE receiver to improve the system sum rate by mitigating intracell interference. However, there is a need to perform a matrix inversion per energy update during iterative energy calculation when implemented with the ES allocation schemes. The receiver in [63] employs Cayley-Hamilton theorem which uses polynomial expansion to solve the complexity of the matrix inversion process. In this chapter, the proposed SIC receiver simplifies the matrix inversions by forming each matrix inverse as a function of the matrix inverse of the previously detected signals. This decreases the complexity especially during iterative energy allocation as well as calculation of the system values. Unlike the chip-level SIC receiver that only cancels inter-stream interferences between MIMO streams [64], where MMSE equalisation and interference cancellation is performed prior to despreading; the symbol-level SIC proposed in this chapter integrates equalisation and despreading. In other words, the interference cancellation process is carried out for each spreading sequence leading to spatial temporal interference cancellation including both inter-stream and inter-code interference. In the next section, the SIC receiver

model will be described. Then, the integration of SIC receiver with ES allocation is discussed. Following that, the proposed simplified covariance matrix inverse formation is introduced and the EEER, EETG as well as ESER and ESTG for the simplified SIC approach is described. Afterwards, an evaluation of the proposed SIC receiver in terms of system value sum rate as well as system throughput for ES and EE schemes are carried out. Before ending this chapter, the SIC formation is tested under experimental conditions based on the NI-PXIe testbed system. It is shown that the simulation results and experimental results agree. Furthermore, a comparative study is carried out for the HSDPA system with SIC receiver and the more ISI resilient LTE scheme [53] in terms of sum rate.

3.2 The System Model for the SIC receiver

The system model of the MMSE SIC receiver is shown in Figure 3.1. The transmitter model remains the same as Section 2.2 in Chapter 2 (page 35).

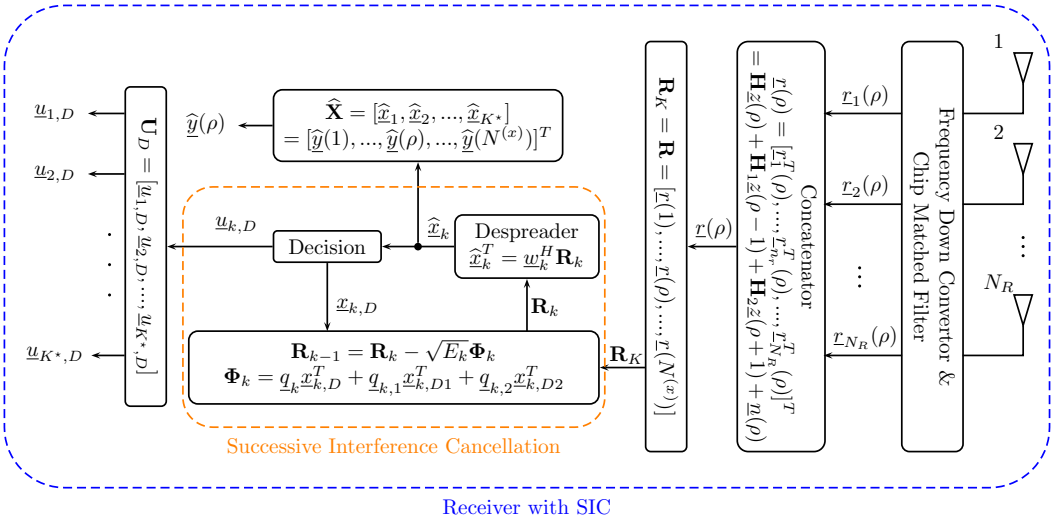


FIGURE 3.1: SIC Receiver for the HSDPA System

This receiver is applicable to both SISO and MIMO configurations and cancels detected signal per spreading code basis. Therefore, channel ordering (ordering of signature sequences) is required for the SIC receiver so that the spread channels under better conditions (those with the stronger SINR or higher channel gain) will be detected and canceled first. Initially, all the received signals from all antennas and all symbols

in the packet are collected at the receiver to produce a received matrix:

$$\mathbf{R} = \left[\underline{r}(1), ..., \underline{r}(\rho), ..., \underline{r}(N^{(x)})\right] \in \mathbb{C}^{(N_R(N+L-1))\times N^{(x)}}. \tag{3.1}$$

Starting from spread channel $K^\star$, where $\mathbf{R}_{K^\star} = \mathbf{R}$, the receiver iteratively cancels the received signal from each spread channel to form $\mathbf{R}_{k-1}$ using the following equation:

$$\mathbf{R}_{k-1} = \mathbf{R}_k - \sqrt{E_k}\mathbf{\Phi}_k \in \mathbb{C}^{(N_R(N+L-1))\times N^{(x)}} \tag{3.2}$$

where

$$\mathbf{\Phi}_k = \underline{q}_k \underline{x}_{k,D}^T + \underline{q}_{k,1}\underline{x}_{k,D1}^T + \underline{q}_{k,2}\underline{x}_{k,D2}^T \in \mathbb{C}^{(N_R(N+L-1))\times N^{(x)}}. \tag{3.3}$$

The vectors $\underline{q}_k$,$\underline{q}_{k,1}$ and $\underline{q}_{k,2}$ are defined in Equation (2.11) to Equation (2.13). The vector $\underline{x}_{k,D}$ is the decision taken after despreading the symbol $\underline{\hat{x}}_k$ (see Equation (2.19) in page 41). When signals are detected in a spread channel by spread channel basis, $\underline{\hat{x}}_k$ can be found by rewriting Equation (2.18) into the following form:

$$\underline{\hat{x}}_k^T = \underline{w}_k^H \mathbf{R} \in \mathbb{C}^{1\times N^{(x)}} \tag{3.4}$$

The vectors $\underline{x}_{k,D1}$ and $\underline{x}_{k,D2}$ are the previous and next symbol period of $\underline{x}_{k,D}$ formed by using $\mathbf{J}_{N^{(x)}} \in \mathbb{C}^{N^{(x)}\times N^{(x)}}$ matrix in Equation (1.7), such that

$$\underline{x}_{k,D1} = \mathbf{J}_{N^{(x)}}\underline{x}_{k,D} \in \mathbb{C}^{N^{(x)}\times 1}, \tag{3.5}$$

$$\underline{x}_{k,D2} = \mathbf{J}_{N^{(x)}}^T\underline{x}_{k,D} \in \mathbb{C}^{N^{(x)}\times 1}. \tag{3.6}$$

After each decision of $\underline{x}_{k,D}$, the symbol stream will be converted to bit stream $\underline{u}_{k,D}$. This iterative cancellation process will continue until $k = 1$.

As shown in Equation (3.2) and Equation (3.4), this SIC receiver minimises both MSE and cancels the detected signal spreading code by spreading code basis. When MSE is minimised, the relationship between system value, MSE and SINR in Equation (2.22) still holds. In the next section, the SIC using SV approach is described.

3.3 SV Approach with the SIC Receiver

The SV approach proposed in Chapter 2 can also be integrated with the SIC receiver. For the SIC receiver, since the detected symbols of the corresponding signature sequence are subtracted from the receive matrix, a different covariance matrix $\mathbf{C}_k$ is required for each cancellation process from $k = K^\star$ to $k = 1$. The system value for the SIC can be written as

$$\lambda_k = E_k \underline{q}_k^H \mathbf{C}_k^{-1} \underline{q}_k. \tag{3.7}$$

The $\mathbf{C}_k$ can be found by firstly initialising $\mathbf{C}_0 = \sigma_n^2 \mathbf{I}_{(N_R(N+L-1))}$, then calculate $\mathbf{C}_k$ using the following equation:

$$\begin{aligned} \mathbf{C}_k &= E_k \underline{q}_k \underline{q}_k^H + E_k \underline{q}_{k,1} \underline{q}_{k,1}^H + E_k \underline{q}_{k,2} \underline{q}_{k,2}^H + \mathbf{C}_{k-1} & (3.8) \\ &= \mathbf{D}_k + E_k \underline{q}_k \underline{q}_k^H & (3.9) \end{aligned}$$

where

$$\mathbf{D}_k = E_k \underline{q}_{k,1} \underline{q}_{k,1}^H + E_k \underline{q}_{k,2} \underline{q}_{k,2}^H + \mathbf{C}_{k-1} \tag{3.10}$$

until $k = K^\star$ is reached.

With the formulation of $\mathbf{C}_k$ as shown above and the λ_k in Equation (3.7), the minimum system value $\lambda_{\min}$, the system value sum rate C_T in Equation (2.35) and λ_{mean} in Equation (2.48) can be found easily. Because each λ_k calculation requries one matrix inversion on $\mathbf{C}_k$, the parameters C_T, λ_{mean} and hence b_p, m and R_T for EE and ES approaches are only found after $K^\star$ matrix inversions. When considering iterative energy calculation, the process becomes more complicated. According to [24], the iterative energy calculation for the i^{th} iteration can be done using the following equation:

$$E_{k,i} = \frac{\gamma_{tar,k}}{\underline{q}_k^H \mathbf{D}_{k,i}^{-1} \underline{q}_k} \tag{3.11}$$

where $\gamma_{tar,k}$ is the target SINR for the k^{th} spread channel, which is either a function of b_p or b_{p+1} depending whether ESER or ESTG is used. As shown in Equation (3.10), the matrix $\mathbf{D}_k$ is a function of E_k. This means that $\mathbf{D}_{k,i}$ is a function of $E_{k,i-1}$ during iterative energy allocation. Hence, there needs to be $I_{\max}$ matrix inversions of $\mathbf{D}_{k,i}^{-1}$

for each k^{th} signature sequence during the iterative energy updates, where $I_{\max}$ is the number of iterations required during the ES energy allocation process as defined in Chapter 2. Thus, when SIC receiver is used together with the system value approach for ES allocations, $K^{\star}I_{\max} + K^{\star}$ matrices inversions are required. This is because:

- $K^{\star}$ matrix inversions are required to find the system values λ_k for $k = 1, ..., K^{\star}$ and a further
- $K^{\star}I_{\max}$ matrix inversions are needed for the whole iterative energy adjustment process for all signature sequences.

On the other hand, if traditional constraint optimisation approach (non-SV based approach) is used for SIC receiver, $K^{\star}PI_{\max}$ and $K^{\star}\left(P + K - 1\right)I_{\max}$ inverses are required for ESER and ESTG allocation respectively. This shows that there is a need to further reduce this complexity especially in ES schemes, which is the aim of this chapter. To achieve this, the following simplifications were considered:

1. The matrix inversion $\mathbf{D}_k^{-1}$ needs to be formed as a function of $\mathbf{C}_{k-1}^{-1}$. Since $\mathbf{C}_{k-1}^{-1}$ is only dependent on $E_{k-1}, \ldots, E_1$, the matrix inverse $\mathbf{C}_{k-1}^{-1}$ remains a constant during the iterative energy process. Hence, only one matrix inversion $\mathbf{D}_k^{-1}(\mathbf{C}_{k-1}^{-1})$ is required per signature sequence, and a total of $K^{\star}$ matrix inversions are required for the whole iterative energy allocation process to be completed.

2. To further decrease the complexity in the iterative energy allocation process and in the system value calculation, the matrix inverse $\mathbf{C}_k^{-1}$ should be formulated as a function of $\mathbf{C}_{k-1}^{-1}$. By doing so, the total number of matrix inversions for forming $\mathbf{C}_k^{-1}$ from $k = 1, \ldots, K^{\star}$ reduces from $K^{\star}$ to 1. Similarly, the total number of matrix inversions of forming $\mathbf{D}_k$ from $k = 1, \ldots, K^{\star}$ is 1. Based on these formulations, the number of matrix inversions during the iterative energy calculation process reduces from $K^{\star}$ to 1. This means that the iterative energy calculation with the SIC receiver is even less complex than the one without SIC in Chapter 2.

The formulations of the simplified $\mathbf{D}_k^{-1}$ and the $\mathbf{C}_k^{-1}$ will be described in the next section, while the proofs of the formulations is shown in Appendix A in page 129.

3.4 Simplification of Covariance Matrix Inversion for SIC

Simplified matrix inversions $\mathbf{D}_k^{-1}$ and $\mathbf{C}_k^{-1}$ for the SIC receiver is proposed in this section. The simplification is done by performing the matrix inversion lemma on $\mathbf{D}_k$ and $\mathbf{C}_k$ respectively, where the proofs are given in Appendix A. In contrast to the previous chapter, no approximations were used to form the simplified covariance matrix inversion. The matrix inversion $\mathbf{D}_k^{-1}$, covariance matrix inverse $\mathbf{C}_k^{-1}$, along with the calculation system value λ_k and SINR γ_k are described in the Algorithm 5 in page 72.

Defining $\alpha = N_R(N+L-1) > 32$, which is the dimension of matrix $\mathbf{C}_k$, performing matrix inversion on each $\mathbf{C}_k$ for $k = 1, \ldots, K^\star$ will usually require a complexity of $O(\alpha^3)$. In contrast, as shown in Algorithm 5, the biggest complexities in the proposed algorithm are performing matrix-vector products as well as matrix additions where both require computational complexity of $O(\alpha^2)$; while vector-vector products involve computational complexity of $O(\alpha)$. In this algorithm, there are a total of 12 operations that need $O(\alpha^2)$ to perform and 10 operations that need $O(\alpha)$. This shows that the proposed simplified matrix inversion formulation has a reduced amount of complexity compared to the matrix inversion.

In the next two sections, the calculations of the rate(s) b_p (as well as b_{p+1} and m) together with the total rate using the system value approach with the simplified matrix inversion methods for EEER, EETG, ESER and ESTG allocation will be shown. A simplified iterative energy calculation for the ESER and ESTG allocation will also be presented.

Algorithm 5 Simplified Covariance Matrix Inverse Formulation

1: *Initialisation:*
2: Set $\mathbf{C}_0^{-1} = \frac{1}{\sigma_n^2}\mathbf{I}_{N_R(N+L-1)}$ and $k = 1$
3: *Loop:*
4: Calculate the set of distance vectors $\underline{d}$, $\underline{d}_1$ and $\underline{d}_2$

$$\underline{d} = \mathbf{C}_{k-1}^{-1}\underline{q}_k, \tag{3.12a}$$
$$\underline{d}_1 = \mathbf{C}_{k-1}^{-1}\underline{q}_{k,1}, \tag{3.12b}$$
$$\underline{d}_2 = \mathbf{C}_{k-1}^{-1}\underline{q}_{k,2}. \tag{3.12c}$$

5: Find ξ, ξ_1, ξ_2, ξ_3, ξ_4, ξ_5, and ξ_6

$$\xi = \underline{q}_k^H\underline{d}, \quad \xi_1 = \underline{q}_{k,1}^H\underline{d}_1, \quad \xi_2 = \underline{q}_{k,2}^H\underline{d}_2, \tag{3.13a}$$
$$\xi_3 = \underline{q}_k^H\underline{d}_1, \quad \xi_4 = \underline{q}_k^H\underline{d}_2, \quad \xi_5 = \underline{q}_{k,1}^H\underline{d}_2, \quad \xi_6 = \mathrm{Re}\left(\xi_3\xi_4^*\xi_5\right). \tag{3.13b}$$

6: Obtain $\mathbf{Z}_1$, $\mathbf{Z}_2$ and $\mathbf{Z}_3$

$$\mathbf{Z}_1 = \underline{d}_1\,\underline{d}_1^H, \quad \mathbf{Z}_2 = \underline{d}_2\,\underline{d}_2^H, \quad \mathbf{Z}_3 = \underline{d}_1\,\underline{d}_2^H. \tag{3.14}$$

7: Calculate ζ_1 and ζ_2

$$\zeta_1 = \frac{E_k}{1 + E_k\,\xi_1}, \quad \zeta_2 = \frac{E_k}{1 + E_k\,\left(\,\xi_2 - \zeta_1\,|\xi_5|^2\,\right)}. \tag{3.15}$$

8: Form

$$\begin{aligned}\mathbf{D}_k^{-1} &= \mathbf{C}_{k-1}^{-1} - \left(\zeta_1^2\zeta_2\,|\xi_5|^2 + \zeta_1\right)\mathbf{Z}_1 \\ &\quad - \zeta_2\mathbf{Z}_2 + \zeta_1\zeta_2\left(\xi_5\,\mathbf{Z}_3 + \xi_5^*\,\mathbf{Z}_3^H\right).\end{aligned} \tag{3.16}$$

9: Calculate $\underline{d}_3$, $\mathbf{Z}_4$ and ζ as follows:

$$\underline{d}_3 = \mathbf{D}_k^{-1}\underline{q}_k, \tag{3.17}$$
$$\mathbf{Z}_4 = \underline{d}_3\underline{d}_3^H, \tag{3.18}$$

$$\zeta = \frac{E_k}{1 + E_k\left(\xi - \zeta_1\,|\xi_3|^2 - \;\zeta_2\left(\;|\xi_4|^2 - 2\zeta_1\xi_6 + \;\zeta_1^2|\xi_5|^2\;\;|\xi_3|^2\right)\;\right)}. \tag{3.19}$$

10: The covariance inverse $\mathbf{C}_k^{-1}$ can be found by performing

$$\mathbf{C}_k^{-1} = \mathbf{D}_k^{-1} - \zeta\mathbf{Z}_4. \tag{3.20}$$

11: The system value λ_k and the SINR γ_k can be obtained from

$$\lambda_k = E_k\underline{q}_k^H\mathbf{C}_k^{-1}\underline{q}_k, \tag{3.21}$$
$$\gamma_k = E_k\underline{q}_k^H\mathbf{D}_k^{-1}\underline{q}_k. \tag{3.22}$$

12: Repeat steps 2 to 9 until $k = K^\star$ is reached.

3.5 EEER Approach with the Simplified SIC Receiver

The EEER for the MMSE receiver has been described in Section 2.4.1 in Chapter 2 (page 48). Similarly, it is possible to use the SIC receiver for the EEER approach by using the SINR calculation in Equation (3.22) and the simplified covariance matrix inversion method as proposed in Section 3.4. The steps for the simplified EEER approach for the SIC receiver are described in Algorithm 6.

Algorithm 6 EEER Allocation with SIC Receiver

1: Allocate energy equally for all spreading codes $E_k = \frac{E_T}{K^\star}$ for $k = 1, ..., K^\star$
2: Calculate $\mathbf{Q}$, $\mathbf{Q}_1$ and $\mathbf{Q}_2$ as in Equation (2.11) to Equation (2.13)
3: Initialize $\mathbf{C}_0^{-1} = \frac{1}{\sigma_n^2}\mathbf{I}_{N_R(N+L-1)}$
4: **for** $k = 1$ to $k = K^\star$ **do**
5: Form $\mathbf{C}_k$ using Equation (3.12) to Equation (3.20)
6: Calculate λ_k and γ_k as shown in Equation (3.21) and Equation (3.22)
7: Form $\underline{\gamma} = [\gamma_1, ..., \gamma_k, ..., \gamma_{K^\star}]$ and identify its minimum element
8: Estimate the corresponding b_p using Table 2.3 or

$$b_p = \log_2\left(\frac{\gamma_{tar}}{\Gamma} + 1\right) \tag{3.23}$$

which is based on Equation (2.36)

The total rate for EEER allocation for the SIC receiver will be $R_T = K^\star b_p$. The EETG for SIC can be done the same way as the non-SIC scheme, by loading $\gamma_k \geq \gamma_{tar}(b_{p+1})$ with rate b_{p+1} to achieve $R_T = (K^\star - m)b_p + mb_{p+1}$.

3.6 ES Approaches with the Simplified SIC Receiver

The system value approach proposed in Chapter 2 can also be used to find b_p (as well as b_{p+1} and m) for the ESER (or ESTG) optimisation by using $\mathbf{C}_k^{-1}$ formation instead of $\mathbf{C}^{-1}$. The parameter $\mathbf{C}_k^{-1}$ can be obtained by using the simplified covariance matrix inversion method proposed in Section 3.4 (page 71). The way to obtain b_p, b_{p+1} and m for the SIC receiver with ESER and ESTG allocation using the system value approach can be summarised in Algortihm 7.

Algorithm 7 Finding b_p & m for ES Allocations with SIC Receiver

1: Allocate energy equally for all spreading codes $E_k = \frac{E_T}{K^\star}$ for $k = 1, ..., K^\star$
2: Calculate $\mathbf{Q}$, $\mathbf{Q}_1$ and $\mathbf{Q}_2$ as in Equation (2.11) to Equation (2.13)
3: Calculate λ_{mean} using Equation (2.48)
4: Find the b_p and b_{p+1} that satisfy:

$$\lambda_{tar}(b_p) \leq \lambda_{mean} < \lambda_{tar}(b_{p+1}) \tag{3.24}$$

5: The m value is found by using Equation (2.51)

The total rate for ESER and ESTG are $R_T = K^\star b_p$ and $R_T = (K^\star - m)b_p + mb_{p+1}$ respectively. The iterative energy allocation process as a function of the simplified covariance matrix inverse will be described next.

3.6.1 Iterative Energy Calculation for SIC

The formation of the simplified matrix inversion proposed in Section 3.4 decreases the number of matrix inversions required to calculate the system value in Equation (3.7) for the SIC receiver from $K^\star$ to 1. In addition, the simplified matrix inversion can also be applied to the iterative energy adjustment process which greatly reduces the complexity. With $\gamma_{tar,k}$ (see Equation (2.36)) defined as the target SINR of the k^{th} spread channel which is either a function of b_p or b_{p+1}, the simplified matrix inverse described in the previous section can be used to reduce the complexity in calculating energy allocations. Therefore, the energy iteration in Equation (3.16) can be further simplified (for proof see Appendix A, page 129) to

$$E_{k,i} = \frac{\gamma_{tar,k}}{\xi - \zeta_{1,(i-1)} |\xi_3|^2 - \zeta_{2,(i-1)} \left(|\xi_4|^2 - 2\zeta_{1,(i-1)}\xi_6 + \zeta_{1,(i-1)}^2 |\xi_5|^2 |\xi_3|^2 \right)}. \tag{3.25}$$

With this simplification, during the iterative energy adjustment process, the only part that requires iterative adjustments are ζ_1 and ζ_2 in Equation (3.15) and E_k in Equation (3.25). Therefore, the total number of matrix inversions required during the iterative energy adjustment process decreases from $K^\star I_{\max}$ to 1. The iterative energy calculation using Equation (3.25) and the simplified matrix inverse formation can be calculated as shown in Algorithm 8.

Algorithm 8 Iterative Energy Allocation Algorithm for SIC Receiver

Initialisation
Set covariance matrix inverse $\mathbf{C}_0^{-1} = \frac{1}{\sigma_n^2}\mathbf{I}_{N_R(N+L-1)}$
Set energy $E_{k,0} = \frac{E_T}{K^\star}$ for $k = 1, ..., K^\star$
Obtain $\mathbf{Q}$,$\mathbf{Q}_1$, and $\mathbf{Q}_2$
Set target SINR $\gamma_{tar,k}$ for each k channels to either $\gamma_{tar}(b_p)$ or $\gamma_{tar}(b_{p+1})$ depending on the allocation scheme
for $k = 1, ..., K^\star$ **do**
    Find $\underline{d}$, $\underline{d}_1$ and $\underline{d}_2$ as in Equation (3.12)
    Find ξ, ξ_1, ξ_2, ξ_3, ξ_4, ξ_5, and ξ_6 in Equation (3.13)
    Calculate $\mathbf{Z}_1$, $\mathbf{Z}_2$ and $\mathbf{Z}_3$ from Equation (3.14)
    Set $i = 1$ and $\varepsilon = 1$
    for $i \leq I_{\max}$ or$\varepsilon = \left|\sum_{k=1}^{K^\star}\left(E_{k,i} - E_{k,(i-1)}\right)\right| < 0.01\%$ **do**
        Calculate $\zeta_{1,(i-1)}$ and $\zeta_{2,(i-1)}$

$$\zeta_{1,(i-1)} = \frac{E_{k,(i-1)}}{1 + E_{k,(i-1)}\xi_1}, \tag{3.26}$$

$$\zeta_{2,(i-1)} = \frac{E_{k,(i-1)}}{1 + E_{k,(i-1)}\left(\xi_2 - \zeta_{1,(i-1)}\left|\xi_5\right|^2\right)}. \tag{3.27}$$

        Calculate energy $E_{k,i}$ using Equation (3.25)
    Find $\zeta_{1,I_{\max}}$ using Equation (3.26)
    Find $\zeta_{2,I_{\max}}$ using Equation (3.27)
    Find ζ from Equation (3.19).
    Calculate $\mathbf{D}_k^{-1}$ from Equation (3.16).
    Find $\underline{d}_3 = \mathbf{D}_k^{-1}\underline{q}_k$ and $\mathbf{Z}_4 = \underline{d}_3\underline{d}_3^H$.

The ESER and ESTG algorithm is illustrated in Figure 3.2.

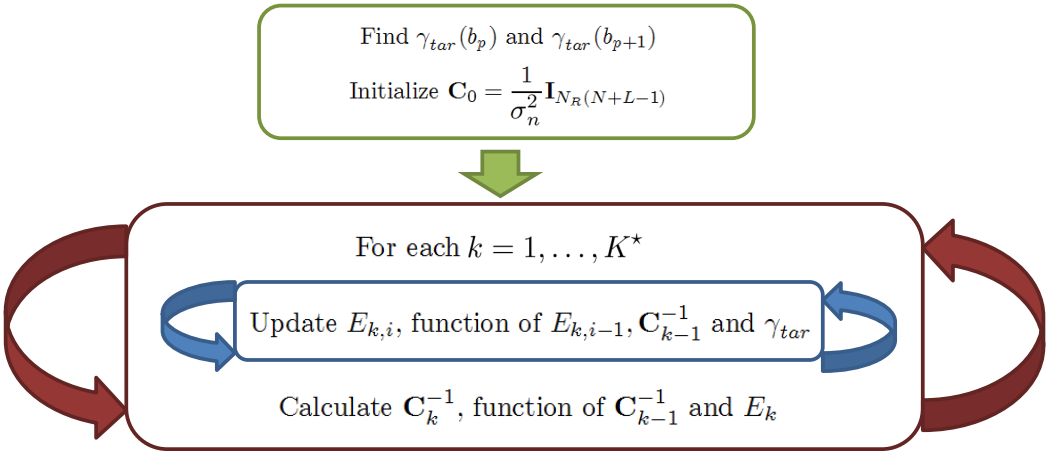


FIGURE 3.2: System Value SIC Algorithm

3.7 Complexity Analysis of the Proposed SIC Schemes

An analysis in terms of complexity for the traditional SIC, the SV SIC and the simplified SV SIC has been presented in Table 3.1. It is shown that the number of matrix inversions required for the whole process of finding rates and energy allocation is

- $K^{\star}PI_{\max}$ using constraint optimisation ESER approach with SIC receiver and
- $K^{\star}(P+K^{\star}-1)I_{\max}$ for ESTG with SIC receiver

which shows the computational complexity is very high. For ESER and ESTG using system value approach without the simplified covariance matrix inversion, the total number of matrix inversions for the SIC system value calculation and iterative energy adjustments is $K^{\star}I_{\max}+K^{\star}$. With the simplification of the covariance matrix inversions, the total number of matrix inversions required is two:

- one for the calculation of the SIC system values and
- one for the whole iterative energy allocation process.

It is also interesting to note that during the iterative energy allocation process, the use of the simplified matrix inversion formation in this chapter for the SIC receiver requires even less computational complexity than the non-SIC receiver in the previous chapter.

TABLE 3.1: Computational Complexity for Different Schemes

Optimisation	No. of matrix inversions to find rates & energies	No. of matrix inversions to find rates
Traditional SIC ESER	$K^{\star}PI_{\max}$	$K^{\star}PI_{\max}$
Traditional SIC ESTG	$K^{\star}(P+K^{\star}-1)I_{\max}$	$K^{\star}(P+K^{\star}-1)I_{\max}$
SV SIC ESER	$K^{\star}I_{\max}+K^{\star}$	$K^{\star}$
SV SIC ESTG	$K^{\star}I_{\max}+K^{\star}$	$K^{\star}$
Simplified SV SIC ESER & ESTG	2	1
Simplified SIC EEER	1	1
Simplified SIC EETG	1	1
Non-SIC SV ESER & ESTG	$I_{\max}+K^{\star}$	$I_{\max}$

3.8 The Performance of SIC Schemes

The SIC and non-SIC receiver under the ESTG and EETG schemes for Pedestrian-A channels and Pedestrian-B channels are shown in Figures 3.3 and 3.4 respectively. The dotted lines in these figures denotes the use of SIC receiver while the normal lines represent the non-SIC receiver. In the same figures, the new system value sum rate curves for SIC receiver using the covariance matrix $\mathbf{C}_k$ instead of $\mathbf{C}$ (black dotted lines) are also presented for both channels. Similar to the non-SIC case, the SIC ESTG scheme achieves system throughput close to the SIC system value sum rate for both Pedestrian-A and Pedestrian-B channels. For the EETG scheme, the use of SIC receiver improves the system throughput close to the more complicated ESTG non-SIC case at high SNR. The use of SIC receiver improves the non-SIC receiver system performance by 5Mbps for the Pedestrian-A channels for both EETG and ESTG schemes at SNR of 20dB. Similarly, improvements of 12Mbps and 9Mbps are observed in ESTG and EETG schemes when using the SIC receiver. This shows that the use of SIC scheme can eliminate a lot of the interference for the Pedestrian-B channel to improve its system throughput performance.

The symbol-level SIC receiver proposed in this chapter which cancels out spatial temporal interference is compared against the chip-level SIC receiver in [64] where only inter-stream interference between the two MIMO streams are canceled as illustrated in Figure 3.5. The detail formulation of this chip-level SIC is also given in Appendix B. In Figure 3.5, it is shown that the symbol-level SIC receiver has a higher SIC sum rate compared to the chip-level one. The improvements in terms of sum rates are 2.5Mbps and 8Mbps at SNR of 20dB for the Pedestrian-A and Pedestrian-B Channels respectively. This shows that it is very important to cancel out the remaining interference in the time domain in addition to space domain especially in a channel with long delay spread.

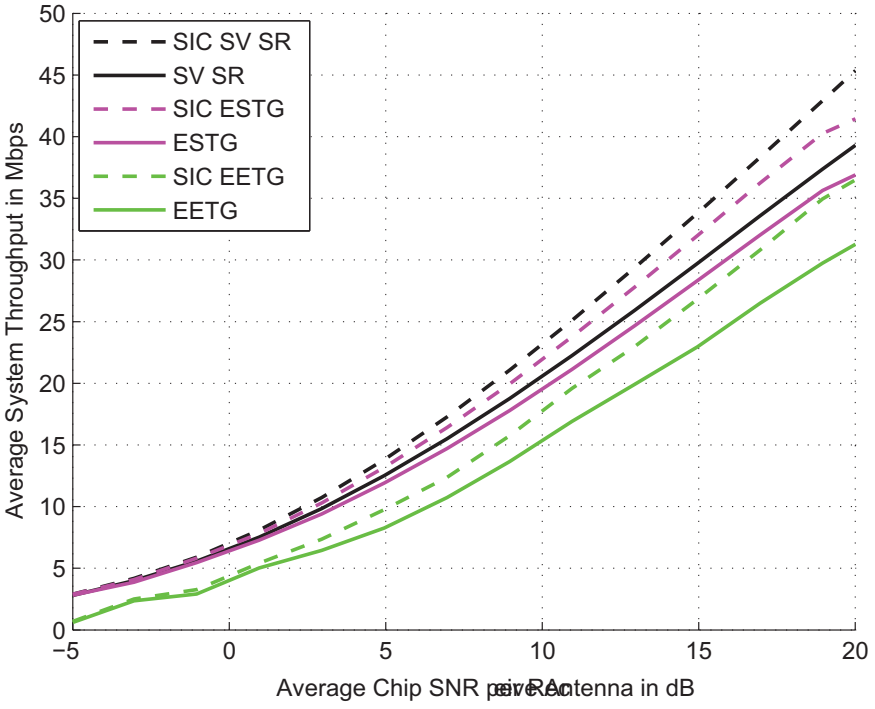


FIGURE 3.3: Comparison of SIC and Non-SIC Schemes (Pedestrian-A)

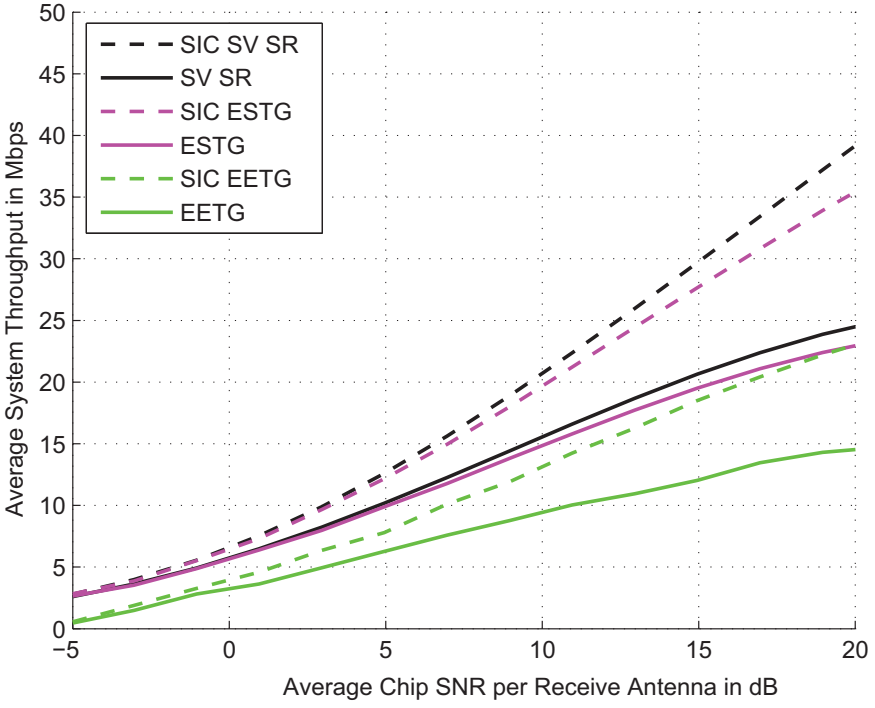


FIGURE 3.4: Comparison of SIC and Non-SIC Schemes (Pedestrian-B)

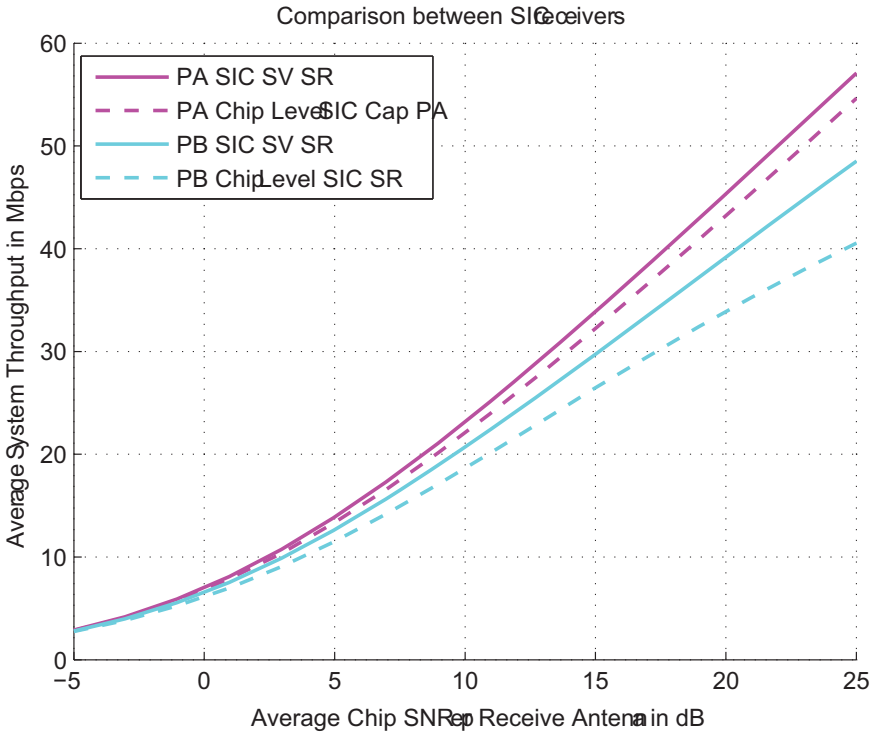


FIGURE 3.5: Comparison of Different SIC Receivers

A simplified SIC receiver that can improve the system throughput while reducing the complexity (in terms of matrix inversions) when calculating the system values and during the energy allocation process for the ES energy allocation process was proposed in this chapter. Experiments can be conducted to further verify the behaviour of algorithms under real-world conditions [65, 66]. Therefore, in this chapter, some experimental results are presented to further verify the validity of the proposed SIC receiver in terms of SV sum rate and EEER allocation.

3.9 Experimental Results

In this section, the experimental results for the proposed SIC receiver using the NI-PXIe platform is compared to the MATLAB simulations to further verify its validity. In our testbed system, the algorithms for the HSDPA transmitter as well as both the MMSE non-SIC and MMSE SIC receivers were transferred/mapped from the MATLAB language to LabVIEW language. During the experiment, signals are sent and received over the radio and the channel is then estimated at the receiver. The LabVIEW SIC algorithm then uses these received signal and channel estimates to perform processing. Should both simulation and MATLAB results agree, it brings us one step closer to the implementation of the SIC in mobile handset.

The experimental setup described in this chapter [67] is based on the NI-PXIe platform, and it operates with the LabVIEW language for both host processing at high-level mode and for controlling the FPGAs with fixed point operation. Other testbeds for HSDPA systems include [68] which is also known as the Vienna testbed. In the Vienna testbed, transmit data blocks are pre-generated in MATLAB. When the signals arrive at the receiver, the received samples are evaluated for synchronisation, channel estimation and feedback purposes. The receive signals are stored in hard disks and the rest of the signal processing are evaluated offline. The results are tested under the "Alpine scenario" and "urban scenario" where the antennas are situated in "Drautal" valley and Vienna city respectively. Although the use of a channel in the real world environment is the most realistic to test the validity of an algorithm, it is often not repeatable especially by other researchers [69, 70]. This is because even with the same

experimental set up, the changes in the surrounding environment will not yield the same channel [70]. The experimental set up in this thesis uses a channel emulator that can emulate different channel environments while allowing transmissions to be carried over the RF path. Resampling is done in real time using FPGAs while channel estimation, different receiver designs (including both MMSE and SIC receivers) and further data processing are carried out in the host for each packet transmission.

3.9.1 NI-PXIe Based Experimental Setup

The experiment conducted in this chapter uses the National Instrument (NI)-PXIe based testbed. This testbedding system contains a modular FPGA with detachable RF front-ends which enable modularity and expandability while enabling physical layer processing via host computer for flexibility. The channel emulator embedded in the system allows the physical layer algorithms to be tested under various realistic channel scenarios while allowing repeatable experiments when the same scenarios in the channel emulator are configured. Real-time channel emulations are carried out using the FPGA based channel emulator with RF front-ends. The hardware platform for the testbedding system consists of an NI-7966 FlexRIO FPGA module and the NI-5791 RF front-end which is installed on the NI-PXIe 1062Q chassis. This platform can be configured to operate for SISO mode and 2×2 MIMO mode.

The testbed consists of the host processing unit and the channel processing unit as illustrated in Figure C.1 of Appendix C. The host processing unit provides flexibility of implementing different wireless standards including the HSDPA and LTE schemes; as well as different receivers including the MMSE receiver and the MMSE-based SIC receiver by using high level LabVIEW programming language. The channel processing unit can be run on a software channel emulator, to verify the results against the ones produced from MATLAB before running on the real-time FPGA based RF channel emulator. The specifications and system parameters for the NI 5791 RF front-end, NI PXIe 7966 FPGA and for the channel emulator can be found in [71–73] which are summarised in Tables 3.2, 3.3 and 3.4 respectively.

TABLE 3.2: Specifications for NI 5791 RF Transceiver Adapter Module

System Parameters	Value
Radio Frequency Range	200MHz to 4.4GHz
RF Bandwidth	100MHz
Maximum Sample Rate	130MS/s
DAC Resolution	16 bits
ADC Resolution	14 bits
RF Power Range	−58dBm to 8dBm
Analogue Input Noise Floor	−162dBm/Hz
Analogue Output Noise Floor	−138dBm/Hz

TABLE 3.3: Specifications for NI 7966R FPGA

System Parameters	Value
DSP FPGA	Virtex-5 SX95T
PC Interface	NI-PXI
Maximum Data Rate / Channel	800MB/s
MIMO Support	Up to 8×8 in real-time

TABLE 3.4: Specifications for the Channel Emulator

System Parameters	Value
Tapped Delay Line Sample Rate	100MHz
Channel Coefficients Interpolation Rate	8192
Channel Coefficients Sample Rate	8100MHz/8192 = 12.207kHz
Maximum No. of Taps per Channel	Up to 36 taps
Delay Resolution	10ns
Delay Range	0 to 20.6μ s

3.9.2 Comparison between Measurements and Simulations

To verify if the algorithms are correctly transferred, the first step was to use the exact same channel impulse responses to see if the results are identical for system value sum rate and equal energy allocation with and without implementing the SIC receiver. After that, the results for the different schemes were run in the software based channel emulator with digital processing and channel estimation in the host were compared and verified. Finally, the schemes were run in the hardware based channel emulator over the RF and with digital signal processing capabilities in the FPGA. Three different channel power delay profiles were used in these tests. In addition to Pedestrian-A and Pedestrian-B channels, the Extended Vehicular-A (EVA) channel specified in TS36.211 [23] were implemented where the PDP is illustrated in Table 3.5.

TABLE 3.5: Extended Vehicular-A Power Delay Profile

Excess tap delay (ns)	Relative power (dB)
0	0
30	−1.5
150	−1.4
310	−3.6
370	−0.6
710	−9.1
1090	−7
1730	−12
2510	−16.9

The experimental results using the NI-PXIe testbed for the Pedestrian-A channel are shown in Figures 3.6 for the system value sum rate (red solid line) and EEER allocation (red dotted line) for the (non-SIC) MMSE receiver; while the system value sum rate (red solid line) and EEER allocation (red dotted line) for the SIC receiver proposed earlier in this chapter are illustrated in Figures 3.7. In the same figures, the experimental results are compared against the MATLAB simulations (green lines) and the simulations over the software channel emulator during the migration process from MATLAB to LabVIEW (blue lines). These figures shows that even under experimental conditions with RF paths, the results for system value sum rates and EEER allocation with and without SIC receiver has similar performance which further proves the validity of the SIC formation proposed in this chapter. Apart from verifying over the Pedestrian-A channel, the experiments were also carried out over the EVA channel and are compared to its MATLAB simulations which shows similar behaviour. These figures are shown in Appendix C.

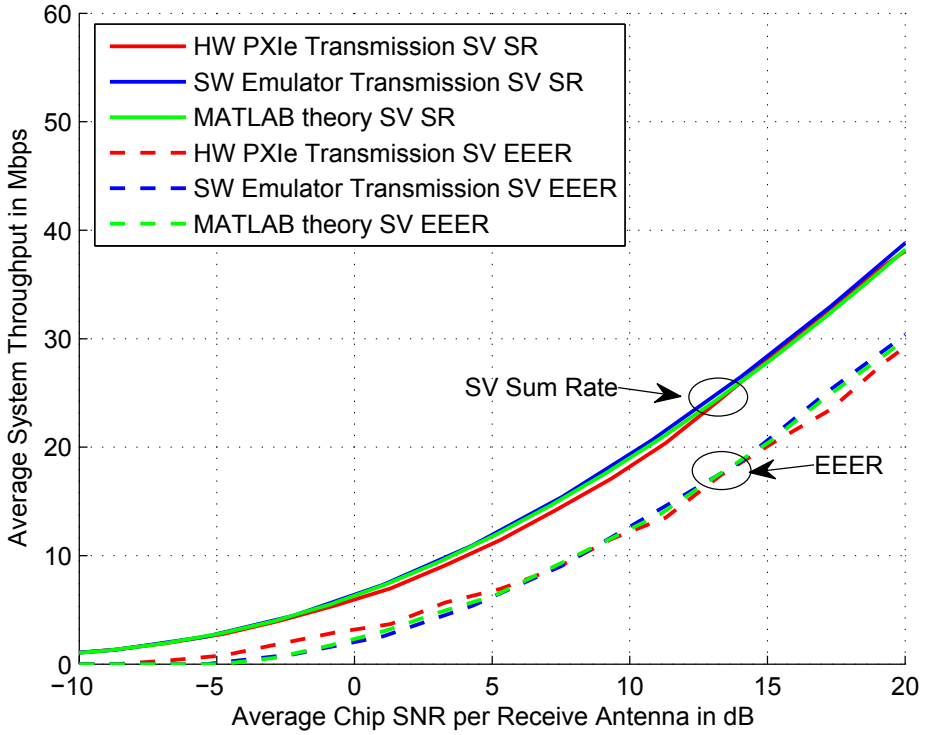


FIGURE 3.6: Simulations & Experiments Comparisons over Pedestrian-A (non-SIC)

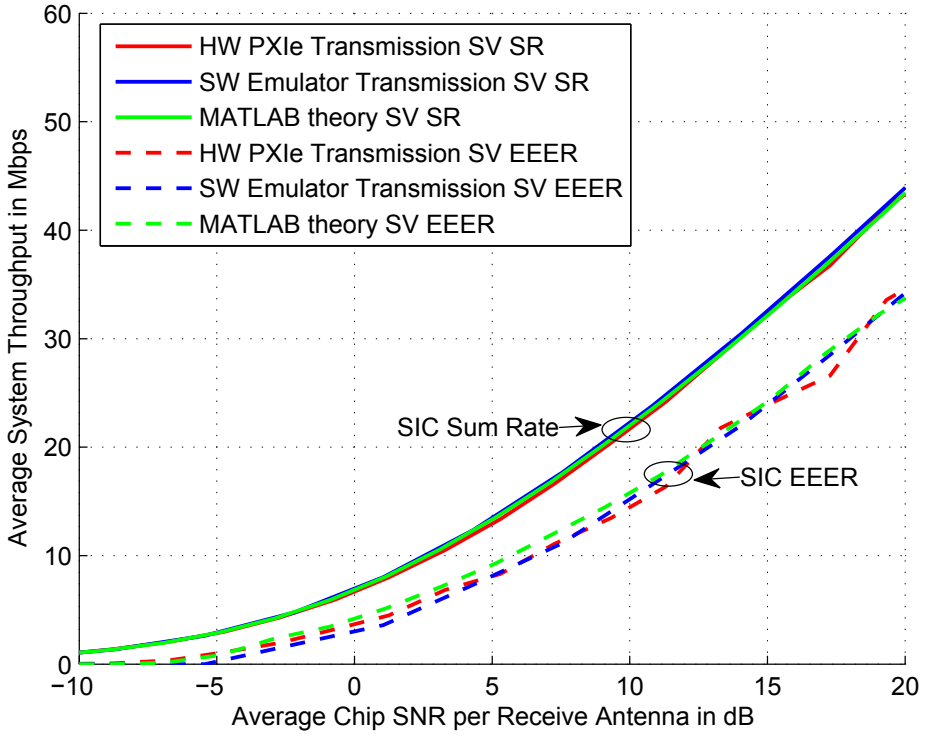


FIGURE 3.7: Simulations & Experiments Comparisons over Pedestrian-A (SIC)

In Figures 3.8, 3.9 and 3.10, comparisons between the EEER with and without SIC receiver (solid lines), system value sum rate with and without SIC receiver (dotted lines) and the LTE sum rate (black dotted lines) carried over the testbed are illustrated for the Pedestrian-A, Pedestrian-B and the EVA channels. For the Pedestrian-A channel, the use of SIC receiver gives a 4Mbps improvement in both EEER system throughput and system value sum rate at SNR of 20dB. When using the proposed SIC on the HSDPA system under the same bandwidth, the sum rate for the HSDPA system is 1.5Mbps lower than the LTE sum rate with MMSE receiver for the Pedestrian-A channel in most SNR regions. For the Pedestrian-B channel, the use of SIC receiver brings 8.5Mbps improvement in the EEER system throughput and 12.5Mbps improvement in terms of sum rate at SNR of 20dB. The HSDPA sum rate with SIC receiver and the LTE sum rate curves diverge at high SNR and the difference is 4.5Mbps at SNR of 20dB. For the EVA channel, the use of SIC improves the EEER system throughput by 7Mbps, and a 9Mbps improvement is observed over the sum rate at SNR of 20dB. By using the SIC receiver in the HSDPA system, the system throughput is only 3Mbps lower than the LTE system with MMSE receiver at SNR of 20dB. This shows that even under the experimental conditions, the SIC receiver proposed in this chapter has significant improvements in terms of system throughput and sum rate in all Pedestrian-A, Pedestrian-B and EVA channel conditions. Furthermore, it is shown that with the use of the SIC receiver over the HSDPA, which is more susceptible to ISI in multipath channels achieves only a slightly lower sum rate than the LTE which uses orthogonal frequency division multiplexing (OFDM) and guard period to deal with ISI, but without the need to change the whole infrastructure.

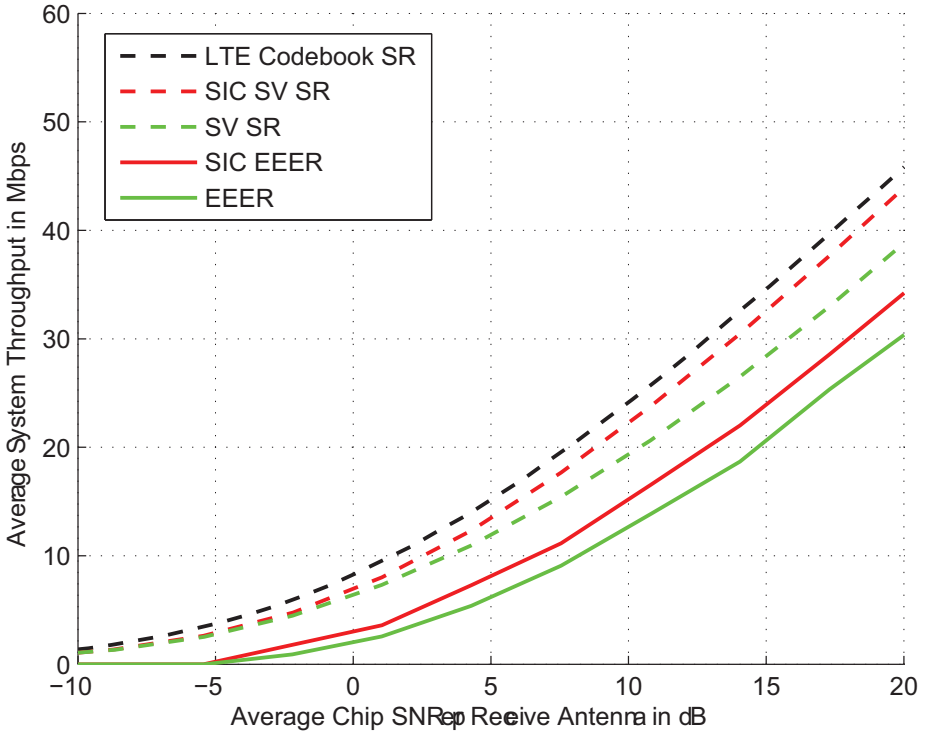


FIGURE 3.8: Comparison of Different Schemes over the Testbed (Pedestrian-A)

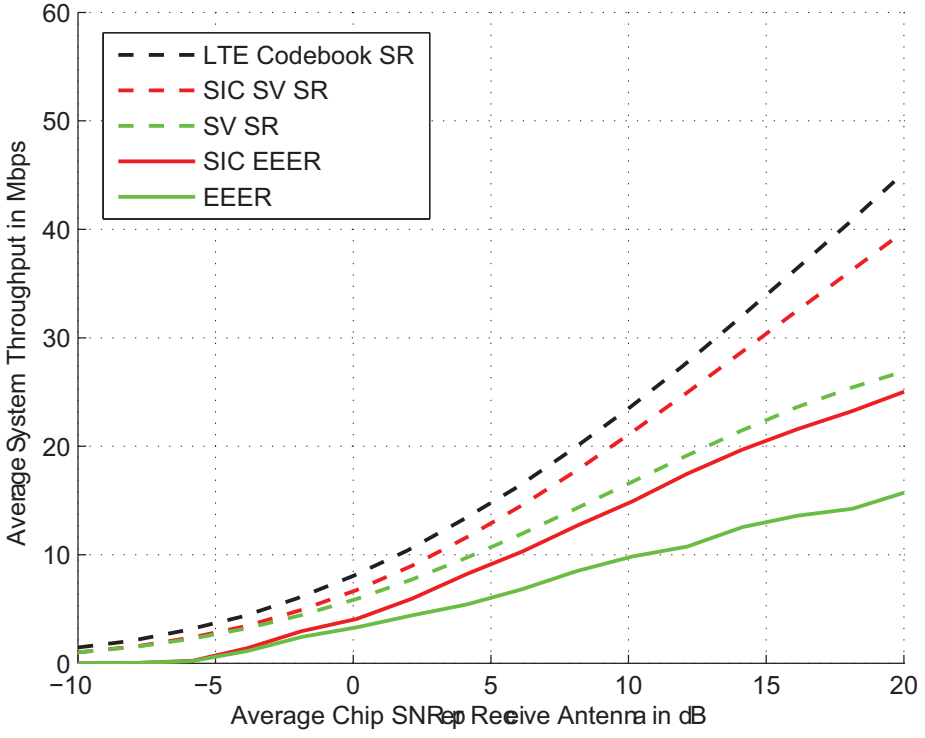


FIGURE 3.9: Different Schemes over Testbed for (Pedestrian-B)

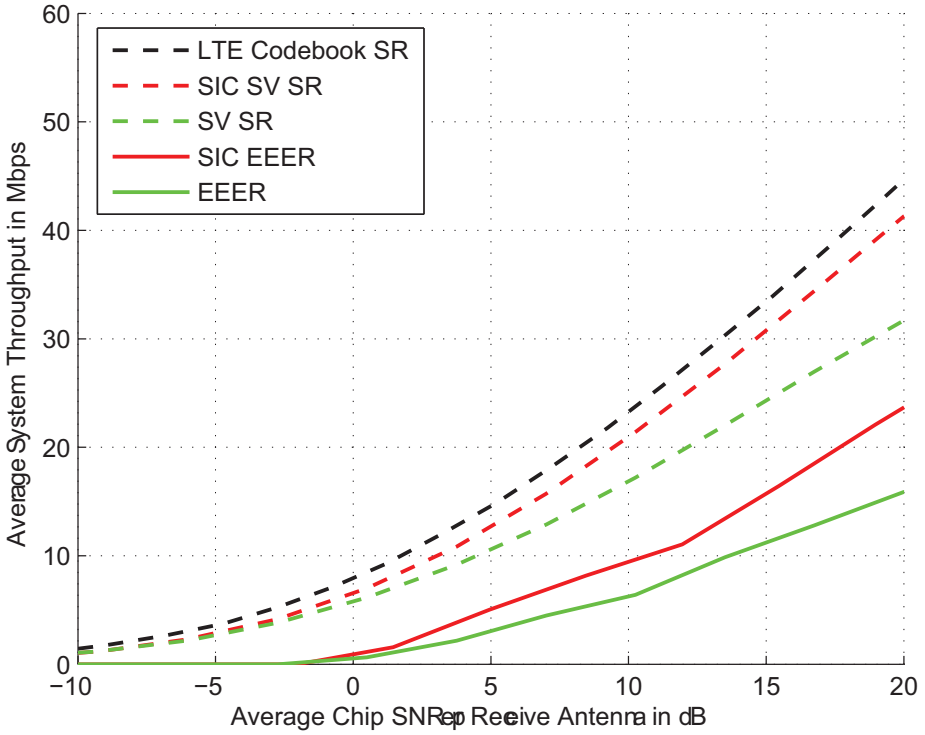


FIGURE 3.10: Comparison of Different Schemes over Testbed for (EVA)

3.10 Summary

In this chapter, a new complexity reduced SIC receiver is proposed. This receiver can be integrated with the SV approach proposed in the previous chapter to further increase the system throughput while reducing the complexity during the iterative energy adjustment process for the ES allocation schemes. Unlike the SIC receiver proposed in [24] which requires:

- $K^{\star}PI_{\max}$ for the ESER SIC scheme and
- $K^{\star}\left(P+K-1\right)I_{\max}$ matrix inversions for ESTG SIC scheme.

By using the proposed simplified SIC formation with SV approach, the total number of matrix inversion for the whole process reduces to two, where:

- one matrix inversion is required for the system values calculations and a further

- one matrix inversion is required for the iterative energy calculation process.

Furthermore, it is observed that the proposed SIC receiver significantly improves the system throughput especially for the Pedestrian-B channels but without much additional complexity. Finally, the proposed SIC receiver has been examined using the testbed system over the RF where it is shown that the behaviour is the same as the the simulations. On top of that, it has been analysed that the sum rate improvements using the SIC over the HSDPA system is very close to the sum rate in the more ISI resilient LTE sum rate with MMSE receiver.

Chapter 4

Signature Sequence Optimisation and Feedback Analysis

In Chapter 2, a transmitter optimisation strategy based on the use of power allocation has been studied. In this chapter, this transmitter optimisation strategy is further exploited using signature sequences. Given full Channel State Information (CSI) is available at the transmitter, a signature sequence design is proposed in this chapter to minimise the correlations between spreading codes while reducing both Inter-Symbol Interference (ISI) and noise to increase the system's sum rate. When Frequency Division Duplex (FDD) system is used, CSI is only available at the transmitter through feedback. Therefore, another signature sequence optimisation strategy – signature sequence selection method is proposed which is based on removing those signature sequences that are heavily affected by interference and does not require full CSI at the transmitter. This method can be applied to both EE and ES schemes and for cases with and without the proposed SIC receiver to further optimise their system throughputs. Additionally, the amount of CSI feedback required for the optimisation schemes proposed in this thesis is evaluated. Furthermore, the sum rate loss due to partial CSI at the Transmitter (CSIT) of the HSDPA systems with more transmit antennas than receive antennas and vice versa is studied for both SIC and non-SIC schemes.

4.1 Signature Sequence Optimisation

Apart from power allocation as discussed in Chapter 2, another transmitter optimisation strategy is to carry out signature sequence optimisation. In the HSDPA system, a fixed set of orthogonal signature sequences known as the Orthogonal Variable Spreading Factor (OVSF) codes are used for SISO system. In the case of MIMO systems, the OVSF codes are used in conjunction with the precoding, creating an effective MIMO signature sequences. The formation of these signature sequences were shown in Section 2.2.3 in Chapter 2 (page 41). Although signature sequences are orthogonal to each other at the transmitter, the received signature sequences overlap with each other and are no longer orthogonal at the receiver which causes degradation in system performance. Therefore, designing good spreading sequences to ensure low interference between spreading codes has been widely explored in literature such as [29, 38, 74–76] where iterative signature sequence design algorithms with power allocation were investigated to minimise the Mean Square Error (MSE) in [38, 74, 76]. On the other hand, a more straight forward way is to minimise inter-code interference such that the received signature sequences are orthogonal to each other is by performing eigen decomposition on the square of the channel matrix, $\mathbf{H}^H\mathbf{H}$ where $\mathbf{H}$ is defined in Equation (1.4) in Section 1.3 of Chapter 1 (see page 27), and setting the eigenvectors as signature sequence [77]. This formulation is also equivalent to performing Singular Value Decomposition (SVD) on the channel matrix, $\mathbf{H}$ and use the conjugate transpose of the right singular value as the signature sequence. In [78, 79], the pair of precoder and decoder for MIMO channels was designed to minimise the MSE by jointly diagonalising the MIMO channel into eigen subchannels. In this case, power allocation strategies were used where the noise covariance was taken into account during the eigen decomposition of the square of the channel matrix. Based on that idea, a signature sequence design is proposed in this chapter to consider the noise covariance as well as the channel from the previous and next symbol periods to further minimise the MSE. In the next two sections, the formation of this signature sequence design is described. After that, the signature sequence selection will be introduced. Following that, the practicality of the different optimisation strategies explored in this thesis are evaluated in terms of the amount of feedback bits required when considering FDD mode in the HSDPA system.

Finally, in this chapter, the sum rate loss due to partial CSIT is examined for MIMO systems with more transmit antennas than receive antennas and vice versa, with and without the proposed SIC receiver.

4.2 Optimised Signature Sequence

To minimise the cross-correlations between the received signature sequences of the i^{th} and j^{th} spread channels $\forall i, j$, i.e.

$$\underline{q}_i^H \underline{q}_j = 0 \quad \text{for } i, j = 1, \ldots, K \text{ and } i \neq j, \tag{4.1}$$

the most straight forward way is to obtain the set of signature sequence by performing SVD on channel matrix $\mathbf{H}$ as follows:

$$\mathbf{H}^H\mathbf{H} = \mathbf{V}\mathbf{D}\mathbf{V}^H \tag{4.2}$$

where $\mathbf{V}$ is the eigenvectors of matrix $\mathbf{H}^H\mathbf{H}$ and $\mathbf{D}$ is a diagonal matrix containing the eigenvalues. The signature sequence set can be formulated such that:

$$\mathbf{S} = \mathbf{V}. \tag{4.3}$$

By setting the signature sequence set equals to $\mathbf{V}$, the received signature sequence set satisfy the following properties:

$$\mathbf{Q}^H\mathbf{Q} = (\mathbf{H}\mathbf{S})^H\mathbf{H}\mathbf{S} = \mathbf{V}^H\mathbf{V}\mathbf{D}\mathbf{V}^H\mathbf{V} = \mathbf{D}. \tag{4.4}$$

This shows that the received signature sequences has zero cross-correlations and are orthogonal to each other.

To further optimise the signature sequence set, the covariance matrix that includes ISI terms and additive white Gaussian noise can be considered during the eigen decomposition by using :

- the channel matrix of the previous symbol period $\mathbf{H}_1$ (as defined in Equation (1.5) in page 27),
- the next symbol period $\mathbf{H}_2$ (see Equation (1.6) in page 27), as well as
- the amplitude matrix that contains energy terms, $\mathbf{A}$, (see Equation (2.4) in page 38).

Then, given that the full number of spreading sequences are used, the interference plus noise covariance matrix $\mathbf{C}_I$ can be defined as follows:

$$\mathbf{C}_I = \mathbf{H}_1\mathbf{A}^2\mathbf{H}_1^H + \mathbf{H}_2\mathbf{A}^2\mathbf{H}_2^H + \sigma_n^2\mathbf{I}_{N_R(N+L-1)} \tag{4.5}$$

where σ_n^2 is the additive white Gaussian noise power per dimension. In the case of equal energy allocation, the interference plus noise covariance matrix can be rewritten as:

$$\mathbf{C}_I = \frac{E_T}{K^\star}\mathbf{H}_1\mathbf{H}_1^H + \frac{E_T}{K^\star}\mathbf{H}_2\mathbf{H}_2^H + \sigma_n^2\mathbf{I}_{N_R(N+L-1)}. \tag{4.6}$$

The optimised signature sequence set is obtained by setting:

$$\mathbf{S} = \mathbf{V}_I \tag{4.7}$$

where $\mathbf{V}_I$ is the matrix with eigenvectors for the matrix $\mathbf{H}^H\mathbf{C}_I^{-1}\mathbf{H}$ and $\mathbf{D}_I$ is a diagonal matrix containing the corresponding eigenvalues.

4.3 Evaluation of Different Signature Sequences

An evaluation of the performance of different signature sequences including the OVSF codes with precoding, signature sequence provided in Equation (4.3) and in Equation (4.7) have been evaluated in terms of system value sum rate. This is shown in Figure 4.1 for the Pedestrian-A channel and Figure 4.2 for the Pedestrian-B channel. For the SIC schemes, there is no noticeable difference in performance to which signature sequence set is used. However, it is clear from these figures that for non-SIC schemes, the difference between the OVSF and the more optimised non-OVSF codes is about

7Mbps for SNR> 20dB (high SNR regions). Furthermore, from Figure 4.2, the proposed approach based on Equation (4.7) has similar performance to the signature sequence in Equation (4.3) up to 20dB but has more improvements above 20dB when ISI is minimised.

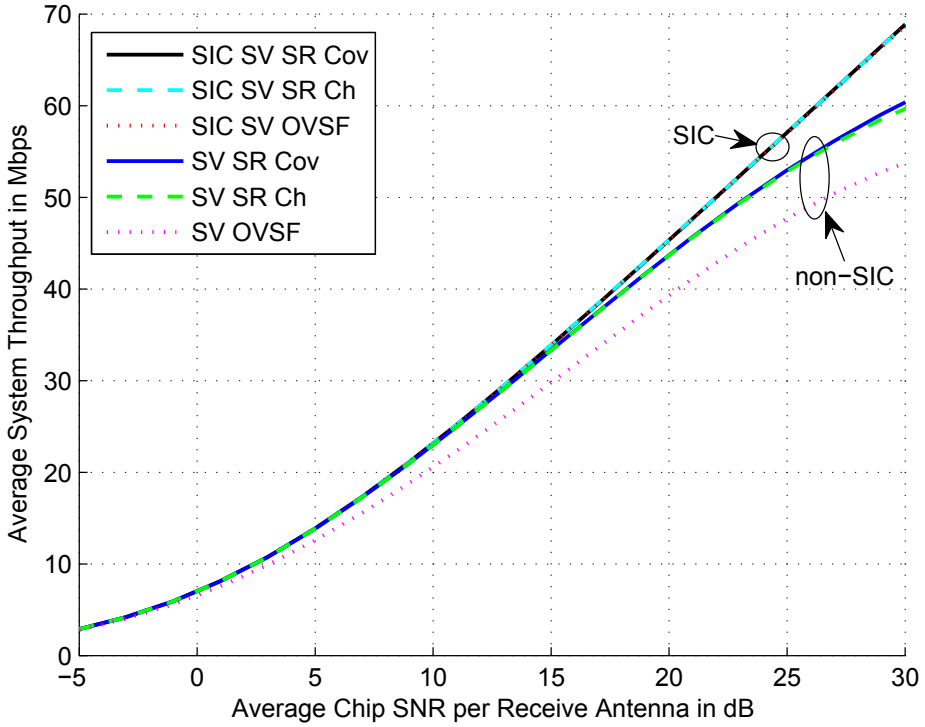


FIGURE 4.1: Comparisons of Different Signature Sequences (Pedestrian-A)

Despite the good performance achieved using signature sequences in Equation (4.3) and Equation (4.7) over non-SIC receivers, full channel information is hard to obtain at the transmitter when Frequency Division Duplex (FDD) systems are used. This motivates the formation of an alternative signature sequence optimisation method without requiring full channel knowledge at the transmitter. This can be done by selecting an an optimal subset of signature sequences (or equivalently, by removing or switching off those with low received SINRs).

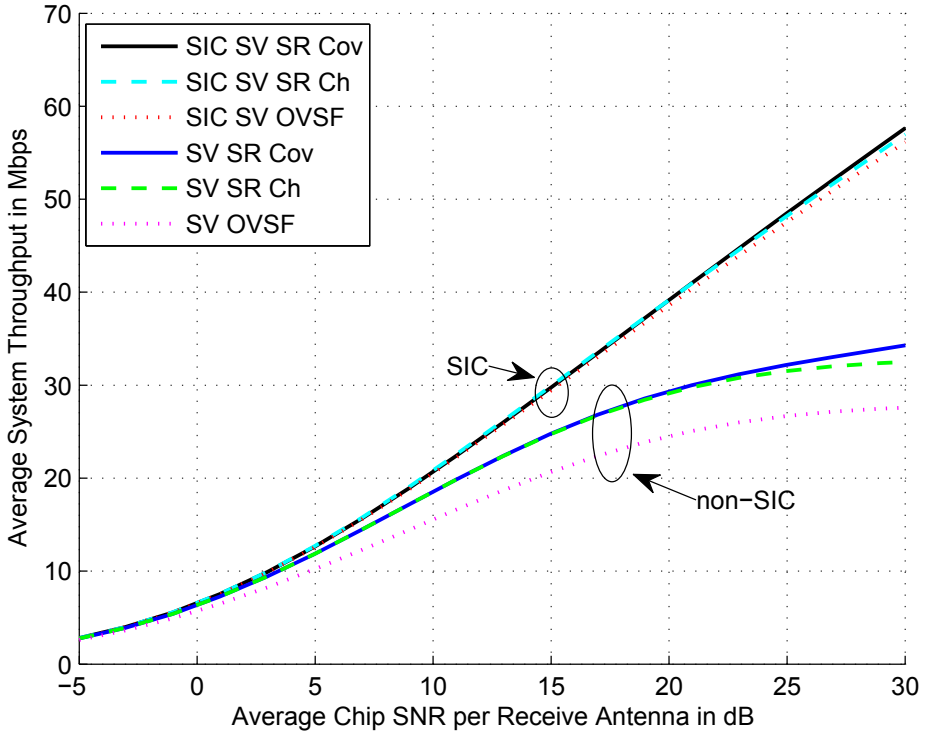


FIGURE 4.2: Comparisons of Different Signature Sequences (Pedestrian-B)

4.4 Feedback and Channel Removal

The availability of CSIT can further increase the data throughput through transmitter adaptation such as power allocation as shown in Chapter 2 and signature sequence optimisation as discussed in this chapter. Other purposes of obtaining CSIT include interference avoidance and better scheduling for multi-user scenario [80]; and to further exploit spatial diversity and multiplexing gain [81]. CSIT can be obtained by exploiting the channel reciprocity [82] for Time Division Duplex (TDD) system where both the uplink and downlink share the same frequency. However, channel reciprocity approach does not apply to the FDD mode which is more widely used in the HSDPA system where both uplink and downlink are on different frequencies.

Feedback of instantaneous channel conditions can be analogue or digital. Examples of analogue feedback include [83,84] where downlink channel coefficients are transmitted using unquantised QAM symbols. Digital feedback aims to quantise CSI while reducing the number of feedback bits required. For digital feedback, it is shown that with

proper design, a small number of bits about the channel conditions is required for feedback to obtain near optimal channel adaptation [80, 85]. This is known as finite-rate feedback systems as defined in [86] which minimises the CSI feedback required while exploiting transmitter adaptations. As full CSIT is hard to obtain in the FDD system, an alternative signature sequence optimisation is also proposed in this chapter to minimise the CSI feedback required. This can be done by selecting an optimal subset of signature sequences (based on the precoded OVSF codes) and by removing those with low received SINR.

In literature, subchannel removal has been considered in various algorithms. For instance, in the water-filling algorithm in [87], the subchannels that have low gains with respect to the total sum rate are removed. Other subchannel removal methods include the use of eigen decomposition of the covariance matrix and isolate the bad data streams to minimise the sum MSE [88]. In [48], switching off methods have been proposed for the low SINR data streams so that power can be allocated to the remaining streams with better SINR. In [89], the use of rounding rates down to zero has been proposed for the low rate subchannels. Nevertheless, the removal of bad signature sequences to increase the system throughput is not yet explored in the HSDPA or the CDMA systems. In this chapter, a novel algorithm is proposed to find the optimal subset of the signature sequence using the system value approach developed in Chapter 2. This approach is appropriate for both ES and EE allocation schemes.

The ESER approach is used to equalise the received SINRs of all spread channels to the target SINR as described in Chapter 2. However, signature sequence selection can further optimise the system throughput by removing those signature sequences that require more energy to reach the target SINR, so that the energy is more efficiently used. An algorithm for the signature sequence selection to further increase the system throughput of ESER and ESTG approaches is proposed. Similarly, an algorithm for signature sequence selection is proposed for the EEER and EETG schemes to improve the system throughput. This is done by switching off those spread channels that has a low received SINR, so that a higher data rate can be allocated to the spread channels in better conditions.

4.5 Selecting the Optimum Signature Sequence Set

In this section, the signature sequence selection procedure [26] is proposed by using the system value calculations in Equation (2.38) of page 47 and Equation (3.7) of page 69. The selection of signature sequences involves two steps: the first process is to find the signature sequence sets starting from $\widetilde{K} = K$ to $\widetilde{K} = 1$ by eliminating the signature sequence with the smallest system value for each set. This generates a new set of signature sequences for each $\widetilde{K}$ iteration. Using the stored signature sequence sets, the second process is to find the optimum number of signature sequences that maximise the total rate for the intended energy allocation scheme (ES or EE).

4.5.1 Signature Sequence Selection for Each $\widetilde{K}$

The first process of signature sequence selection starts from $\widetilde{K} = K$ and continues by iteratively adjusting $\widetilde{K} = \widetilde{K} - 1$ until it reaches $\widetilde{K} = 1$. The selection starts from $\widetilde{K} = K$ because for each $\widetilde{K}^{th}$ iteration, the signature sequence corresponding to the spread channel with the worst SINR (lowest system value) is removed. In other words, a smaller set of signature sequences with good conditions are retained after each iteration. The set of signature sequences corresponding to each $\widetilde{K}^{th}$ loop should be stored for further processing in Section 4.5.2 for either ES or EE allocation schemes.

To find the system values and signature sequence set for each $\widetilde{K}^{th}$ iteration, the first step is to find the system values $\underline{\lambda}_{\widetilde{K}} = \left[\lambda_1, ..., \lambda_{\widetilde{K}}\right]^T$ according to Equation (2.38) (see page 47) for non-SIC scheme and Equation (3.7) (see page 69) for SIC scheme.

The second step is to perform channel ordering by sorting the elements in $\underline{\lambda}_{\widetilde{K}}$ in an ascending manner to form $\underline{\lambda}_{ord,\widetilde{K}}$ and obtain its ordering $\underline{k}_{ord} = [a_1, ..., a_{\widetilde{K}}]^T \in \mathbb{N}^{\widetilde{K}\times 1}$. This means:

$$\left[\underline{\lambda}_{ord,\widetilde{K}}\right]_k = \left[\underline{\lambda}_{\widetilde{K}}\right]_{a_k}. \tag{4.8}$$

Then, obtain $[\underline{\lambda}_{\min}]_{\widetilde{K}}$ which is to the minimum element of $\underline{\lambda}_{\widetilde{K}}$. This also corresponds to the first element of $\underline{\lambda}_{ord,\widetilde{K}}$ such that:

$$[\underline{\lambda}_{\min}]_{\widetilde{K}} = \left[\underline{\lambda}_{ord,\widetilde{K}}\right]_1. \tag{4.9}$$

After that, obtain the mean system value $[\underline{\lambda}_{mean}]_{\widetilde{K}}$ as shown in Equation (2.48) (see page 55).

By initialising $\mathbf{S}_{\widetilde{K}}^{temp} = \mathbf{S}$ as in Equation (2.5) in page 38, the signature sequence set is ordered according to the corresponding ordered system values such that:

$$\left[\mathbf{S}_{\widetilde{K}}^{ord}\right]_k = \left[\mathbf{S}_{\widetilde{K}}^{temp}\right]_{a_k} \text{ for } k = 1, ..., \widetilde{K} \tag{4.10}$$

where

$$\mathbf{S}_{\widetilde{K}}^{ord} = \left[\underline{s}_{\widetilde{K},1}^{ord}, ..., \underline{s}_{\widetilde{K},k}^{ord}, ..., \underline{s}_{\widetilde{K},\widetilde{K}}^{ord}\right]. \tag{4.11}$$

Then, form the received signature sequence set using:

$$\mathbf{Q} = \mathbf{H}\mathbf{S}_{\widetilde{K}}^{ord}, \tag{4.12a}$$

$$\mathbf{Q}_1 = \mathbf{H}_1\mathbf{S}_{\widetilde{K}}^{ord}, \tag{4.12b}$$

$$\mathbf{Q}_2 = \mathbf{H}_2\mathbf{S}_{\widetilde{K}}^{ord}. \tag{4.12c}$$

After that, perform signature sequence removal by removing the first column of $\mathbf{S}_{\widetilde{K}}^{ord}$ (which corresponds to the signature sequence with the lowest system value) to form $\mathbf{S}_{\widetilde{K}-1}^{temp}$ for the next iteration:

$$\mathbf{S}_{\widetilde{K}-1}^{temp} = \left[\underline{s}_{\widetilde{K},2}^{ord}, ..., \underline{s}_{\widetilde{K},k}^{ord}, ..., \underline{s}_{\widetilde{K},\widetilde{K}}^{ord}\right]. \tag{4.13}$$

Set $\widetilde{K} = \widetilde{K} - 1$. This process is repeated until $\widetilde{K} = 1$. The algorithm is summarised in Algorithm 9.

After storing the optimum signature sequence sets for each $\widetilde{K}$, the optimum set can be selected according to the energy allocation scheme (ES or EE) and this will be described next.

Algorithm 9 Algorithm to Remove the "Bad" Signature Sequences

Initialisation
Form $\mathbf{S}_{\widetilde{K}}^{temp}$=$\mathbf{S}$ and $\mathbf{S}_{\widetilde{K}}^{ord}$=$\mathbf{S}$
Form $\mathbf{Q}, \mathbf{Q}_1$ and $\mathbf{Q}_2$ as shown in Equation (4.12) using $\mathbf{S}_{\widetilde{K}}^{ord}$
for $\widetilde{K} = K$ to $\widetilde{K} = 1$ **do**
    Find the system values
    Allocate energy equally to all spread channels $E_k = \frac{E_T}{\widetilde{K}}$ for $k = 1, ..., \widetilde{K}$
    Form $\mathbf{A}$ as shown in Equation (2.4)
    for $k = 1, \ldots, \widetilde{K}$ **do**
        if MMSE receiver is used **then**
            Find $\lambda_k = E_k \underline{q}_k^H \mathbf{C}^{-1} \underline{q}_k$ and $\mathbf{C}$ from Equation (2.38)
        else
            if SIC receiver is used **then**
                Find $\lambda_k = E_k \underline{q}_k^H \mathbf{C}_k^{-1} \underline{q}_k$ and $\mathbf{C}_k$ from Equation (3.7)
    Form $\underline{\lambda}_{\widetilde{K}} = \left[\lambda_1, ..., \lambda_k, ..., \lambda_{\widetilde{K}}\right]^T$
    Reorder of the signature sequences
    Order $\underline{\lambda}_{\widetilde{K}}$ in an ascending manner to form $\underline{\lambda}_{ord,\widetilde{K}}$
    Obtain its ordering $\underline{k}_{ord} = \left[a_1, ..., a_{\widetilde{K}}\right]^T$
    if EEER or EETG **then**
        Find the minimum system value $\lambda_{\min,\widetilde{K}}$ as:

$$\lambda_{\min,\widetilde{K}} = \left[\underline{\lambda}_{ord,\widetilde{K}}\right]_1 \tag{4.14}$$

    else
        if ESER or ESTG **then**
            Calculate the mean system value $\lambda_{mean,\widetilde{K}}$:

$$\lambda_{mean,\widetilde{K}} = \frac{\underline{\lambda}_{\widetilde{K}}^T \underline{1}_{\widetilde{K}}}{\widetilde{K}} \tag{4.15}$$

            where $\underline{1}_{\widetilde{K}}$ is a vector containing ones with a length of $\widetilde{K}$.
    Order the signature sequence set $\left[\mathbf{S}_{\widetilde{K}}^{ord}\right]_k = [\mathbf{S}_{\widetilde{K}}^{temp}]_{a_k}$ for $k = 1, ..., \widetilde{K}$.
    Perform signature sequence removal by removing the first column of $\mathbf{S}_{\widetilde{K}}^{ord}$:

$$\mathbf{S}_{\widetilde{K}-1}^{temp} = \left[\underline{s}_{\widetilde{K},2}^{ord}, ..., \underline{s}_{\widetilde{K},k}^{ord}, ..., \underline{s}_{\widetilde{K},\widetilde{K}}^{ord}\right] \tag{4.16}$$

    Set $\widetilde{K} = \widetilde{K} - 1$

4.5.2 Signature Sequence Selection for ES and EE Allocations

Selecting the optimum signature sequence set is to find the combination of $\widetilde{K}$ and b_p that maximises the total rate for a specific energy allocation scheme (ES or EE). Firstly, for a given set of discrete rate represented by the vector $\underline{b} = [b_1, \ldots, b_p, \ldots, b_P]$, find the corresponding target system value vector $\underline{\lambda}_{tar}$ using the following equation:

$$[\underline{\lambda}_{tar}]_p = \frac{\Gamma\left(2^{b_p} - 1\right)}{1 - \Gamma\left(2^{b_p} - 1\right)}. \tag{4.17}$$

where Γ is the gap value. Then, if ES allocations are performed, use $\lambda_{mean,\widetilde{K}}$ obtained in Equation (4.15), find the rate to be allocated for the $\widetilde{K}^{th}$ channel, $b_{p_{\widetilde{K}}}$, $\forall\ \widetilde{K} = 1, \ldots, K$ which satisfies the following inequatlity:

$$[\underline{\lambda}_{tar}]_{p_{\widetilde{K}}} \leq [\underline{\lambda}_{mean}]_{\widetilde{K}} < [\underline{\lambda}_{tar}]_{(p+1)_{\widetilde{K}}} \tag{4.18}$$

where $(p+1)_{\widetilde{K}}$ is the index of the next discrete rate $(p+1)$ for the $\widetilde{K}$ channel.

Otherwise, if EE allocations are performed, use $\lambda_{\min,\widetilde{K}}$ obtained in Equation (4.14) and find $p_{\widetilde{K}}$ $\forall\ \widetilde{K} = 1, \ldots, K$ which satisfies the following inequality:

$$[\underline{\lambda}_{tar}]_{p_{\widetilde{K}}} \leq [\underline{\lambda}_{\min}]_{\widetilde{K}} < [\underline{\lambda}_{tar}]_{(p+1)_{\widetilde{K}}}\,. \tag{4.19}$$

Find the total rate for all $\widetilde{K} = 1, \ldots, K$ by using the following equation:

$$[\underline{R}_T]_{\widetilde{K}} = \widetilde{K}\,[\underline{b}]_{P_{\widetilde{K}}} \tag{4.20}$$

The optimum number of signature sequences and total rate $R_T^\star$ for either ESER or EEER allocation is given by the following equations:

$$K^\star = \arg\left(\max_{\widetilde{K}=1,\cdots,K}(\underline{R}_T)\right), \tag{4.21}$$

$$b_p^\star = [\underline{b}]_{p_{K^\star}}\,, \tag{4.22}$$

$$R_T^\star = [\underline{R}_T]_{K^\star} = K^\star b_p^\star. \tag{4.23}$$

After obtaining $K^\star$, the corresponding signature sequence is $\mathbf{S}_{K^\star}^{ord}$ (refer to Section 4.5.1). The algorithm can be summarised in Algorithm 10.

Algorithm 10 Algorithm to Find $K^\star$ for ES and EE Schemes

1: Find $\underline{\lambda}_{tar}$ corresponding to each data rate $\underline{b} = [b_1, \ldots, b_p, \ldots, b_P]$ using Equation (4.17)
2: Find $p_{\widetilde{K}}$ $\forall$ $\widetilde{K} = 1, \ldots, K$
3: **if** ESER or ESTG **then**
4: Obtain $p_{\widetilde{K}}$ using Equation (4.18)
5: **else**
6: **if** EEER or EETG **then**
7: Compute $p_{\widetilde{K}}$ using Equation (4.19)
8: Calculate $\underline{R}_T$ using Equation (4.20).
9: Obtain $K^\star$ using Equation (4.21), $b_p^\star$ using Equation (4.22) and $R_T^\star$ using Equation (4.23).
10: Select the optimum signature sequence set $\mathbf{S}_{K^\star}^{ord}$ for ES allocation.
11: **if** ESER or ESTG **then**
12: Find $\lambda_{mean}^\star$ using the following equation:

$$\lambda_{mean}^\star = [\underline{\lambda}_{mean}]_{K^\star} \tag{4.24}$$

13: **else**
14: **if**
15: **then**Find $\lambda_{\min}^\star$ using the following equation:

$$\lambda_{\min}^\star = [\underline{\lambda}_{\min}]_{K^\star} \tag{4.25}$$

The rate $R_T^\star$ given in Equation (4.20) is for equal rate allocation. When ESTG is performed, the number of spread channels that can carry $b_{p+1}^\star$, m can be found by finding the maximum m that satisfy:

$$(K^\star - m)\,[\underline{\lambda}_{tar}]_{p_{K^\star}} + m\,[\underline{\lambda}_{tar}]_{(p+1)_{K^\star}} \leq K^\star\,[\lambda_{mean}]_{K^\star} \tag{4.26}$$

Similarly, EETG allocation can also be performed by loading spread channels that has system values $\lambda_k > [\underline{\lambda}_{tar}]_{(p+1)_{K^\star}}$ with $b_{p+1}^\star$. Then the total rate for two-group allocation is given by:

$$R_{T,TG}^\star = (K^\star - m)\,b_p^\star + m\lambda_{tar}(b_{p+1}^\star) \tag{4.27}$$

4.6 Complexity of Signature Sequence Selection

The complexity of signature sequence selection mainly arises from Algorithm 9 where matrix and vector multiplications as well as sorting and ordering operations were performed. On the other hand, in Algorithm 10, only rate calculations and selecting the signature sequence set (computed in Algorithm 9) that optimises the total rate were carried out.

Defining $\alpha = N_R(N + L - 1)$, the main computational complexity in Algorithm 9 includes:

- Operation $\underline{q}_k^H \mathbf{C}^{-1} \underline{q}_k$ (or $\underline{q}_k^H \mathbf{C}_k^{-1} \underline{q}_k$) in step 10 (or 12), which requires a complexity of $2O(\alpha^2)$ for each k, and a total of $2K$ of $O(\alpha^2)$ operations for $k = 1, \ldots, K^\star$.
- Sorting of $\underline{\lambda}_{\widetilde{K}}$ in step 16, which has an average complexity of $O(\alpha \log \alpha)$ for most sorting algorithms and
- Ordering signature sequence to find $\mathbf{S}_{\widetilde{K}}^{ord}$ which can be done by performing matrix multiplication between the matrix to be ordered and a permutation matrix, requiring a complexity of $O(\alpha^3)$.

A permutation matrix is a reordered identity matrix where there is only one 1 in each row and column. For example, let $\mathbf{\Psi} = [\underline{\psi}_1, \underline{\psi}_2, \underline{\psi}_3]$ and the intended order is $\mathbf{\Psi}_{ord} = [\underline{\psi}_3, \underline{\psi}_1, \underline{\psi}_2]$. The ordering can be done by forming the permutation matrix

$$\mathbf{P} = \begin{bmatrix} 0 & 1 & 0 \\ 0 & 0 & 1 \\ 1 & 0 & 0 \end{bmatrix} \tag{4.28}$$

and performing matrix multiplication $\mathbf{\Psi}_{ord} = \mathbf{\Psi}\mathbf{P}$.

Therefore, this algorithm will require less than $2O(\alpha^3)$ in complexity.

4.7 Performance of Signature Sequence Selection

The average system throughput for signature sequence selection using the ESTG scheme for both SIC and non-SIC receivers are shown in Figures 4.3 and 4.4 for the Pedestrian-A and Pedestrian-B channels respectively. The dotted lines represent the use of optimum signature sequence selection while the normal lines denote the use of full set of signature sequences. For Pedestrian-A channel in Figure 4.3, the use of $K^\star$ signature sequences improves the performance by 2 to 2.5Mbps for most SNR regions (SNR of 5 to 20dB) when SIC receiver is not implemented. The improvements are more significant in Pedestrian-B channel in Figure 4.4, where the difference between the use of $K^\star$ and K signature sequences reaches 5Mbps at high SNR regions. However, the improvement of using $K^\star$ signature sequences are less obvious when SIC receiver is used.

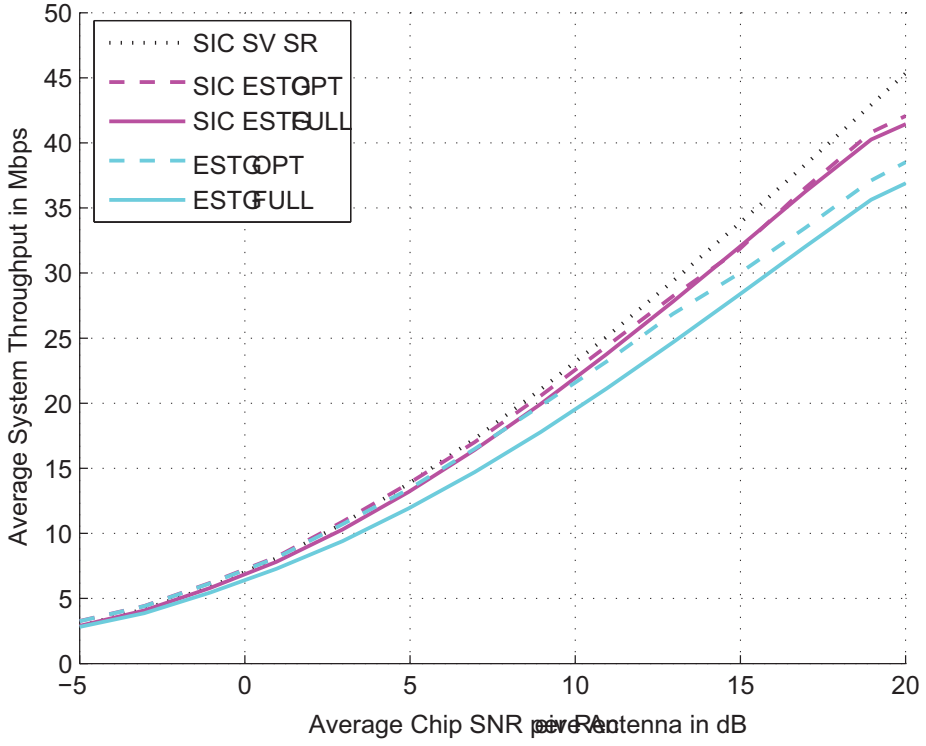


FIGURE 4.3: ESTG Schemes with K and $K^\star$ Spreading Sequences (Pedestrian-A)

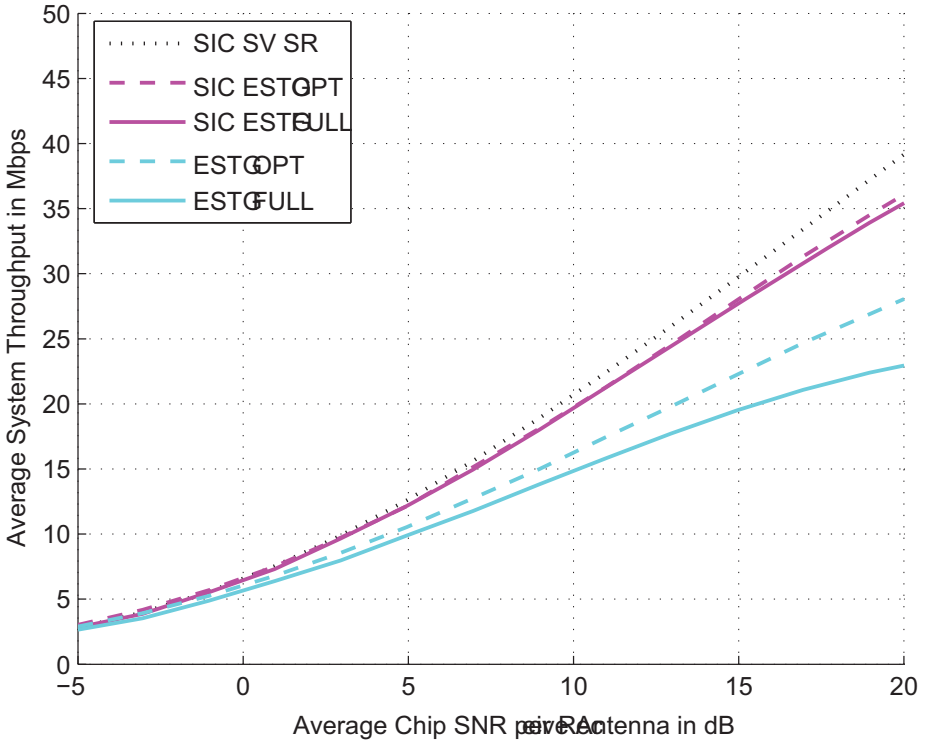


FIGURE 4.4: ESTG Schemes with K and $K^{\star}$ Spreading Sequences (Pedestrian-B)

On the other hand, the use of signature sequence selection shows significant improvements in EETG allocations with and without SIC receiver as shown in Figures 4.5 and 4.6 for the Pedestrian-A and Pedestrian-B channel respectively. For the Pedestrian-A channel in Figure 4.5, the improvement by using signature sequence selection improves the EETG non-SIC scheme by 3 to 5Mbps, while a 2.5 to 3Mbps enhancement is seen for the EETG SIC scheme. The improvement by using signature sequence selection is very significant in Pedestrian-B channel (see Figure 4.6). When non-SIC receiver is used, the improvement reaches 11Mbps at high SNR regions. Similarly, when SIC receiver is used, the improvement became as high as 7Mbps at high SNR regions.

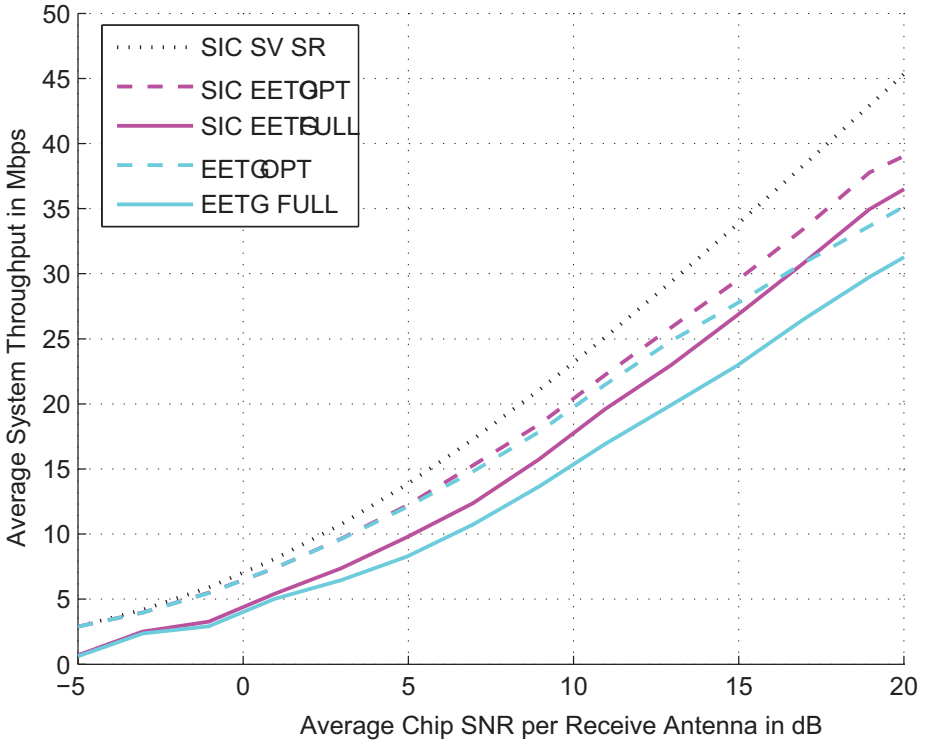


FIGURE 4.5: EETG Schemes with K and $K^\star$ Spreading Sequences (Pedestrian-A)

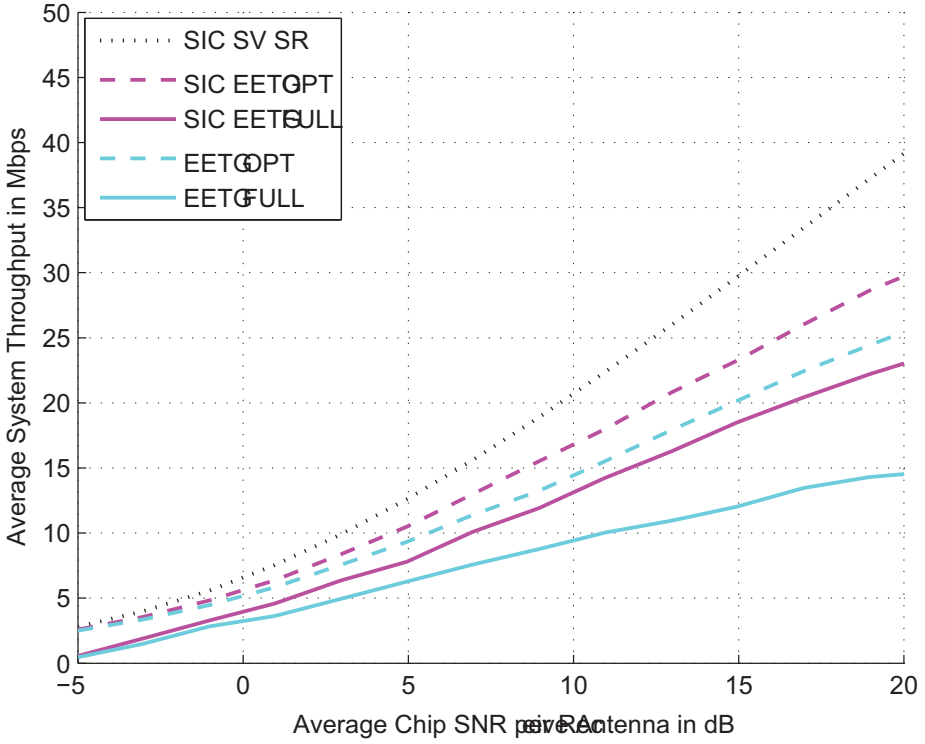


FIGURE 4.6: EETG Schemes with K and $K^\star$ Spreading Sequences (Pedestrian-B)

In Figures 4.7 and 4.8, the use of signature sequence selection for the EETG scheme with and without SIC against the more complicated ESTG scheme without any further optimisation is compared. For the Pedestrian-A channels in Figure 4.7, EETG non-SIC and SIC with $K^\star$ signature sequences is 1 to 1.5Mbps less than the non-optimised ESTG scheme for low SNR regions (SNR $<$ 10dB). At high SNR, the use of SIC receiver with $K^\star$ EETG scheme achieves similar performance.

For Pedestrian-B channels in Figure 4.8, the $K^\star$ EETG non-SIC scheme is at most 3Mbps lower than the non-optimised ESTG scheme at high SNR regions. However, when the SIC receiver is implemented on the the $K^\star$ EETG scheme, the system throughput is similar to or even 2Mbps higher the non-optimised ESTG scheme at high SNR region. This is because the Pedestrian-B channel has a long delay spread and causes some spread channels to have really low received SINR or require a lot of energy to achieve the target rate. Therefore, the gain in switching off the spread channels with very low SINR greatly improves the system throughput. Morover, when SIC receiver optimisation is also carried out, the gain arising from this two optimisation schemes is more than using ESTG scheme alone.

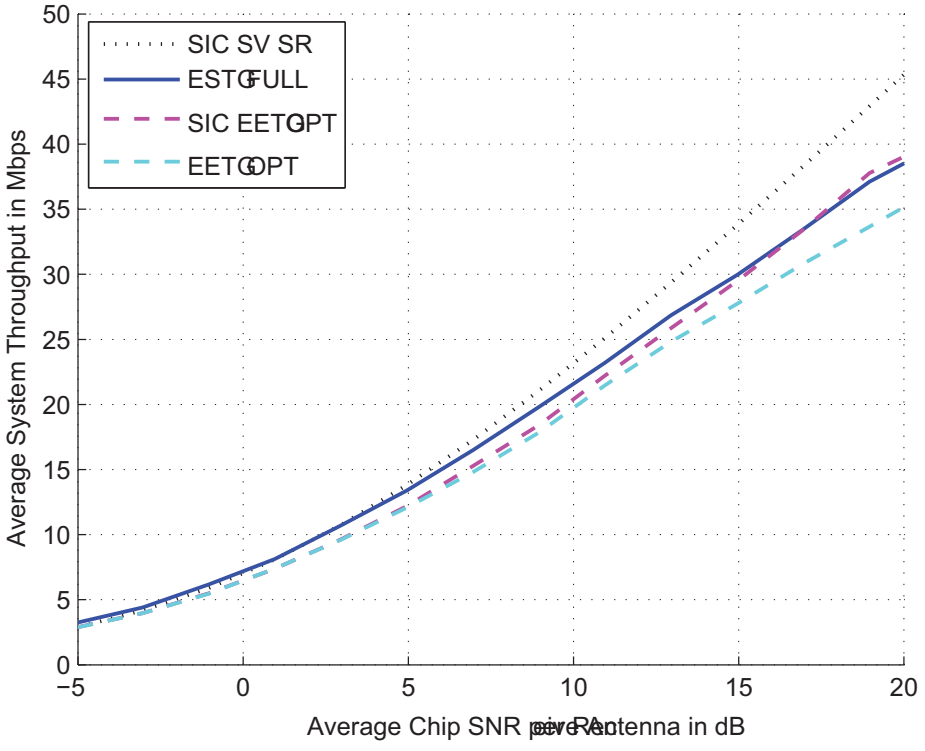


FIGURE 4.7: Comparison of Improved EETG against ESTG (Pedestrian-A)

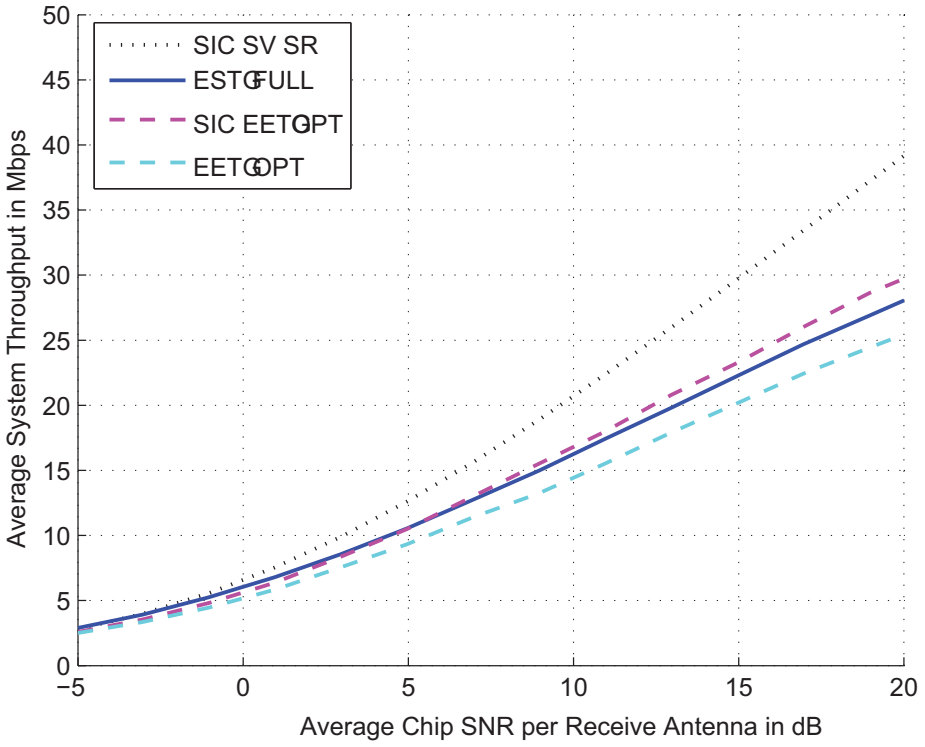


FIGURE 4.8: Comparison of Improved EETG against ESTG (Pedestrian-B)

4.8 Obtaining Channel State Information at Transmitter

In the previous sections, the use of optimum signature sequence selection method which employs the precoded OVSF codes was proposed to reduce the amount of CSI feedback. In literature, CSI feedback can be divided into three categories [86]:

- scalar quantisation of channel such as [85,90] where the magnitude of the channel response is quantised,
- codebook design such as [86,91] and
- random vector quantisation (for larger systems) such as [92,93].

For the HSDPA and LTE systems, predefined codebooks are used to minimise the feedback required. Usually, one set of codebooks is related to link adaptation providing information such as:

- modulation scheme,

- transport-block size and
- number of channelisation codes

that each MIMO stream should operate under the estimated channel conditions at the receiver. Another set of codebooks is related to the precoding weights for MIMO systems.

The aim of codebook design is to create a set of codewords which represent the different states of channel conditions. These codewords and their respective indices are known to both the receiver and the transmitter. Therefore, only the index of the selected codeword is required. The number of bits, B required to be fed back depends on the codebook size 2^B. There are two sets of codebooks for the HSDPA system. The first set is known as Channel Quality Indicator (CQI) and the second set is the Precoding Control Indicator (PCI) which is only used for MIMO configuration. CQI contains information related to link adaptation, while PCI contains the precoding vector that is best suited for MIMO transmissions under the current channel conditions. The CQI tables for the HSDPA system is outlined in TS25.214 v.11.6.0 Section 6.2.3 [43]. Each of these tables are catered for different User Equipment (UE) categories as some UE supports limited channelisation codes or lower order of modulation scheme. In these tables, each CQI index contains information including the transport block size N_{TBS}, the number of channelisation codes, K, and the modulation scheme to be employed. Given the following parameters:

- the number of bits for cyclic redundancy check, $N_{CRC} = 24$,
- the number of symbols per TTI, $N^{(x)} = 480$, together with
- the transport block size N_{TBS},
- the number of channelisation codes, K and
- the number of bits in the modulation scheme b

from the tables, the effective code rate r_{code} can be calculated as follows:

$$r_{code} = \frac{N_{TBS} + N_{CRC}}{KN^{(x)}b}. \tag{4.29}$$

Hence, b_p can be obtained using the following equation:

$$b_p = br_{code}. \tag{4.30}$$

An example of a CQI table together with the calculated r_{code} and b_p is given in Table 4.1.

TABLE 4.1: CQI Table Corresponding to TS25.214 v.11.6.0 7Ib

CQI Index	N_{TBS}	K	Modulation	b	r_{code}	b_p	Equivalent AWGN
0	4592	15	QPSK	2	0.32	0.64	-3
1	4592	15	QPSK	2	0.32	0.64	-1
2	5296	15	QPSK	2	0.37	0.74	0
3	7312	15	QPSK	2	0.51	1.02	0
4	9392	15	QPSK	2	0.65	1.31	0
5	11032	15	QPSK	2	0.77	1.54	0
6	14952	15	16QAM	4	0.52	2.08	0
7	17880	15	16QAM	4	0.62	2.49	0
8	21384	15	16QAM	4	0.74	2.97	0
9	24232	15	16QAM	4	0.84	3.37	0
10	27960	15	64QAM	6	0.65	3.89	0
11	32264	15	64QAM	6	0.75	4.48	0
12	36568	15	64QAM	6	0.85	5.08	0
13	39984	15	64QAM	6	0.93	5.56	0
14	42192	15	64QAM	6	0.98	5.86	0

As there are many CQI tables for different handsets, this thesis assumes that the b_p values are from 0 to 6 with 0.5 intervals as shown in Table 2.3 in page 58. This corresponds to 4 bits feedback.

4.9 Analysis of Link Adaptation Feedback

So far, the practicality of different optimisation schemes was evaluated in terms of computational complexity (number of matrix inversion required). When an FDD system is used, the practicality of transmitter optimisation has to be further evaluated in terms of

the amount of CSI required for feedback[1] . An analysis in terms of number of feedback bits required for link adaptation is carried out for the different optimisation schemes proposed in this thesis.

For the EEER schemes, since energy available at the transmitter is equally allocated, only the rates to be allocated (in this case, 4 bits) are required to be fed back. For the EETG scheme, since two rates b_p and b_{p+1} are allocated to different spread channels, information is required about which spread channels can transmit at rate b_{p+1}. Since b_{p+1} is the next discrete rate in the CQI table, feeding back such information is not required. Therefore, the total number of feedback bits required for the EEER scheme is 4 bits; while the EETG scheme requires $4 + \log_2 K$ bits, where K is the total number of signature sequences used for transmission.

When signature sequence selection is used, information regarding which spread channel to be switched off is required. Therefore, a total of $4+\log_2 K$ feedback bits are required for the EEER scheme with $K^\star$ signature sequences and $4 + 2\log_2 K$ feedback bits are required for the EETG scheme with $K^\star$ schemes.

For the system value based ESER scheme proposed in Chapter 2, power adaptation is used to improve the system throughput. In this scheme, energy allocation for each spread channel (which varies across vast values and requires great accuracy) is required to be fed back to the transmitter. This means that a large set of feedback bits are required compared to the EETG scheme with $K^\star$ for a small improvement as shown in Figures 4.7 and 4.8. Therefore, although the ES approaches achieve a better performance and can be applied to the TDD system where CSI can be exploited much easily, the use of signature sequence selection scheme has an upper hand when balancing the amount of feedback and system throughput for the FDD system. The above analysis is summarised in Table 4.2.

[1]Note that the SIC receiver does not contribute to additional feedback as it does not require transmitter adaptation.

TABLE 4.2: Link Adaptation Feedback for Different Optimisation Schemes

Optimisation Scheme	Total Feedback Bits
EEER	4
EETG	$4 + \log_2 K$
EEER $K^\star$	$4 + \log_2 K$
EETG $K^\star$	$4 + 2\log_2 K$
ESER	$>> 4 + 2\log_2 K$

4.10 Multiplexing & Array gains in MIMO FDD Systems

So far, a 2×2 MIMO system for spatial multiplexing has been considered and evaluated based on system value sum rate and system throughput. The use of MIMO technologies can improve the performance of a communication system without the need of additional bandwidth. The main enhancements of MIMO systems include diversity gain, spatial multiplexing gain and beamforming gain (power gain) [94]. The aim of a diversity system is to combat fading and to improve error performance through sending and/or receiving replicas of a signal and is measured in terms of error rate. Transmit diversity techniques include the use of Alamouti codes [95], Orthogonal Space-Time Block Codes (OSTBCs) [96] and Space-Time Trellis Codes (STTCs) [97]; while receive diversity is usually achieved through antenna selection or receiver combining techniques such as Maximum Ratio Combining (MRC) and linear combining [98, 99]. A spatial multiplexing system [10, 11] aims to increase data rate by sending different signal through different spatial streams and the multiplexing gain in given by $\min(N_T, N_R)$ where N_T is the total number of transmit antennas and N_R is the total number of receive antennas as defined in Chapter 1. On the other hand, trade-offs between diversity and multiplexing gain has been studied in [100, 101] to balance between bit error rate performance and system throughput. Transmit beamforming gain can be achieved by transmitting the signals towards the desired directions of the designed user and nulls towards the directions to the other users [102]. Given some form of channel information is available at the transmitter, precoding or beamforming techniques can be applied to diversity or multiplexing systems to further boost their performance. These techniques include zero-forcing beamforming, regularised zero-forcing beamforming [103] and beamforming based on MUltiple SIgnal Classification (MUSIC) algorithm [104]. As channel coding is used in modern systems which provide coding gain to achieve

error performance [105, 106], this thesis only considers multiplexing systems and the power gain achieved through increasing the number of antennas on one side (either on the transmitter or receiver side) while keeping the other side constant to further increase the total data rate.

Defining the MIMO systems containing N_T transmit antennas and N_R transmit antennas as a $N_T \times N_R$ system, this section focus on examining the sum rate of MIMO systems including the 2×3, 3×2, 2×4, 4×2, 3×4 and 4×3 systems with partial CSIT (precoding codebook only). In [102], the difference in terms of ergodic capacity between having full CSIT and only having statistical channel information at the transmitter was explored for the 2×2, 2×4, 4×2 and 4×4 MIMO systems. It was observed that when $N_R \geq N_T$, the capacities are the same between having full CSIT or partial CSIT. However, when $N_R < N_T$, there is a difference between the ergodic capacities of having full CSIT and partial CSIT where the gain comes from the energy saved by not emitted energy to the subspace that is not seen by the receiver [102]. The difference between the systems with $N_R < N_T$ and the systems with $N_R > N_T$ (with partial or full CSIT) because the receiver has full channel knowledge.

For downlink systems, it is more attractive to increase the number of antennas at the transmitter (base station) rather than increasing the number of antennas at the receiver (handset) due to space constraints and processing capabilities in handsets. Therefore, CSIT is very important. To reduce the feedback while achieving partial CSIT when the FDD system is used, precoding codebooks are defined for the two transmit antennas and four transmit antennas MIMO HSDPA systems. However, there is a loss of beamforming gain due to partial CSIT [2] in a MIMO system with $N_T > N_R$. This chapter evaluates the loss of beamforming gain in MIMO systems with $N_T > N_R$ in terms of system value sum rate for both SIC and non-SIC schemes. Furthermore, a comparison study of the non-SIC scheme with $N_R > N_T$ and the SIC scheme with $N_T > N_R$ is also carried out.

[2]Note that this does not affect a MIMO system with $N_R > N_T$ as the receiver has full channel knowledge.

4.10.1 Evaluation of Partial CSIT in MIMO FDD Systems

The MIMO signature sequences used in this section is based on the precoding codebook in Section 2.2.4 in page 42 for the 2 transmit antennas system and Appendix D in page 145 for the 3 and 4 transmit antenna schemes. The codeword is selected according to the sum rate maximisation criteria by using the system value sum rate calculation in Equation (2.35) in page 46 where the codeword that gives the highest sum rate will be selected. In theory, when $N_R \geq N_T$ as described in the previous section, the ergodic capacity is the same whether full CSIT or partial CSIT is available. The sum rate for systems with $N_R \geq N_T$ using the worst precoding codeword, i.e. choosing the codeword with the lowest sum rate, and the sum rate using the best precoding codeword is evaluated in Figure 4.9 for the Pedestrian-A channel and Figure 4.10 for the Pedestrian-B channel for non-SIC receivers. From these figures, it can be seen that even in the worst scenario where all the signals from the transmit antennas are emitting at wrong directions, the sum rate loss is not very significant. This means that the feedback of PCI is not necessary when $N_R \geq N_T$.

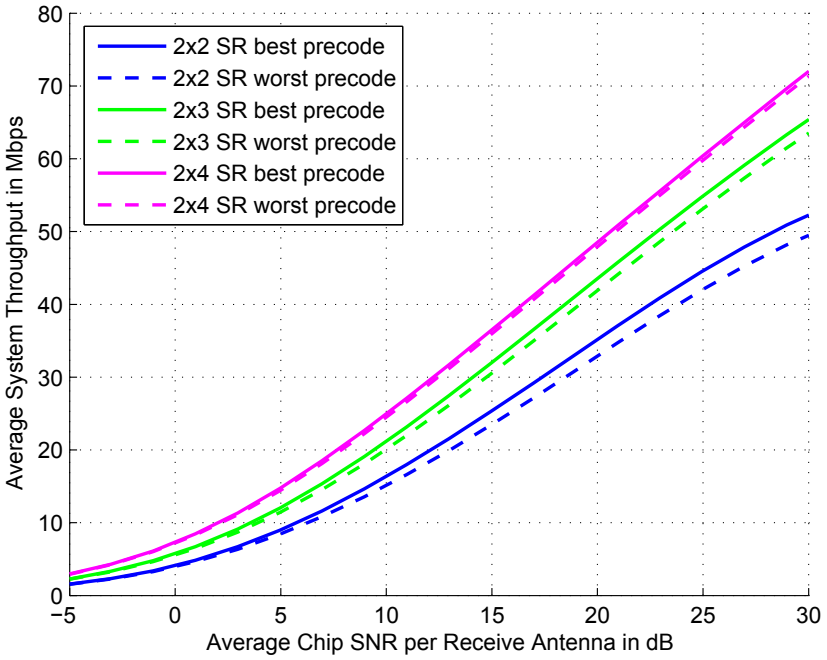


FIGURE 4.9: SV Sum Rate with 2 Transmit Antennas (Pedestrian-A)

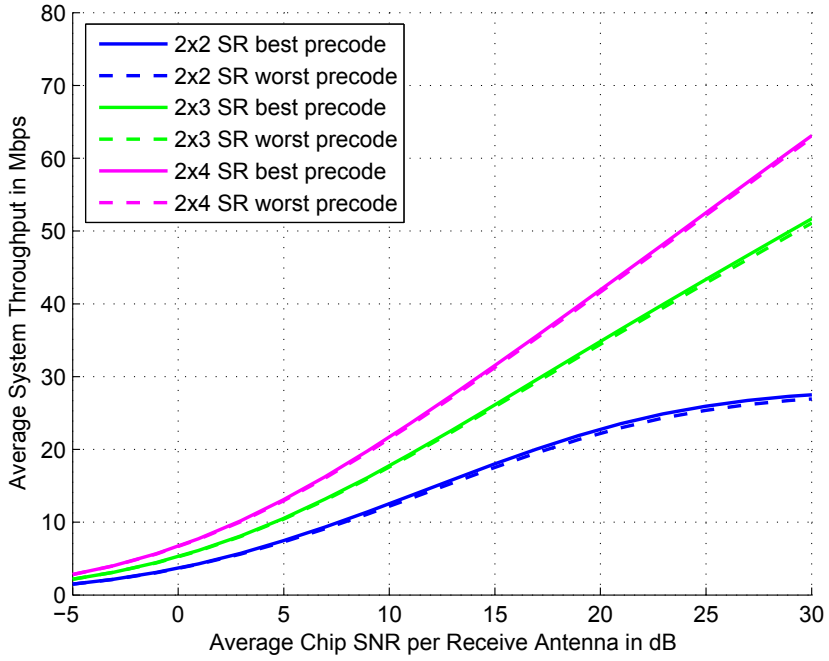


FIGURE 4.10: SV Sum Rate with 2 Transmit Antennas over (Pedestrian-B)

The difference between using more receive antennas than transmit antennas (i.e. 2×3, 2×4 and 3×4 MIMO systems) and using more transmit antennas than receive antennas, (i.e. 3×2, 4×2 and 4×3 MIMO systems) are evaluated. These comparisons are illustrated in Figure 4.11 for the non-SIC scheme and Figure 4.12 for the SIC scheme. Comparing to the systems with $N_R < N_T$ (where full channel information is available at the receiver), the sum rate loss is quite significant with partial CSIT by using the codebooks in standards for systems with $N_R < N_T$. For Pedestrian-A channel without SIC receiver at SNR of 30dB, the loss due to partial CSIT is:

- 7.5Mbps between the 3×4 and 4×3 systems;
- 12Mbps between the 2×4 and 4×2 systems and
- 7.5Mbps between the 2×3 and 3×2 systems.

However, when SIC receiver is applied, the difference in terms of sum rate between:

- 3×4 and 4×3 systems decreases from 7.5Mbps to 3Mbps;
- 2×4 and 4×2 systems decreases from 12Mbps to 5Mbps and
- 2×3 and 3×2 systems decreases from 9Mbps to 4Mbps

at SNR of 30dB.

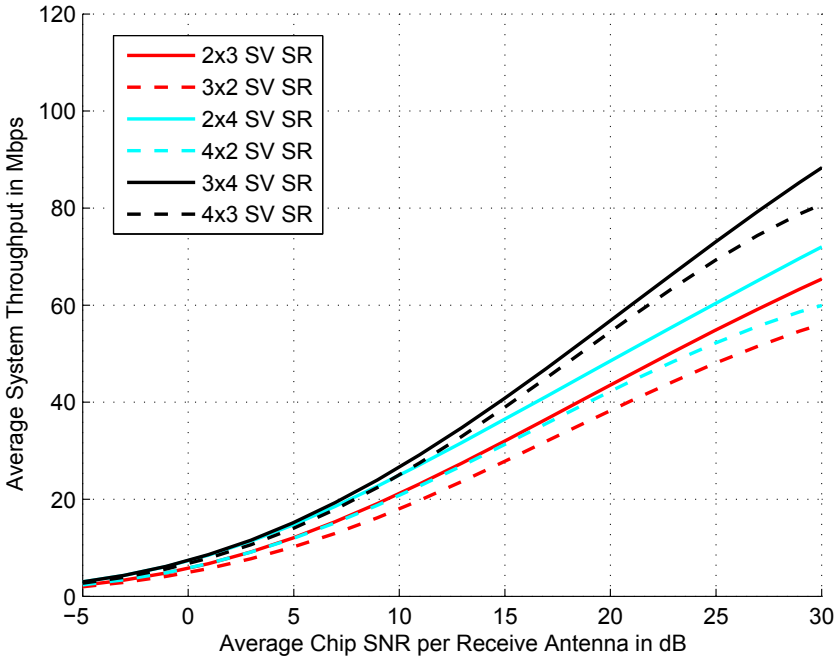


FIGURE 4.11: MIMO with non-SIC schemes for Pedestrian-A channel

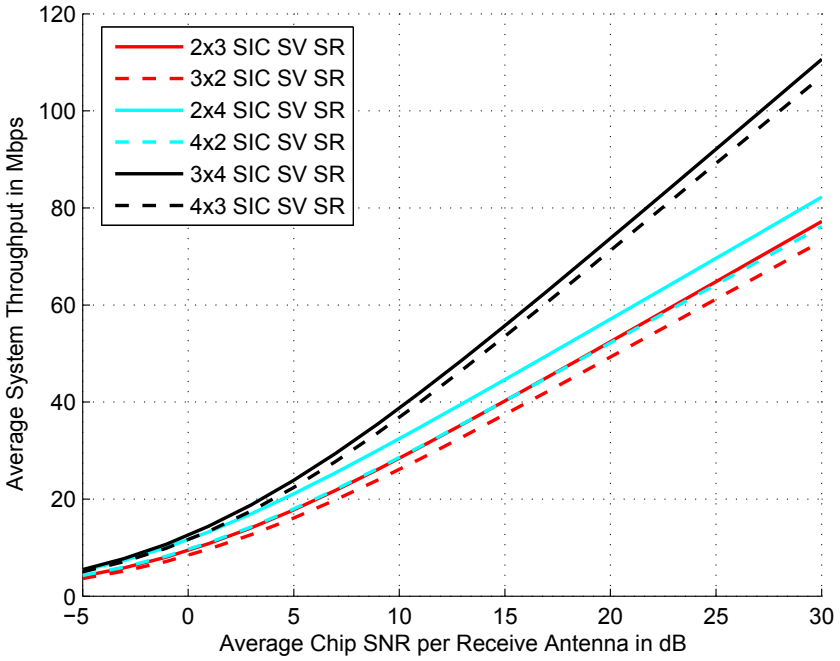


FIGURE 4.12: MIMO with SIC schemes for Pedestrian-B channel

Similar improvements are observed in the Pedestrian-B channel when using the SIC receiver. These results are illustrated in Figures 4.13 and 4.14 for the non-SIC and SIC receiver respectively. For the case without SIC receiver at SNR of 30dB, the loss

due to partial CSIT is:

- 29Mbps between the 3×4 and 4×3 systems;
- 37Mbps between the 2×4 and 4×2 systems and
- 26Mbps between the 2×3 and 3×2 systems.

However, when SIC receiver is applied, the difference in terms of sum rate between:

- 3×4 and 4×3 systems decreases from 29Mbps to 14Mbps;
- 2×4 and 4×2 systems decreases from 37Mbps to 17Mbps and
- 2×3 and 3×2 systems decreases from 26Mbps to 11.5Mbps

at SNR of 30dB. This shows that the use of SIC scheme can decrease the difference between systems with $N_R > N_T$ with partial CSIT and systems with $N_R < N_T$ by over half.

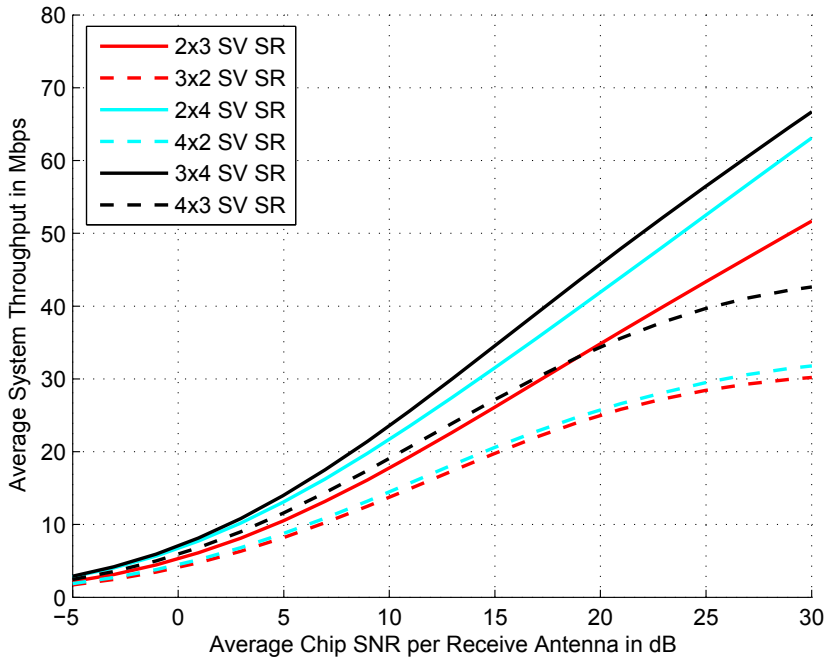


FIGURE 4.13: MIMO with non-SIC schemes for Pedestrian-A channel

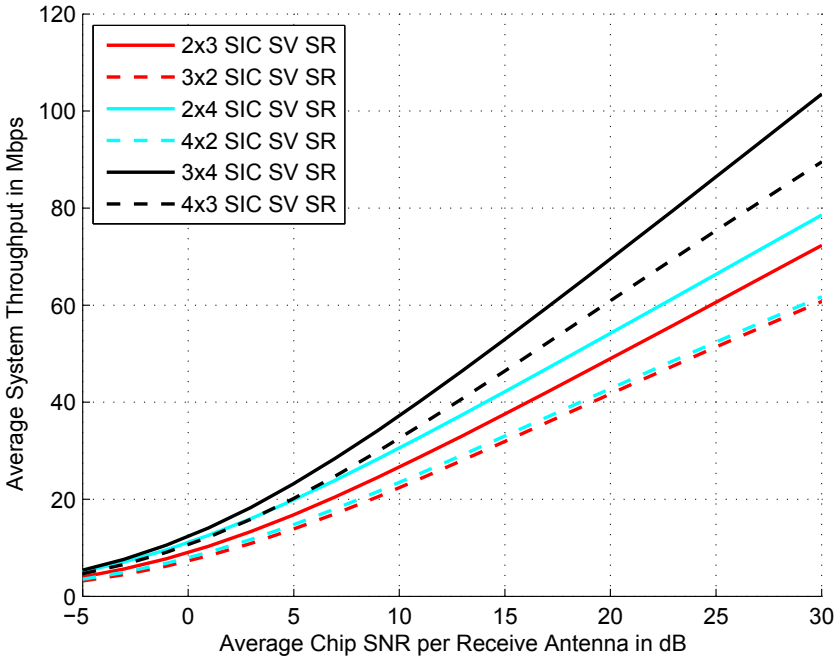


FIGURE 4.14: MIMO with SIC schemes for Pedestrian-B channel

Although increasing the number of receive antennas achieves better results than increasing the number of transmit antennas, it is difficult to install more receive antennas due to space constraints in handsets. Therefore, it will be interesting to find out if the $N_T > N_R$ MIMO systems with the proposed SIC receiver will achieve similar or better performance than the $N_T < N_R$ systems but with a simple MMSE receiver. These results are shown in Figure 4.15 for the Pedestrian-A channel and Figure 4.16 for the Pedestrian-B channel. It is found that for most cases, the use of SIC receiver with $N_T > N_R$ achieves a much higher sum rate than using a simple MMSE receiver in $N_T < N_R$ systems. For instance, at SNR of 30dB an improvement of

- 18Mbps for Pedestrian-A is observed when using 4×3 SIC system instead of the 3×4 non-SIC system;
- 22Mbps for Pedestrian-B is observed when using 4×3 SIC system instead of the 3×4 non-SIC system;
- 8Mbps for Pedestrian-A is observed when using 3×2 SIC system instead of the 2×3 non-SIC system;

- 9Mbps for Pedestrian-B is observed when using 3×2 SIC system instead of the 2×3 non-SIC system;
- 4Mbps for Pedestrian-A is observed when using 4×2 SIC system instead of the 2×4 non-SIC system;
- while similar results are observed for the Pedestrian-B when using 4×2 SIC system instead of the 2×4 non-SIC system.

This shows the significance of the use of SIC receivers to further improve the system value sum rate and provide a tradeoff between space constraints in the mobile handset and the sum rate loss due to partial CSIT when more transmit antennas are used.

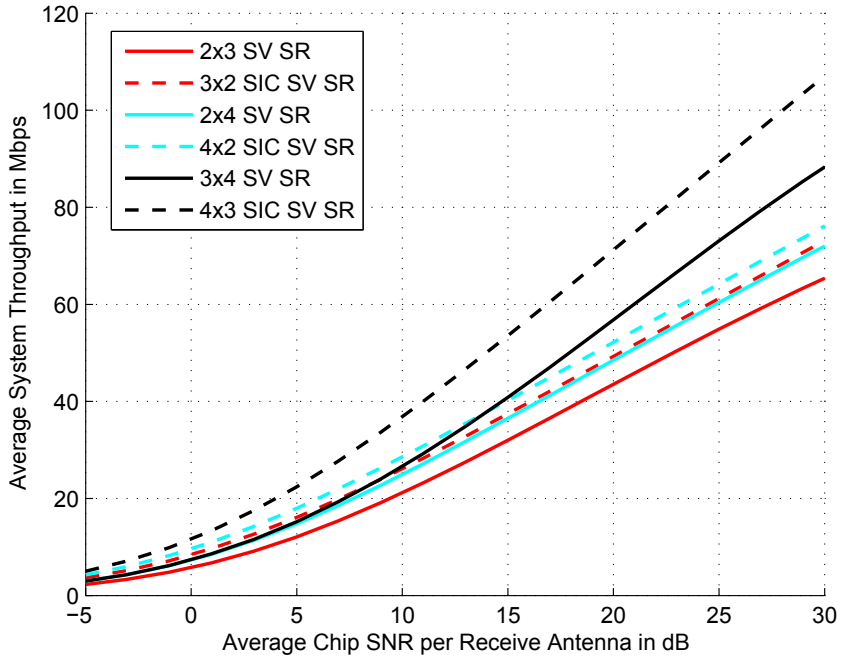


FIGURE 4.15: $2 \times 3, 2 \times 4, 3 \times 4$ non-SIC v.s. $3 \times 2, 4 \times 2, 4 \times 3$ SIC (Pedestrian-A)

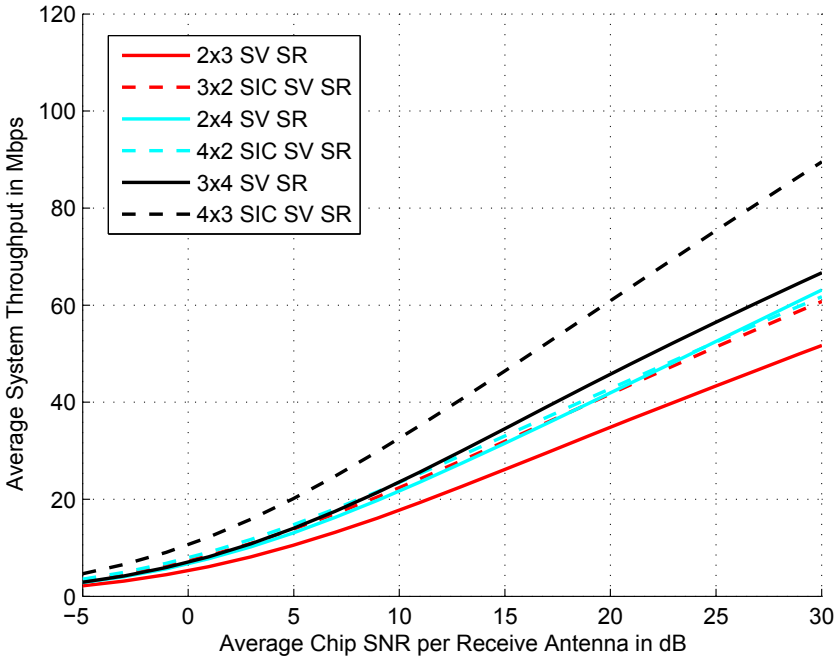


FIGURE 4.16: $2 \times 3, 2 \times 4, 3 \times 4$ non-SIC v.s. $3 \times 2, 4 \times 2, 4 \times 3$ SIC (Pedestrian-B)

4.11 Summary

In this chapter, a signature design optimisation approach that minimises the ISI was proposed. It is observed that when the SIC receiver is not implemented, there is a wide gap in terms of sum rate between the use of precoded OVSF codes and the more optimised signature sequences. However, as full CSIT is hard to obtain in FDD systems, an alternative signature sequence optimisation is proposed by removing those signature sequences with low SVs (equivalently low received SINR). This increases the overall system throughput because transmission energy is allocated to the spread channels in better conditions. Significant improvements were observed in the EETG allocation schemes with and without SIC receivers and in ESTG allocations with the MMSE receivers. Moreover, it is observed that the simple EETG approach with the non-SIC receiver with $K^{\star}$ signature sequences can achieve a system throughput close to the more complicated ESTG approach with the non-SIC receiver and without signature sequence selection.

In a TDD system, the CSIT can be exploited using channel reciprocity. However, when FDD system is used, it is important to consider the practicality of transmitter

optimisation techniques in terms of both computational complexity and the number of bits required to be fed back to the transmitter. The amount of feedback required is evaluated for the schemes proposed in this thesis including EEER, EETG (with and without signature sequence selection) and ES approaches. It is concluded that the use of EEER and EETG schemes with signature sequence selection balances the system throughput performance and the amount of feedback required in the case of FDD system.

Finally, the sum rate loss due to partial CSIT is evaluated in systems with more transmit antennas than receive antennas and vice versa. As there is a limited number of codewords available for the precoding selection, hence limited CSIT, it is expected that the sum rate of systems with $N_T > N_R$ is lower than systems with $N_R > N_T$. However, due to the space constraint at the receiver (mobile phone terminals), it is more practical to install more antennas at the transmitter (base station). By using the SIC receiver in systems with $N_T > N_R$, it is found that the sum rate is higher than in systems with $N_R > N_T$ without using SIC receiver.

Chapter 5

Summary, Conclusions and Future Work

In this thesis different ways to further increase the system throughput were studied. The use of transmitter adaptations including the simplified *system value* based ES power allocation approaches proposed in Chapter 2 and the signature sequence optimisation approaches in Chapter 4 is examined. The optimum signature sequence selection method for EE and ES schemes were proposed to further increase the system throughput without requiring much information to be fed back to the transmitter. The use of receiver optimisation was also investigated in Chapter 3, where a SIC receiver algorithm was proposed. The proposed algorithm reduces the complexity during the calculation of system values as well as the calculation of energies for ES allocations while achieving a higher system throughput.

5.1 Summary and Conclusions

In Chapter 2, the use of different power allocation strategies were studied including EEER, EETG, ESER and ESTG schemes aiming at achieving higher system throughput. However, the traditional constraint optimisation approach to search for the data rate b_p to be allocated and the energy allocation is rather computationally expensive. Therefore, the *system value* criterion was proposed in this chapter to simplify

the complexity. When the proposed system value approach is integrated with the ES allocations, the computation of ESER allocation decreased by P times, where P is the total number of discrete rates available. On the other hand, when the *system value* based ESTG scheme is implemented, the complexity reduces by $P + K^{\star} - 1$ times, where $K^{\star}$ is optimum number signature sequence.

In Chapter 3, the SIC receiver was proposed that cancels interferences in both space and time domain where significant improvement was observed in terms of sum rate compared to the SIC receiver that only cancels interference in space domain in [64]. The SIC formation can also be applied to the system value approach proposed in Chapter 2. This formation decreases the number matrix inversions of the system value calculations from $K^{\star}$ to 1, and further decreases the number of matrix inversions during the iterative energy calculations from $I_{\max}$ to 1. Furthermore, the proposed SIC algorithm was verified in terms of both sum rate and system throughput using both MATLAB simulations and experimental measurements based on the NI-PXIe testbed. In addition, it was shown that under the same conditions, the use of the proposed SIC receiver in the HSDPA system achieved a sum rate close to the more ISI resilient LTE system.

In Chapter 4, signature sequence optimisation was considered. A signature sequence design that minimises ISI and noise was proposed to further increase the sum rate when full CSIT is available. In this chapter, a novel signature sequence optimisation strategy was proposed for the FDD systems that does not require extensive CSI feedback. The proposed approach removes the signature sequences that corresponds to low received SINR so that higher rates can be allocated to the spread channels of high SINRs. The signature sequence selection algorithms were proposed for both EE and ES allocations with and without SIC receiver based on the *system values* criterion proposed in Chapter 2. These algorithms showed very significant improvements in systems without the SIC receiver and in channels with long delay spread (e.g. the Pedestrian-B channel). Finally, the sum rate is evaluated for 2×3, 3×2, 2×4, 4×2, 3×4 and 4×3 systems with partial CSIT. Although the MIMO system with $N_R > N_T$ achieves a higher sum rate than $N_T > N_R$, it is hard to implement a system with more antennas on the handsets than on the transmitter. However, if the proposed SIC

receiver is used at the receiver, the use of $N_T > N_R$ achieve a higher sum rate than the use of $N_R > N_T$ without SIC receiver, where the former set up require much less hardware at the receiver.

5.2 List of Contributions

1. Proposed the use of *system value* based ES allocation scheme which has a much less complexity than the traditional ES allocation scheme.

2. Proposed a novel SIC receiver of reduced complexity while increasing the system throughput.

3. Compared the sum rate of the proposed SIC receiver which cancels out interference in both space and time domain against the chip-level SIC in [64] which only cancels interference in the space domain. By using the proposed SIC receiver, significant increase in the sum rate especially in channels with long power delay profiles were observed.

4. Verified the validity of the proposed SIC algorithm through both MATLAB simulations and experimental measurements based on the NI-PXIe testbed.

5. Compared the sum rate of HSDPA system using the proposed SIC receiver against LTE system with MMSE receiver under similar channel conditions (identical power delay profiles) and equal bandwidth for a 2×2 MIMO configuration. This comparative studies have shown that the HSDPA system with the SIC receiver achieves a sum rate close to the more ISI resilient LTE system.

6. Proposed a signature sequence design that minimises the correlations between codes while taking ISI and noise power into consideration.

7. Proposed the signature sequence selection method that further increases the system throughput of both EE and ES allocation schemes without requiring too much feedback.

8. Studied the amount of feedback required for the different optimisation schemes including EEER, EETG, ESER and ESTG with and without signature sequence optimisation.

9. Evaluated the sum rate loss due to partial CSIT for the HSDPA MIMO system with different antenna combinations with and without the SIC receiver.

5.3 Future Work

5.3.1 Channel model with correlations and Doppler effects

Although a frequency multipath channel was used in this thesis, it has been assumed that there are no correlations between the MIMO channel coefficients. Considering the use of more receive antennas in a mobile station where it only has a limited space, there should be partial correlations between the channel coefficients. Additionally, in a situation where the user is moving in a moderate to high speed, the Doppler effects should also be considered. It is therefore desirable to further investigate the performance of the schemes proposed in this thesis under a channel model with further assumptions.

5.3.2 Extend the work to minimise inter-cell interference

In this thesis, it has been assumed that the mobile station is located at the center of a cell, where the interference between cells are limited and therefore not considered. However, when a user travels to places closer to cell boundaries, the inter-cell interference can be quite severe [107]. A more extensive system model should that considers inter-cell interference should be formed; and the effects and performance of inter-cell interference should be explored. Furthermore, the SIC receiver proposed in this chapter should be extended such that it cancels both intra-cell interference as well as inter-cell interference.

5.3.3 Codebook design with more codewords

The amount of sum rate loss due to partial channel information at the transmitter has been observed in the Chapter 4 when using the current set of precoding. On the other hand, although the number of codewords in the HSDPA and LTE codebooks is the same, equal or more feedback is required in the LTE system depending whether feedback is carried out in a wideband or subband basis. It will be interesting to find out the performance difference for both cases. Similarly, an evaluation can be carried out to find out the improvement in terms of sum rate and system throughput in the HSDPA systems by increasing the size of the codebook. Therefore, a codebook with more codewords can be designed and that the optimum balance between the amount of feedback information and sum rate improvements should be considered.

Publications Arising from This Work

The following papers were accepted for publications during my PhD studies:

1. Mustafa. K. Gurcan, **Irina Ma**, Anusorn Chungtragarn, Hamdi Joudeh, "System Value-based Optimum Spreading Sequence Selection for High-Speed Downlink Packet Access (HSDPA) MIMO", in *EURASIP Journal on Wireless Communications and Networking,* Springer International Publishing, 2013, pp. 1-19.

2. Mustafa. K. Gurcan, **Irina Ma**, Hadhrami Ab Ghani, "The Interference-reduced Energy Loading for Multi-Code HSDPA System", in *EURASIP Journal on Wireless Communications and Networking*, Springer International Publishing, 2012, pp. 1-17.

3. Mustafa. K. Gurcan, Hadhrami Ab Ghani, **Irina Ma**,"Successive Interference Cancellation for Two-group Resource Allocation", in *Personal, Indoor and Mobile Radio Communications (PIMRC), 2011 IEEE 22nd International Symposium on*, pp.157-161, Sep 2011.

4. Mustafa. K. Gurcan, **Irina Ma**, Hadhrami Ab Ghani and Zhenfeng He,"Complexity Reduction for Multi-hop Network End-to-end Delay Minimization" in *Computer and Information Sciences II*, Springer London, 2012, pp. 231-237.

5. Mustafa. K. Gurcan, **Irina Ma**, Hamdi Joudeh, Qinxin Liu, "Building a Next-Generation Test System for Next-Generation Wireless Communication With PXI Express and LabVIEW", 2013.

Available at http://sine.ni.com/cs/app/doc/p/id/cs-15646

This article has been entered for the GSDA awards 2013 by the National Instruments where finalist was awarded under the RF and Communications category

Appendix A

The Proof of $\mathbf{D}_k^{-1}$ and $\mathbf{C}_k^{-1}$ (Chapter 3)

This appendix shows the proof of the simplified $\mathbf{D}_k^{-1}$ as a function of $\mathbf{C}_{k-1}^{-1}$ and the formation of $\mathbf{C}_k^{-1}$ in terms of $\mathbf{C}_{k-1}^{-1}$. The formation/proof of the simplified $\mathbf{D}_k^{-1}$ and $\mathbf{C}_k^{-1}$ requires the use of matrix inversion lemma on $\mathbf{D}_k$ and $\mathbf{C}_k$. The matrix inversion lemma is defined below:

$$(\mathbf{B}+\mathbf{U}\mathbf{V}\mathbf{U}^H)^{-1} = \mathbf{B}^{-1} - \mathbf{B}^{-1}\mathbf{U}(\mathbf{V}^{-1}+\mathbf{U}^H\mathbf{B}^{-1}\mathbf{U})^{-1}\mathbf{U}^H\mathbf{B}^{-1} \tag{A.1}$$

In Chapter 3, it has been shown that the equation for $\mathbf{C}_k$ is given as:

$$\begin{aligned} \mathbf{C}_k &= \mathbf{C}_{k-1} + E_k \underline{q}_k \underline{q}_k^H + E_k \underline{q}_{k,1} \underline{q}_{k,1}^H + E_k \underline{q}_{k,2} \underline{q}_{k,2}^H & \text{(A.2)} \\ &= \mathbf{D}_k + E_k \underline{q}_k \underline{q}_k^H & \text{(A.3)} \end{aligned}$$

where

$$\begin{aligned} \mathbf{D}_k &= \mathbf{C}_{k-1} + E_k \underline{q}_{k,1} \underline{q}_{k,1}^H + E_k \underline{q}_{k,2} \underline{q}_{k,2}^H & \text{(A.4)} \\ &= \mathbf{D}_{1,k} + E_k \underline{q}_{k,2} \underline{q}_{k,2}^H & \text{(A.5)} \end{aligned}$$

with

$$\mathbf{D}_{1,k} = \mathbf{C}_{k-1} + E_k \underline{q}_{k,1} \underline{q}_{k,1}^H. \tag{A.6}$$

A.1 The formation of $\mathbf{D}_k^{-1}$

To find $\mathbf{D}_k^{-1}$ as a function of $\mathbf{C}_{k-1}^{-1}$, perform the matrix inversion lemma on Equation (A.5) to obtain:

$$\begin{aligned} \mathbf{D}_k^{-1} &= \mathbf{D}_{1,k}^{-1} - \mathbf{D}_{1,k}^{-1} \underline{q}_{k,2} (E_k^{-1} + \underline{q}_{k,2}^H \mathbf{D}_{1,k}^{-1} \underline{q}_{k,2})^{-1} \underline{q}_{k,2}^H \mathbf{D}_{1,k}^{-1} && \text{(A.7)} \\ &= \mathbf{D}_{1,k}^{-1} - \frac{E_k \mathbf{D}_{1,k}^{-1} \underline{q}_{k,2} \underline{q}_{k,2}^H \mathbf{D}_{1,k}^{-1}}{1 + E_k \underline{q}_{k,2}^H \mathbf{D}_{1,k}^{-1} \underline{q}_{k,2}}. && \text{(A.8)} \end{aligned}$$

Similarly, perform matrix inversion lemma on Equation (A.6) which yields:

$$\mathbf{D}_{1,k}^{-1} = \mathbf{C}_{k-1}^{-1} - \frac{E_k \mathbf{C}_{k-1}^{-1} \underline{q}_{k,1} \underline{q}_{k,1}^H \mathbf{C}_{k-1}^{-1}}{1 + E_k \underline{q}_{k,1}^H \mathbf{C}_{k-1}^{-1} \underline{q}_{k,1}}. \tag{A.9}$$

By substituting Equation (A.9) into Equation (A.8),

$$\begin{aligned} \mathbf{D}_k^{-1} &= \mathbf{C}_{k-1}^{-1} - \frac{E_k \mathbf{C}_{k-1}^{-1} \underline{q}_{k,1} \underline{q}_{k,1}^H \mathbf{C}_k^{-1}}{1 + E_k \underline{q}_{k,1}^H \mathbf{C}_{k-1}^{-1} \underline{q}_{k,1}} - \frac{E_k \mathbf{D}_{1,k}^{-1} \underline{q}_{k,2} \underline{q}_{k,2}^H \mathbf{D}_{1,k}^{-1}}{1 + E_k \underline{q}_{k,2}^H \mathbf{D}_{1,k}^{-1} \underline{q}_{k,2}} && \text{(A.10)} \\ &= \mathbf{C}_{k-1}^{-1} - \frac{E_k \mathbf{C}_{k-1}^{-1} \underline{q}_{k,1} \underline{q}_{k,1}^H \mathbf{C}_k^{-1}}{1 + E_k \underline{q}_{k,1}^H \mathbf{C}_{k-1}^{-1} \underline{q}_{k,1}} && \text{(A.11)} \\ &\quad - \frac{E_k \left(\mathbf{C}_{k-1}^{-1} - \frac{E_k \mathbf{C}_{k-1}^{-1} \underline{q}_{k,1} \underline{q}_{k,1}^H \mathbf{C}_{k-1}^{-1}}{1 + E_k \underline{q}_{k,1}^H \mathbf{C}_{k-1}^{-1} \underline{q}_{k,1}} \right) \underline{q}_{k,2} \underline{q}_{k,2}^H \left(\mathbf{C}_{k-1}^{-1} - \frac{E_k \mathbf{C}_{k-1}^{-1} \underline{q}_{k,1} \underline{q}_{k,1}^H \mathbf{C}_{k-1}^{-1}}{1 + E_k \underline{q}_{k,1}^H \mathbf{C}_{k-1}^{-1} \underline{q}_{k,1}} \right)}{1 + E_k \underline{q}_{k,2}^H \left(\mathbf{C}_{k-1}^{-1} - \frac{E_k \mathbf{C}_{k-1}^{-1} \underline{q}_{k,1} \underline{q}_{k,1}^H \mathbf{C}_{k-1}^{-1}}{1 + E_k \underline{q}_{k,1}^H \mathbf{C}_{k-1}^{-1} \underline{q}_{k,1}} \right) \underline{q}_{k,2}}. \end{aligned}$$

Using $\underline{d}_1 = \mathbf{C}_{k-1}^{-1} \underline{q}_{k,1}, \underline{d}_2 = \mathbf{C}_{k-1}^{-1} \underline{q}_{k,2}, \xi_1 = \underline{q}_{k,1}^H \underline{d}_1, \xi_2 = \underline{q}_{k,2}^H \underline{d}_2, \xi_5 = \underline{q}_{k,1}^H$ and $\zeta_1 = \frac{E_k}{1 + E_k \xi_1}$, the above expression becomes:

$$\begin{aligned} \mathbf{D}_k^{-1} &= \mathbf{C}_{k-1}^{-1} - \zeta_1 \underline{d}_1 \underline{d}_1^H && \text{(A.12)} \\ &\quad - \frac{E_k \left(\mathbf{C}_{k-1}^{-1} \underline{q}_{k,2} - \zeta_1 \underline{d}_1 \underline{q}_{k,1}^H \mathbf{C}_{k-1}^{-1} \underline{q}_{k,2} \right) \left(\underline{q}_{k,2}^H \mathbf{C}_{k-1}^{-1} - \underline{q}_{k,2}^H \zeta_1 \mathbf{C}_{k-1}^{-1} \underline{q}_{k,1} \underline{d}_1^H \right)}{1 + E_k \left(\underline{q}_{k,2}^H \mathbf{C}_{k-1}^{-1} \underline{q}_{k,2} - \underline{q}_{k,2}^H \zeta_1 \mathbf{C}_{k-1}^{-1} \underline{q}_{k,1} \underline{q}_{k,1}^H \mathbf{C}_{k-1}^{-1} \underline{q}_{k,2} \right)}. \end{aligned}$$

By substituting $\underline{d}_2 = \mathbf{C}_{k-1}^{-1}\underline{q}_{k,2}$, $\xi_5 = \underline{q}_{k,1}^H\underline{d}_2, \xi_2 = \underline{q}_{k,2}^H\underline{d}_2$, the above expression is simplified to:

$$\mathbf{D}_k^{-1} = \mathbf{C}_{k-1}^{-1} - \zeta_1\underline{d}_1\underline{d}_1^H - \frac{E_k\left(\underline{d}_2 - \zeta_1\underline{d}_1\xi_5\right)\left(\underline{d}_2^H - \zeta_1\xi_5^*\underline{d}_1^H\right)}{1 + E_k\left(\xi_2 - \zeta_1\left|\xi_5\right|^2\right)}. \tag{A.13}$$

Through expanding the above equation and substituting $\mathbf{Z}_1 = \underline{d}_1\underline{d}_1^H, \mathbf{Z}_2 = \underline{d}_2\underline{d}_2^H, \mathbf{Z}_3 = \underline{d}_1\underline{d}_2^H$ into the expression to yield:

$$\mathbf{D}_k^{-1} = \mathbf{C}_{k-1}^{-1} - \zeta_1\mathbf{Z}_1 - \frac{E_k\left(\mathbf{Z}_2 - \zeta_1\xi_5^*\mathbf{Z}_3^H - \zeta_1\xi_5\mathbf{Z}_3 + \zeta_1^2\left|\xi_5\right|^2\mathbf{Z}_1\right)}{1 + E_k\left(\xi_2 - \zeta_1\left|\xi_5\right|^2\right)}. \tag{A.14}$$

By letting $\zeta_2 = \frac{E_k}{1+E_k\left(\xi_2-\zeta_1\left|\xi_5\right|^2\right)}$, the above expression can be simplified to:

$$\begin{aligned}\mathbf{D}_k^{-1} &= \mathbf{C}_{k-1}^{-1} - \zeta_1\mathbf{Z}_1 - \zeta_2\left(\mathbf{Z}_2 - \zeta_1\xi_5^*\mathbf{Z}_3^H - \zeta_1\xi_5\mathbf{Z}_3 + \zeta_1^2\left|\xi_5\right|^2\mathbf{Z}_1\right) &\text{(A.15)}\\ &= \mathbf{C}_{k-1}^{-1} - \left(\zeta_1 + \zeta_1^2\zeta_2\left|\xi_5\right|^2\right)\mathbf{Z}_1 - \zeta_2\mathbf{Z}_2 + \zeta_1\zeta_2\left(\xi_5\mathbf{Z}_3 + \xi_5^*\mathbf{Z}_3^H\right). &\text{(A.16)}\end{aligned}$$

The above expression is the same as Equation (3.16).

A.2 The formation of $\mathbf{C}_k^{-1}$

To find $\mathbf{C}_k^{-1}$ in terms of $\mathbf{D}_k^{-1}$, perform matrix inversion lemma on $\mathbf{C}_k = \mathbf{D}_k + E_k\underline{q}_k\underline{q}_k^H$

$$\mathbf{C}_k^{-1} = \mathbf{D}_k^{-1} - \frac{E_k\mathbf{D}_k^{-1}\underline{q}_k\underline{q}_k^H\mathbf{D}_k^{-1}}{1 + E_k\underline{q}_k^H\mathbf{D}_k^{-1}\underline{q}_k}. \tag{A.17}$$

Then, substitute $\underline{d}_3 = \mathbf{D}_k^{-1}\underline{q}_k$ to form:

$$\mathbf{C}_k^{-1} = \mathbf{D}_k^{-1} - \frac{E_k\underline{d}_3\underline{d}_3^H}{1 + E_k\underline{q}_k^H\mathbf{D}_k^{-1}\underline{q}_k}. \tag{A.18}$$

By letting $\mathbf{Z}_4 = \underline{d}_3\underline{d}_3^H$, the above expression is simplified to:

$$\mathbf{C}_k^{-1} = \mathbf{D}_k^{-1} - \frac{E_k\mathbf{Z}_4}{1+E_k\underline{q}_k^H\mathbf{D}_k^{-1}\underline{q}_k} \tag{A.19}$$

$$= \mathbf{D}_k^{-1} - \frac{E_k\mathbf{Z}_4}{1+E_k\underline{q}_k^H\left(\mathbf{C}_{k-1}^{-1} - \left(\zeta_1+\zeta_1^2\zeta_2\left|\xi_5\right|^2\right)\mathbf{Z}_1 - \zeta_2\mathbf{Z}_2 + \zeta_1\zeta_2\left(\xi_5\mathbf{Z}_3 + \xi_5^*\mathbf{Z}_3^H\right)\right)\underline{q}_k}. \tag{A.20}$$

Substitute $\xi = \underline{q}_k^H\underline{d}, \xi_3 = \underline{q}_k^H\underline{d}_1, \xi_4 = \underline{q}_k^H\underline{d}_2, \xi_6 = \mathrm{Re}(\xi_3\xi_4^*\xi_5), \underline{d}_1\underline{d}_1^H = \mathbf{Z}_1, \underline{d}_2\underline{d}_2^H = \mathbf{Z}_2$ and $\underline{d}_1\underline{d}_2^H = \mathbf{Z}_3$, to yield

$$\mathbf{C}_k^{-1} = \mathbf{D}_k^{-1} - \frac{E_k\mathbf{Z}_4}{1+E_k\left(\xi-\zeta_1\left|\xi_3\right|^2 - \left|\xi_3\right|^2\zeta_1^2\zeta_2\left|\xi_5\right|^2 - \zeta_2\left|\xi_4\right|^2 + \zeta_1\zeta_2\left(\xi_5\xi_3\xi_4^* + \xi_5^*\xi_3^*\xi_4\right)\right)} \tag{A.21}$$

$$= \mathbf{D}_k^{-1} - \frac{E_k\mathbf{Z}_4}{1+E_k\left(\xi-\zeta_1\left|\xi_3\right|^2 - \zeta_2\left(\left|\xi_3\right|^2\zeta_1^2\left|\xi_5\right|^2 + \left|\xi_4\right|^2 - 2\zeta_1\xi_6\right)\right)}. \tag{A.22}$$

Defining $\zeta = \frac{E_k}{1+E_k\left(\xi-\zeta_1\left|\xi_3\right|^2-\zeta_2\left(\left|\xi_4\right|^2-2\zeta_1\xi_6+\zeta_1^2\left|\xi_3\right|^2\left|\xi_5\right|^2\right)\right)}$, the above expression is simplified to:

$$\mathbf{C}_k^{-1} = \mathbf{D}_k^{-1} - \zeta\mathbf{Z}_4 \tag{A.23}$$

which is the same as Equation (3.20).

Similarly, by substituting $\mathbf{D}_k^{-1}$ in Equation (A.16) and letting $\xi = \underline{q}_k^H\underline{d}, \xi_3 = \underline{q}_k^H\underline{d}_1, \xi_4 = \underline{q}_k^H\underline{d}_2, \xi_6 = \mathrm{Re}(\xi_3\xi_4^*\xi_5), \underline{d}_1\underline{d}_1^H = \mathbf{Z}_1, \underline{d}_2\underline{d}_2^H = \mathbf{Z}_2$ and $\underline{d}_1\underline{d}_2^H = \mathbf{Z}_3$, the iterative energy calculation can be reformed as:

$$E_{k,i} = \frac{\gamma_{tar}}{\underline{q}_k^H\mathbf{D}_{k,i}^{-1}\underline{q}_k} \tag{A.24}$$

$$= \frac{\gamma_{tar}}{\xi - \zeta_{1,(i-1)}\left|\xi_3\right|^2 - \zeta_{2,(i-1)}\left(\left|\xi_4\right|^2 - 2\zeta_1\xi_6 + \zeta_{1,(i-1)}^2\left|\xi_3\right|^2\left|\xi_5\right|^2\right)} \tag{A.25}$$

which is the same as Equation (3.25).

Appendix B

The Chip Level SIC receiver (Chapter 3)

This appendix provides the chip level SIC formulation in [64] that was used for comparison purposes in Chapter 3. This chip-level SIC receiver detects and cancels MIMO signals in a stream by stream basis starting from stream 1. The total number of MIMO streams as $N_S = \min(N_T, N_R)$ with streams $n_s = 1, \ldots, N_S$. In this chip-level SIC receiver formation, three precoding matrices is defined:

- the full precoding matrix $\mathbf{F}$,
- the precoding matrix for the detected streams $\mathbf{F}_d^{(n_s)}$ and
- the precoding matrix for the remaining streams $\mathbf{F}_r^{(n_s)}$.

In Chapter 3, the 2×2 MIMO HSDPA system was examined. Therefore, the formation of the precoding matrix in this appendix is based on the codebook described in Section 2.2.4 in page 42. The full precoding matrix given in Equation (2.26) is formed as:

$$\mathbf{F} = \begin{bmatrix} F_1 & F_1 \\ F_2 & -F_2 \end{bmatrix}. \tag{B.1}$$

At the start of processing stream 2, the precoding matrix for the detected stream (stream 1 in this case) is given as follows:

$$\mathbf{F}_d^{(2)} = \begin{bmatrix} F_1 & 0 \\ F_2 & 0 \end{bmatrix} \tag{B.2}$$

while the precoding matrix of the remaining stream (stream 2) can be formed as follows:

$$\mathbf{F}_r^{(2)} = \begin{bmatrix} 0 & f_1 \\ 0 & -f_2 \end{bmatrix}. \tag{B.3}$$

However, because no detection/cancellation has taken place at the start of processing stream 1 ($n_s = 1$), hence, $\mathbf{F}_r^{(1)} = \mathbf{F}$ and $\mathbf{F}_d^{(1)}$ is a zero matrix.

The signature sequence for MIMO system is formed by combining precoding with the OVSF codes $\mathbf{S}_{OVSF}$such that $\mathbf{S}_F = \mathbf{F} \otimes \mathbf{S}_{OVSF} \in \mathbb{C}^{N_T N \times N_S N}$. Simiarly, the MIMO signature sequence set with precoding of the detected stream is formed as:

$$\mathbf{S}_d^{(n_s)} = \mathbf{F}_d^{(n_s)} \otimes \mathbf{S}_{OVSF} \tag{B.4}$$

and the signature sequence set of the remaining MIMO streams is formed as

$$\mathbf{S}_r^{(n_s)} = \mathbf{F}_r^{(n_s)} \otimes \mathbf{S}_{OVSF}. \tag{B.5}$$

Therefore, when $n_s = 1, \mathbf{S}_{r,n_s}^{(1)} = \mathbf{S}_F$.

Assuming all the spreading sequences are used, the transmit signal of the current symbol period is then given by:

$$\underline{z}(\rho) = \begin{bmatrix} \underline{z}_1(\rho) \\ \underline{z}_2(\rho) \\ \vdots \\ \underline{z}_{N_T}(\rho) \end{bmatrix} = \mathbf{S}_F \mathbf{A} \underline{y}(\rho) \in \mathbb{C}^{N_T N \times 1} \tag{B.6}$$

where $\underline{y}(\rho)$ is defined in Equation (2.2) and $\mathbf{A}$ is defined in Section 2.4. Similarly, the transmit signal for the detected signal of the current symbol period is given by:

$$\underline{z}_d^{(n_s)}(\rho) = \begin{bmatrix} \underline{z}_{d,1}^{(n_s)}(\rho) \\ \underline{z}_{d,2}^{(n_s)}(\rho) \\ \vdots \\ \underline{z}_{d,N_T}^{(n_s)}(\rho) \end{bmatrix} = \mathbf{S}_d^{(n_s)} \mathbf{A} \underline{y}(\rho) \in \mathbb{C}^{N_T N \times 1}. \tag{B.7}$$

Then, the entire packet containing $N^{(x)}$ transmit symbol for each n_t^{th} antenna can be represented as:

$$\underline{z}_{n_t} = \left[\underline{z}_{n_t}(1), ..., \underline{z}_{n_t}(\rho), ..., \underline{z}_{n_t}(N^{(x)}) \right] \in \mathbb{C}^{NN^{(x)} \times 1} \tag{B.8}$$

and for the detected signal at each n_t^{th} antenna for the n_s^{th} stream as:

$$\underline{z}_{d,n_t}^{(n_s)} = \left[\underline{z}_{d,n_t}^{(n_s)}(1), ..., \underline{z}_{d,n_t}^{(n_s)}(\rho), ..., \underline{z}_{d,n_t}^{(n_s)}(N^{(x)}) \right] \in \mathbb{C}^{NN^{(x)} \times 1}. \tag{B.9}$$

Since there are no detected signals at the start of processing stream 1, $\underline{z}_{d,n_t}^{(1)} = \underline{0}_{NN^{(x)}}$.

B.1 Channel

Given the channel impulse response between the n_t^{th} and n_r^{th} antenna paris as:

$$\underline{h}^{(n_r n_t)} = \left[h_0^{(n_r n_t)}, ..., h_{L-1}^{(n_r n_t)} \right]^T, \tag{B.10}$$

the convolution matrix for this chip level formulation is formed as:

$$\mathbf{H}_c^{(n_r, n_t)} = \begin{bmatrix} h_0^{(n_r n_t)} & \cdots & h_{L-1}^{(n_r n_t)} & 0 & \cdots & 0 \\ 0 & h_0^{(n_r n_t)} & \cdots & h_{L-1}^{(n_r n_t)} & \ddots & \vdots \\ \vdots & \ddots & \ddots & \ddots & \ddots & 0 \\ 0 & \cdots & 0 & h_0^{(n_r n_t)} & \cdots & h_{L-1}^{(n_r n_t)} \end{bmatrix} \in \mathbb{C}^{L_f \times (L + L_f - 1)} \tag{B.11}$$

where L_f is the length of the MMSE filter ($L_f = 30$ was used in this thesis). The overall MIMO channel is given as:

$$\mathbf{H}_c = \begin{bmatrix} \mathbf{H}_c^{(1,1)} & \cdots & \mathbf{H}_c^{(1,N_T)} \\ \vdots & \ddots & \vdots \\ \mathbf{H}_c^{(N_R,1)} & \cdots & \mathbf{H}_c^{(N_R,N_T)} \end{bmatrix} \in \mathbb{C}^{N_R L_f \times N_T(L+L_f-1)}. \tag{B.12}$$

The channel matrix with precoding is then given as:

$$\mathbf{H}_F = \mathbf{H}_c(\mathbf{F} \otimes \mathbf{I}_{L_f+L-1}) \in \mathbb{C}^{N_R L_f \times N_T(L+L_f-1)} \tag{B.13}$$

while the channel matrix with the precoding of the remaining (yet to be detected) streams is given as:

$$\mathbf{H}_{F_r}^{(n_s)} = \mathbf{H}_c(\mathbf{F}_r^{(n_s)} \otimes \mathbf{I}_{L_f+L-1}) \in \mathbb{C}^{N_R L_f \times N_T(L+L_f-1)}. \tag{B.14}$$

Similarly, at the start of processing stream 1, i.e. $n_s = 1$, $\mathbf{H}_{F_r}^{(1)} = \mathbf{H}_F$.

B.2 Receiver

The received signal of each n_r^{th} antenna is formed as a convolution of the transmitted streams and the channel impulse responses as follows:

$$\underline{r}_{o,n_r} = \underline{z}_1 * \underline{h}^{(n_r 1)} + ... + \underline{z}_{N_T} * \underline{h}^{(n_r N_T)} + \underline{n} \in \mathbb{C}^{(NN^{(x)}+L-1)\times 1} \tag{B.15}$$

where $\underline{n}$ is the noise vector. The detected signal for each n_r^{th} antenna at each n_s^{th} stream is formed as:

$$\underline{r}_{d,n_r}^{(n_s)} = \underline{z}_{d,1}^{(n_s)} * \underline{h}^{(n_r 1)} + ... + \underline{z}_{d,N_T}^{(n_s)} * \underline{h}^{(n_r N_T)} + \underline{n} \in \mathbb{C}^{(NN^{(x)}+L-1)\times 1} \tag{B.16}$$

while the yet to be detected signal for each n_r^{th} antenna at each n_s^{th} stream is given as:

$$\underline{r}_{r,n_r}^{(n_s)} = \underline{r}_{o,n_r} - \underline{r}_{d,n_r}^{(n_s)} \in \mathbb{C}^{(NN^{(x)}+L-1)\times 1}. \tag{B.17}$$

This implies that at the start of processing stream 1, $\underline{r}_{d,n_r}^{(1)} = \underline{0}_{(NN^{(x)}+L-1)}$ and $\underline{r}_{r,n_r}^{(1)} = \underline{r}_{o,n_r}$.

B.2.1 MMSE Filter

The MMSE filter coefficients of each MIMO stream is given as:

$$\underline{f}^{(n_s)} = \begin{bmatrix} \underline{f}_1^{(n_s)} \\ \vdots \\ \underline{f}_{N_R}^{(n_s)} \end{bmatrix} \in \mathbb{C}^{N_R L_f \times 1} \tag{B.18}$$

where

$$\underline{f}_{n_r}^{(n_s)} = \left[f_{n_r}^{(n_s)}(1), ..., f_{n_r}^{(n_s)}(L_f) \right] \in \mathbb{C}^{L_f \times 1}. \tag{B.19}$$

These filter coefficients are calculated as follows:

$$\underline{f}^{(n_s)} = \begin{bmatrix} \underline{f}_1^{(n_s)} \\ \vdots \\ \underline{f}_{N_R}^{(n_s)} \end{bmatrix} = \frac{1}{g^{(n_s)}} \left(\mathbf{C}_r^{(n_s)} \right)^{-1} \mathbf{H}_{F_r}^{(n_s)} \underline{e}_\tau^{(n_s)} \tag{B.20}$$

where $\underline{e}_\tau^{(n_s)}$ is a vector with zeros except a single "1" at $[(n_s - 1)(L_f + L - 1) + (\tau + 1)]^{th}$ element, with $\tau \geq L$ representing the delay of the equalizer ($\tau = 20$ was used in this thesis); while $\mathbf{C}_r^{(n_s)}$ is the covariance matrix given as:

$$\mathbf{C}_r^{(n_s)} = \frac{E_c}{N_s} \left(\mathbf{H}_{F_r}^{(n_s)} \left(\mathbf{H}_{F_r}^{(n_s)} \right)^H \right) + N_0 \mathbf{I}_{N_R L_f} \in \mathbb{C}^{N_R L_f \times N_R L_f} \tag{B.21}$$

and $g^{(n_s)}$ is the normalisation factor formed as follows:

$$g^{(n_s)} = \left| \left(\mathbf{H}_{F_r}^{(n_s)} \underline{e}_\tau^{(n_s)} \right)^H \left(\mathbf{C}_r^{(n_s)} \right)^{-1} \mathbf{H}_{F_r}^{(n_s)} \underline{e}_\tau^{(n_s)} \right|. \tag{B.22}$$

B.2.2 Estimation and Detection

The estimated signal (with delays) is formed by convoluting the yet to be detected (remaining) received signals $\underline{r}_{r,n_r}^{(n_s)}$ with the conjugate of the filter coefficients.

$$\underline{z}_{est}^{(n_s)} = \underline{r}_{r,1}^{(n_s)} * \left(f^{(1,n_s)}\right)^* + ... + \underline{r}_{r,N_r}^{(n_s)} * \left(f^{(N_R,n_s)}\right)^* \in \mathbb{C}^{(N^{(x)}N+L+L_f-2)\times 1}. \quad \text{(B.23)}$$

However, the above expression contains the delay samples. Therefore, to recover the useful signal, the delay elements (first τ samples) and the last $(L+L_f-\tau-2)$ samples needs to be discarded as shown below:

$$\underline{\hat{z}}_{est}^{(n_s)} = \left[\hat{z}_{est,1}^{(n_s)}, ..., \hat{z}_{est,N^{(x)}N}^{(n_s)}\right] = \left[z_{est,\tau+1}^{(n_s)}, ..., z_{est,\tau+N^{(x)}N1}^{(n_s)}\right] \quad \text{(B.24)}$$

$$= \begin{bmatrix} \underline{\hat{z}}_{est}^{(n_s)}(1) \\ \vdots \\ \underline{\hat{z}}_{est}^{(n_s)}(\rho) \\ \vdots \\ \underline{\hat{z}}_{est}^{(n_s)}(N^{(x)}) \end{bmatrix} \in \mathbb{C}^{NN^{(x)}} \quad \text{(B.25)}$$

where $\underline{\hat{z}}_{est}^{(n_s)}(\rho) \in \mathbb{C}^{N^{(x)}\times 1}$ is the estimated signal of symbol period ρ. Then, form $\mathbf{Z}_{est}^{(n_s)}$ as follows:

$$\mathbf{Z}_{est}^{(n_s)} = \left[\underline{\hat{z}}_{est}^{(n_s)}(1), ..., \underline{\hat{z}}_{est}^{(n_s)}(\rho), ..., \underline{\hat{z}}_{est}^{(n_s)}(N^{(x)})\right] \in \mathbb{C}^{N\times N^{(x)}}. \quad \text{(B.26)}$$

The symbols are then recovered by multiplying $\mathbf{Z}_{est}^{(n_s)}$ and the conjugate transpose of OVSF codes $\mathbf{S}_{OVSF}$:

$$\hat{\mathbf{X}}^{(n_s)} = \left(\mathbf{S}_{OVSF}^H \mathbf{Z}_{est}^{(n_s)}\right)^T \in \mathbb{C}^{N^{(x)}\times N}, \quad \text{(B.27)}$$

and the $\hat{\mathbf{X}}$ matrix can be formed as

$$\hat{\mathbf{X}} = \left[\hat{\mathbf{X}}^{(1)}, ..., \hat{\mathbf{X}}^{(n_s)}, ..., \hat{\mathbf{X}}^{(N_S)}\right] \in \mathbb{C}^{N^{(x)}\times N_s N}. \quad \text{(B.28)}$$

Appendix C

Supplementary Material for the Testbedding System (Chapter 3)

In this appendix, further materials are provided that is related to the testbedding system in Chapter 3. Firstly, an overview of testbeds and prototypes is described. Then, a more detailed system model for the NI-PXIe testbed system used in thesis is presented. Finally, more practical results for the EVA channel are shown in this appendix to illustrate that the proposed SIC receiver achieves similar behaviour as simulations not only in Pedestrian-A channel but also in EVA channel.

C.1 Overview of Testbeds and Prototypes

Experiments for wireless communications can be classified into three categories: demonstrators, testbeds and prototypes [108] . Demonstrators are normally used for a concept that has been finalised to show the technology to customers. Testbeds are more widely used in research to verify developing algorithms under real-world conditions while providing scalability, modularity and extendability. A testbed system usually contains a real-time wireless transmission, but the data are often stored for offline processing in a higher level language. Since the processing is done offline in a higher level language, it allows researchers to test the validity of their algorithms without requiring a group of engineers to build a prototype. Prototypes are used as a "proof of concept"

which involve more hardware processing and the processing functionalities are normally performed in real-time. Channel emulators are often used in prototypes which make repeatable experiments possible.

A testbed system can be divided into three main components [109]: the baseband modules, RF front-ends and software development tools. The baseband modules include the host PC and digital hardware components such as field-programmable gate array (FPGA) which deals with baseband or intermediate frequency (IF) signals and implement digital to analogue (DAC) and analogue to digital (ADC) converters. The radio frequency (RF) front-ends are responsible to convert signals to baseband or IF to RF and vice versa.

To meet the tight time-to-market constraints, and to enable short development time in a prototype system without requiring a large group of engineers, the use of rapid prototyping system by using the "five one approach", which involves the use of one team, one environment, one code, one documentation and one code revision tool was proposed [66]. In addition, the use of automatic tools to convert high level codes to lower design language are promoted to speed up the process and to avoid most errors [66, 108] such as the use of tools in [110] which convert C into VHDL or to use Mathworks tool suite combined with some VHDL code generators [111]. Similarly, the experimental set up described in this thesis uses a high level language based on LabVIEW which translates to VHDL to load the design in the FPGA boards. When verifying a new algorithm in experimental testbed, the software development can be divided into three processes [109] simulation, migrating simulation to testbed and real-time implementation where each migration has to be carefully verified against the previous step.

C.2 Further Details on the NI-PXIe Testbed

The system model for the testbed is illustrated in Figure C.1 where the system can be divided into the host processing unit and the channel emulator hardware. The photo of the tesbed is shown in Figure C.2.

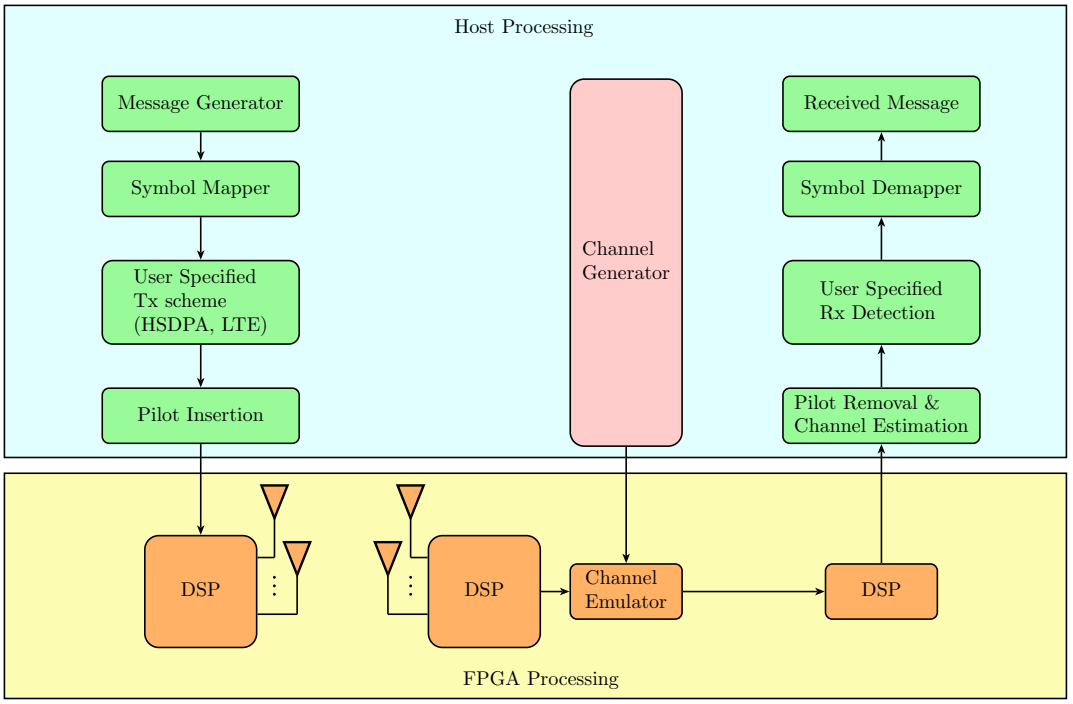


FIGURE C.1: Software & Hardware Processing Unit of the Rapid Prototyping System

The host processing unit uses high level LabVIEW language and its modulation toolkit with floating point operations to handle signal generation, symbol mapping and demapping and the modulation and demodulation for different wireless standards. In this thesis, these three operations are the same as the system model described in Sections 2.2 (see page 35) and 3.1 (see page 67) for the HSDPA system. The pilot signal is inserted after all the physical layer processing is done to enable channel estimation to be carried out at the receiver irrespective of the wireless standard used. The combined signal with both data and pilot are then passed to the channel processing unit. The channel fading generation is done in the host, which is fed into the channel emulator to be processed in FPGA for real-time processing. At the receiver, after the digital signal processing, pulse shaping and frequency down converting the signal; the channel estimation is carried out at the host and the pilot is removed. Based on the channel information estimated, the receiver processing is carried out for non-SIC scheme as shown in Figure 2.1 (page 36) , SIC as shown in Figure 3.1 (67). For the FPGA boards in this testbed, both the FPGA functionalities and channel emulations are written in LabVIEW language with Digital Filter Design toolkit and FPGA toolkit with fixed point operations. At the output of the host processing, after the transmit signals are

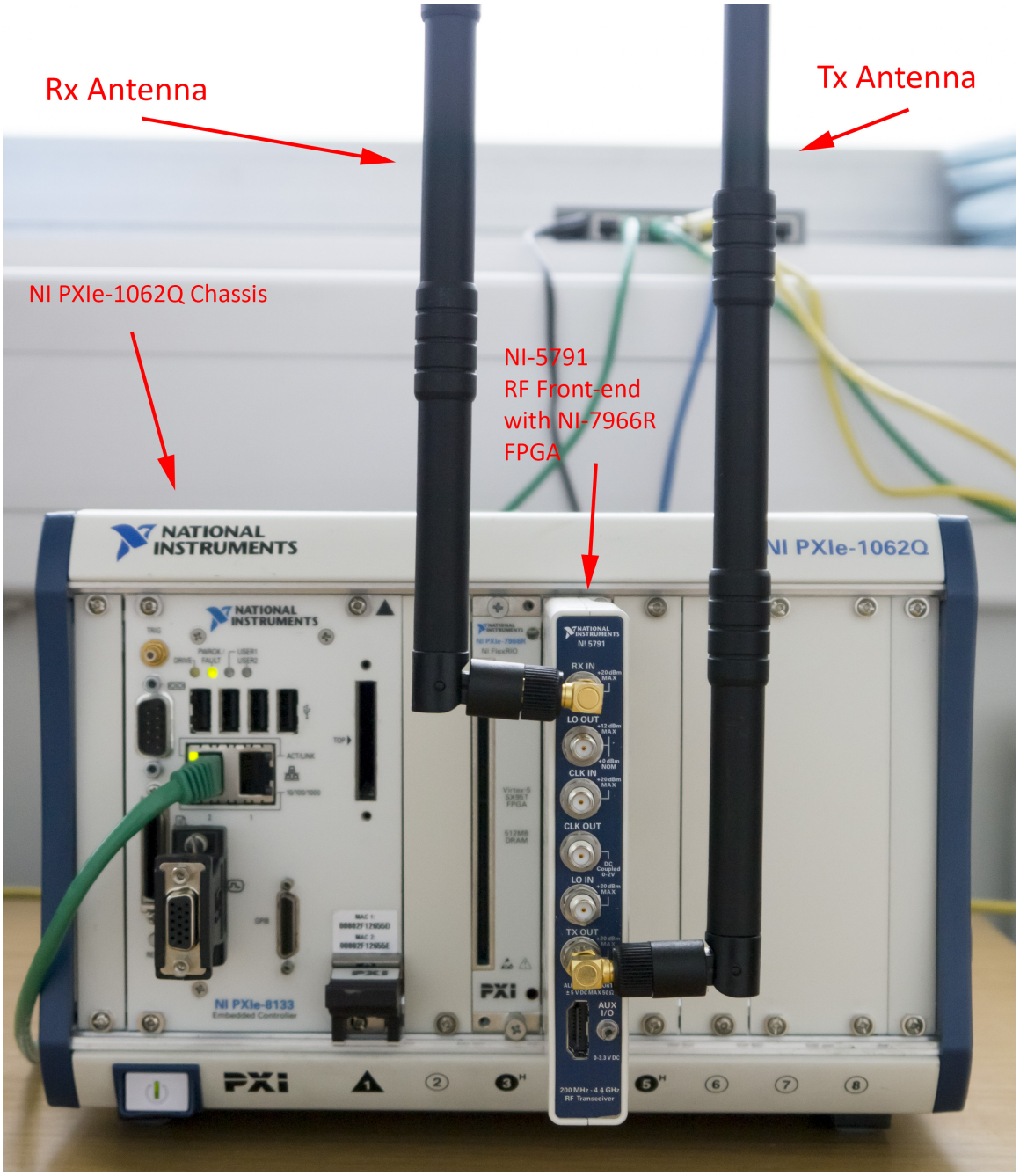


FIGURE C.2: NI PXIe Hardware Platform

generated and pilot insertion in the host, the samples from the transmit vector first pass through a digital up converter (DUC) and a pulse shaping filter. This signal is then sent through the RF channel. At the receiver, the channel gain is applied to the signal which is then convolved with the channel coefficients generated from the channel fading generation block. After this, the signal is passed through a match filter and are digital down converted (DDC). Then, the signal is ready to be passed back to the host processing.

C.3 Further Measurement Results over the EVA Channels

In Chapter 3, the comparison between MATLAB simulations, software channel emulator and hardware channel emulator for the sum rate and the system throughput for the EEER allocation with and without the SIC receiver over the Pedestrian-A channel was described. In this appendix, the above comparisons over the EVA channels are presented. The PDP of the EVA channel is given in Table 3.4 in page 82. In Figure C.3, the sum rate and EEER allocation with (non-SIC) MMSE receiver are shown; while in Figure C.4 the sum rate and EEER allocation with SIC receiver are illustrated. Similar to the case for the Pedestrian-A Channel in Chapter 3, the results transmitted over the EVA channel further proves that the SIC receiver proposed in this thesis works as expected in simulations even under experimental conditions.

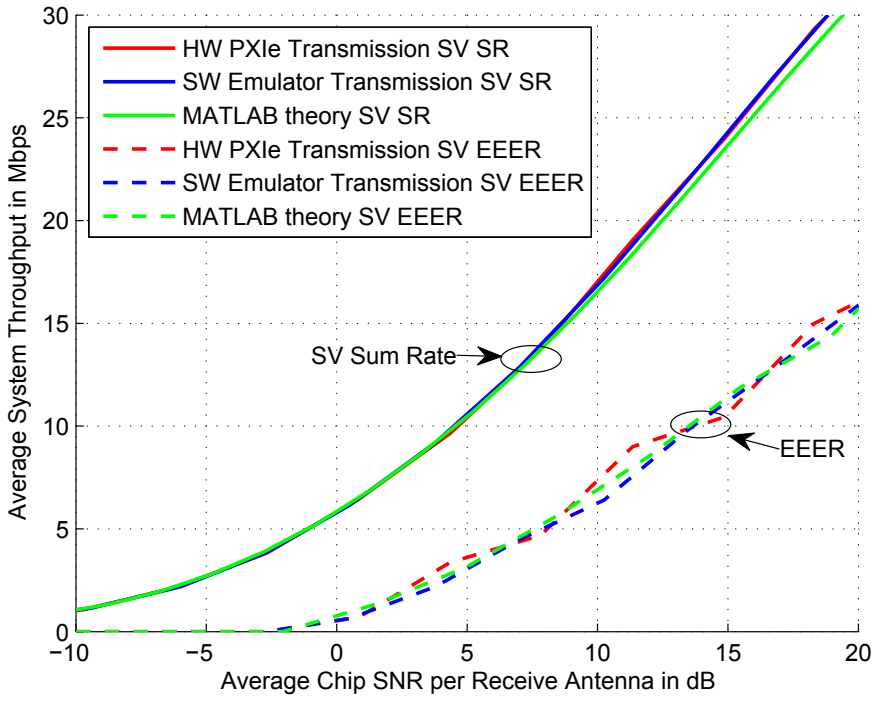


FIGURE C.3: Simulations and Experiments Comparisons over EVA (MMSE)

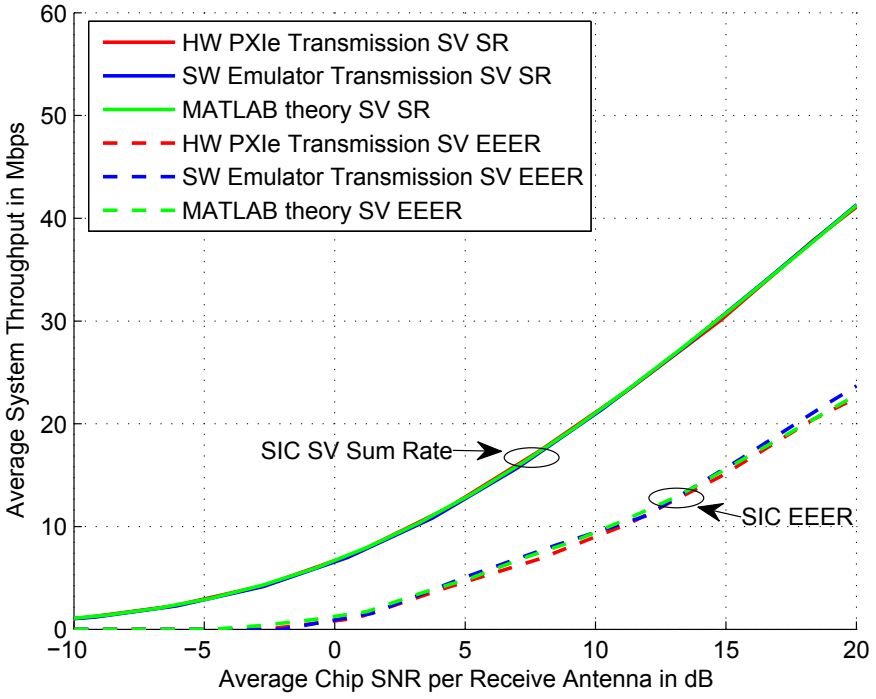


FIGURE C.4: Simulations and Experiments Comparisons over EVA (SIC)

Appendix D

PCI Codebooks (Chapter 4)

The PCI codebooks for the MIMO system with two transmit antennas has been introduced in Section 2.2.3. This section describes the PCI codebooks for the MIMO systems with three and four transmit antennas. Here, each codeword is represented by matrix $\mathbf{F}_n$, where n represents the PCI index. The selected codeword, i.e. the codeword that maximises the system value sum rate as defined in Equation (2.35) in page 46, will be represented by matrix $\mathbf{F}$. With the precoding matrix $\mathbf{F}$, the MIMO spreading sequences are formed by using $\mathbf{S}_F = \mathbf{F} \otimes \mathbf{S}_{OVSF}$. The PCI codebooks for the HSDPA system is only available for two and four transmit antennas. Hence, the WiMAX codebook is used for the case with three transmit antennas. The next part will describe the PCI codebook for three transmit antennas.

D.1 PCI Codebook for Three Transmit Antennas

For a system with three transmit antennas, the WiMAX codebook defined in [112] is used. The codebook is formed using vectors $\underline{u}_n$ as defined in Table D.1. Based on these parameters, the codebook for the three-transmit-antenna scheme is formulated as follows:

1. Given $\underline{u}_n$ for $n = 0, ..., N-1$ in Table D.1 for $N_T = 3$.

2. Form $\underline{w}_n = \underline{u}_n - \underline{e}$, for $n = 0, ..., N-1$, where $\underline{e} = [1, 0, 0]^T \in \mathbb{R}^{N^T \times 1}$.

3. Form the codebook using the formula

$$\mathbf{F}_n = \left\{ \begin{array}{cc} \mathbf{I}_{N_T} & n = 0 \\ \mathbf{I}_{N_T} - 2\underline{w}_n \underline{w}_n^H / \underline{w}_n^H \underline{w}_n & n \neq 0 \end{array} \right\}. \tag{D.1}$$

4. If only two (or one) transmission streams are used in the transmit diversity mode, the codebook will select the last two (or one) of the codebook.

TABLE D.1: PCI Codebook for Three Transmit Antennas

PCI Index	$\underline{u}_n$
0	$\underline{u}_0 = [1, 0, 0]^T$
1	$\underline{u}_1 = [0.5, -0.7201 - j0.3126, 0.2483 - j0.2684]^T$
2	$\underline{u}_2 = [0.5, -0.0659 + j0.1371, -0.6283 - j0.5763]^T$
3	$\underline{u}_3 = [0.5, -0.0063 + j0.6527, 0.4621 - j0.3321]^T$
4	$\underline{u}_4 = [0.5, 0.7171 + j0.3202, -0.2533 + j0.2626]^T$
5	$\underline{u}_5 = [0.4954, 0.4819 - j0.4517, 0.2963 - j0.4801]^T$
6	$\underline{u}_6 = [0.5, 0.0686 - j0.1386, 0.62 + j0.5845]^T$
7	$\underline{u}_7 = [0.5, -0.0054 - j0.6540, -0.4566 + j0.3374]^T$

D.2 PCI Codebook for Four Transmit Antennas

The precoding codebook for four transmit antennas is formed by using householder reflection or unitary householder (HH) matrix, given as

$$\mathbf{F}_n = \mathbf{I}_4 - 2\underline{u}_n \underline{u}_n^H / \underline{u}_n^H \underline{u}_n \qquad \text{for } n = 0, 1, .., N-1. \tag{D.2}$$

where $N = 16$. The codewords of different ranks are constructed as follows:

1. Form the vectors $\underline{u}_n$ for $n = 0, .., N-1$ according to Table D.2.

2. Form the unitary household matrix $\mathbf{F}_n = \mathbf{I}_4 - 2\underline{u}_n \underline{u}_n^H / \underline{u}_n^H \underline{u}_n$ for $n = 0, .., N-1$.

3. According to the rank chosen, formulate the codewords $\mathbf{F}$ by selecting the appropriate columns of $\mathbf{F}_n$ as indicated on the superscript $\mathbf{F}_n^{order}$. For example, $\mathbf{F}_2^{\{3214\}}$ means reordering the columns of $\mathbf{F}_2$ to the order $3, 2, 1, 4$.

TABLE D.2: LTE System with Four Transmit Antennas

Codebook Index	Codeword $\underline{u}_n$	No. of Layers 1	2	3	4
0	$\underline{u}_0 = [1,-1,-1,-1]^T$	$\mathbf{F}_0^{\{1\}}$	$\mathbf{F}_0^{\{14\}}$	$\mathbf{F}_0^{\{124\}}$	$\mathbf{F}_0^{\{1234\}}$
1	$\underline{u}_1 = [1,-j,1,j]^T$	$\mathbf{F}_1^{\{1\}}$	$\mathbf{F}_1^{\{12\}}$	$\mathbf{F}_1^{\{123\}}$	$\mathbf{F}_1^{\{1234\}}$
2	$\underline{u}_2 = [1,1,-1,1]^T$	$\mathbf{F}_2^{\{1\}}$	$\mathbf{F}_2^{\{12\}}$	$\mathbf{F}_2^{\{123\}}$	$\mathbf{F}_2^{\{3214\}}$
3	$\underline{u}_3 = [1,j,1,-j]^T$	$\mathbf{F}_3^{\{1\}}$	$\mathbf{F}_3^{\{12\}}$	$\mathbf{F}_3^{\{123\}}$	$\mathbf{F}_3^{\{3214\}}$
4	$\underline{u}_4 = [1,(-1-j)/\sqrt{2},-j,(1-j)/\sqrt{2}]^T$	$\mathbf{F}_4^{\{1\}}$	$\mathbf{F}_4^{\{14\}}$	$\mathbf{F}_4^{\{124\}}$	$\mathbf{F}_4^{\{1234\}}$
5	$\underline{u}_5 = [1,(1-j)/\sqrt{2},j,(-1-j)/\sqrt{2}]^T$	$\mathbf{F}_5^{\{1\}}$	$\mathbf{F}_5^{\{14\}}$	$\mathbf{F}_5^{\{124\}}$	$\mathbf{F}_5^{\{1234\}}$
6	$\underline{u}_6 = [1,(1+j)/\sqrt{2},-j,(-1+j)/\sqrt{2}]^T$	$\mathbf{F}_6^{\{1\}}$	$\mathbf{F}_6^{\{13\}}$	$\mathbf{F}_6^{\{134\}}$	$\mathbf{F}_6^{\{1324\}}$
7	$\underline{u}_7 = [1,(-1+j)/\sqrt{2},j,(1+j)/\sqrt{2}]^T$	$\mathbf{F}_7^{\{1\}}$	$\mathbf{F}_7^{\{13\}}$	$\mathbf{F}_7^{\{134\}}$	$\mathbf{F}_7^{\{1324\}}$
8	$\underline{u}_8 = [1,-1,1,1]^T$	$\mathbf{F}_8^{\{1\}}$	$\mathbf{F}_8^{\{12\}}$	$\mathbf{F}_8^{\{124\}}$	$\mathbf{F}_8^{\{1234\}}$
9	$\underline{u}_9 = [1,-j,-1,-j]^T$	$\mathbf{F}_9^{\{1\}}$	$\mathbf{F}_9^{\{14\}}$	$\mathbf{F}_9^{\{134\}}$	$\mathbf{F}_9^{\{1234\}}$
10	$\underline{u}_{10} = [1,1,1,-1]^T$	$\mathbf{F}_{10}^{\{1\}}$	$\mathbf{F}_{10}^{\{13\}}$	$\mathbf{F}_{10}^{\{123\}}$	$\mathbf{F}_{10}^{\{1324\}}$
11	$\underline{u}_{11} = [1,j,-1,j]^T$	$\mathbf{F}_{11}^{\{1\}}$	$\mathbf{F}_{11}^{\{13\}}$	$\mathbf{F}_{11}^{\{134\}}$	$\mathbf{F}_{11}^{\{1324\}}$
12	$\underline{u}_{12} = [1,-1,-1,1]^T$	$\mathbf{F}_{12}^{\{1\}}$	$\mathbf{F}_{12}^{\{12\}}$	$\mathbf{F}_{12}^{\{123\}}$	$\mathbf{F}_{12}^{\{1234\}}$
13	$\underline{u}_{13} = [1,-1,1,-1]^T$	$\mathbf{F}_{13}^{\{1\}}$	$\mathbf{F}_{13}^{\{13\}}$	$\mathbf{F}_{13}^{\{123\}}$	$\mathbf{F}_{13}^{\{1324\}}$
14	$\underline{u}_{14} = [1,1,-1,-1]^T$	$\mathbf{F}_{14}^{\{1\}}$	$\mathbf{F}_{14}^{\{13\}}$	$\mathbf{F}_{14}^{\{123\}}$	$\mathbf{F}_{14}^{\{3214\}}$
15	$\underline{u}_{15} = [1,1,1,1]^T$	$\mathbf{F}_{15}^{\{1\}}$	$\mathbf{F}_{15}^{\{12\}}$	$\mathbf{F}_{15}^{\{123\}}$	$\mathbf{F}_{15}^{\{1234\}}$

References

[1] Deloitte. (2013) Technology fast 500: 2013 ranking of the fastest growing technology based companies in north america. http://www.deloitte.com/assets/Dcom-UnitedStates/Local%20Assets/Documents/TMT_us_tmt/us_tmt_fast500_winnersbrochure_111213.pdf.

[2] Fujitsu. (2009) 4G impacts to mobile backhaul, Whtie Paper. http://www.fujitsu.com/downloads/TEL/fnc/whitepapers/4Gimpacts.pdf.

[3] B. Sarikaya, "Packet mode in wireless networks: overview of transition to third generation," *Communications Magazine, IEEE*, vol. 38, no. 9, pp. 164–172, September 2000.

[4] A. Toskala and H. Holma, *WCDMA for UMTS: HSPA evolution and LTE; 4th ed.* Hoboken, NJ: Wiley, 2007.

[5] M. Cvitkovic, B. Modlic, and G. Sisul, "High speed downlink packet access principles," in *ELMAR, 2007*, September 2007, pp. 125 –128.

[6] T. Cui, F. Lu, V. Sethuraman, A. Goteti, S. Rao, and P. Subrahmanya, "Throughput optimization in high speed downlink packet access (hsdpa)," *Wireless Communications, IEEE Transactions on*, vol. 10, no. 2, pp. 474 –483, February 2011.

[7] Cisco. (2014, February) Cisco visual networking index: Global mobile data traffic forecast update, 2013 - 2018, White Paper. http://www.cisco.com/c/en/us/solutions/collateral/service-provider/visual-networking-index-vni/white_paper_c11-520862.pdf.

[8] A. Paulraj, R. Nabar, and D. Gore, *Introduction to Space-Time Wireless Communications*, 1st ed. New York, NY, USA: Cambridge University Press, 2008.

[9] A. Paulraj, D. Gore, R. Nabar, and H. Bolcskei, "An overview of mimo communications - a key to gigabit wireless," *Proceedings of the IEEE*, vol. 92, no. 2, pp. 198–218, 2004.

[10] E. Telatar, "Capacity of multi-antenna gaussian channels," *European Transactions on Telecommunications*, vol. 10, no. 6, pp. 585–595, 1999. [Online]. Available: http://dx.doi.org/10.1002/ett.4460100604

[11] G. Foschini and M. Gans, "On limits of wireless communications in a fading environment when using multiple antennas," *Wireless Personal Communications*, vol. 6, no. 3, pp. 311–335, 1998. [Online]. Available: http://dx.doi.org/10.1023/A%3A1008889222784

[12] 3GPP, "Technical specification group radio access network; Multiple Input Multiple Output in UTRA (Tech. Rep. 25.876 V.7.0.0)," 3rd Generation Partnership Project (3GPP), TR 25.876, March 2007.

[13] ——, "Technical Specification Group Radio Access Network; Multiplexing and Channel Coding (FDD)(Tech. Spec. 25.212 V.11.5.0)," 3rd Generation Partnership Project (3GPP), TS 25.212, June 2013.

[14] B. Sklar, *Digital Communications: Fundamentals & Applications, 2/E.* Pearson Education, 2009.

[15] T. S. Rappaport, *Wireless Communications: Principles And Practice, 2/E.* Pearson Education, 2010.

[16] Y. S. Cho, J. Kim, W. Y. Yang, and C.-G. Kang, *MIMO-OFDM Wireless Communications with MATLAB.* John Wiley & Sons, 2010.

[17] C. Mehlfuhrer, S. Caban, and M. Rupp, "Measurement-based performance evaluation of mimo hsdpa," *Vehicular Technology, IEEE Transactions on*, vol. 59, no. 9, pp. 4354–4367, 2010.

[18] ——, "Cellular system physical layer throughput: How far off are we from the shannon bound?" *Wireless Communications, IEEE*, vol. 18, no. 6, pp. 54–63, 2011.

[19] ——, "MIMO HSDPA throughput measurement results," in *HSDPA/HSUPA Handbook*, S. A. B. Furht, Ed. Boca Raton, FL, USA: CRC Press, 2010, pp. 357–377.

[20] R. Kwan, M. Aydin, C. Leung, and J. Zhang, "Multiuser scheduling in high speed downlink packet access," *Communications, IET*, vol. 3, no. 8, pp. 1363 –1370, August 2009.

[21] A. Mäder and D. Staehle, "Spatial and temporal fairness in heterogeneous hsdpa-enabled umts networks," *EURASIP J. Wirel. Commun. Netw.*, vol. 2009, pp. 13:1–13:12, January 2009.

[22] 3GPP, "Technical specification group radio access network; High Speed Downlink Packet Access: UE Radio Transmission and Reception(Tech. Rep. 25.890 V.1.1.0)," 3rd Generation Partnership Project (3GPP), TR 25.890, May 2002.

[23] ——, "Evolved Universal Terrestrial Radio Access (E-UTRA); Base Station (BS) radio transmission and reception (TS 36.104 V.12.0.0)," 3rd Generation Partnership Project (3GPP), TS 36.104, July 2013.

[24] Z. He, "Efficient radio resource allocation schemes and code optimizations for high speed downlink packet access transmission," Ph.D. dissertation, Imperial College London, January 2011.

[25] M. K. Gurcan, I. Ma, and H. Ab Ghani, "The interference-reduced energy loading for multi-code hsdpa systems," *EURASIP Journal on Wireless Communications and Networking*, vol. 2012, no. 1, pp. 1–17, 2012.

[26] M. K. Gurcan, I. Ma, A. Chungtragarn, and H. Joudeh, "System value-based optimum spreading sequence selection for high-speed downlink packet access (hsdpa) mimo," *EURASIP Journal on Wireless Communications and Networking*, vol. 2013, no. 1, pp. 1–19, 2013.

[27] R. Visoz, A. Berthet, and N. Gresset, "Advanced transceiver architectures for downlink mimo cdma evolution," *Wireless Communications, IEEE Transactions on*, vol. 6, no. 8, pp. 3016–3027, August 2007.

[28] S. Kim, S. Kim, C. Shin, J. Lee, and Y. Kim, "A new multicode interference cancellation method for hsdpa system," in *Communications, Computers and Signal Processing, 2009. PacRim 2009. IEEE Pacific Rim Conference on*, August 2009, pp. 487–490.

[29] T. Wong and T. Lok, "Transmitter adaptation in multicode ds-cdma systems," *Selected Areas in Communications, IEEE Journal on*, vol. 19, no. 1, pp. 69 –82, January 2001.

[30] B. Sayadi, S. Ataman, and I. Fijalkow, "Joint downlink power control and multicode receivers for downlink transmissions in high speed umts," *EURASIP J. Wirel. Commun. Netw.*, vol. 2006, pp. 60–60, April 2006.

[31] N. Vucic, H. Boche, and S. Shi, "Robust transceiver optimization in downlink multiuser mimo systems," *Signal Processing, IEEE Transactions on*, vol. 57, no. 9, pp. 3576 –3587, September 2009.

[32] T. Bogale, B. Chalise, and L. Vandendorpe, "Robust transceiver optimization for downlink multiuser mimo systems," *Signal Processing, IEEE Transactions on*, vol. 59, no. 1, pp. 446 –453, January 2011.

[33] D. I. Kim, E. Hossain, and V. Bhargava, "Dynamic rate and power adaptation for forward link transmission using high-order modulation and multicode formats in cellular wcdma networks," *Wireless Communications, IEEE Transactions on*, vol. 4, no. 5, pp. 2361–2372, 2005.

[34] L. Zhao and J. Mark, "Joint rate and power adaptation for radio resource management in uplink wideband code division multiple access systems," *Communications, IET*, vol. 2, no. 4, pp. 562 –572, April 2008.

[35] A. Soysal and S. Ulukus, "Optimum power allocation for single-user mimo and multi-user mimo-mac with partial csi," *Selected Areas in Communications, IEEE Journal on*, vol. 25, no. 7, pp. 1402–1412, 2007.

[36] A. Tajer, N. Prasad, and X. Wang, "Robust transceiver design for the multi-user interference channel," in *Communications (ICC), 2010 IEEE International Conference on*, May 2010, pp. 1–5.

[37] H.-H. Lee, Y.-C. Ko, and H.-C. Yang, "On robust weighted sum rate maximization for mimo interfering broadcast channels with imperfect channel knowledge," *Communications Letters, IEEE*, vol. 17, no. 6, pp. 1156–1159, June 2013.

[38] S. Ulukus and A. Yener, "Iterative transmitter and receiver optimization for cdma networks," *Wireless Communications, IEEE Transactions on*, vol. 3, no. 6, pp. 1879 – 1884, November 2004.

[39] W. Xu, A. Tajer, X. Wang, and S. Alshomrani, "Power allocation in miso interference channels with stochastic csit," *Wireless Communications, IEEE Transactions on*, vol. 13, no. 3, pp. 1716–1727, March 2014.

[40] G. Li and T. Wong, "Power control and spreading sequence allocation in a cdma forward link," *Information Theory, IEEE Transactions on*, vol. 50, no. 1, pp. 105 – 124, January 2004.

[41] J. W. P. Ng and A. Manikas, "A space-diffused spatial-temporal array (star) receiver for ds-cdma system," *International Journal in Hellenic European Research in Mathematics and Informatics Science (HERMIS)*, vol. 4, pp. 131 – 152, 2003.

[42] 3GPP, "Technical Specification Group Radio Access Network; Universal Mobile Telecommunications System (UMTS); Spreading and modulation (FDD) (Tech. Spec. 25.213 V.11.4.0)," 3rd Generation Partnership Project (3GPP), TS 25.213, January 2013.

[43] ——, "Technical specification group radio access network; physical layer procedures (FDD) (Tech. Spec. 25.214 V.11.6.0)," 3rd Generation Partnership Project (3GPP), TS 25.214, June 2013.

[44] D. Cai, T. Quek, and C. W. Tan, "A unified analysis of max-min weighted sinr for mimo downlink system," *Signal Processing, IEEE Transactions on*, vol. 59, no. 8, pp. 3850 –3862, August 2011.

[45] A. Tenenbaum and R. Adve, "Minimizing sum-mse implies identical downlink and dual uplink power allocations," *Communications, IEEE Transactions on*, vol. 59, no. 3, pp. 686 –688, March 2011.

[46] ——, "Energy optimization across training and data for multiuser minimum sum-mse linear precoding," in *Information Sciences and Systems (CISS), 2010 44th Annual Conference on*, March 2010, pp. 1 –6.

[47] H. Shen, B. Li, M. Tao, and X. Wang, "Mse-based transceiver designs for the mimo interference channel," *Wireless Communications, IEEE Transactions on*, vol. 9, no. 11, pp. 3480 –3489, November 2010.

[48] S. Shi, M. Schubert, and H. Boche, "Rate optimization for multiuser mimo systems with linear processing," *Signal Processing, IEEE Transactions on*, vol. 56, no. 8, pp. 4020 –4030, August 2008.

[49] D. Palomar, J. Cioffi, and M.-A. Lagunas, "Joint tx-rx beamforming design for multicarrier mimo channels: a unified framework for convex optimization," *Signal Processing, IEEE Transactions on*, vol. 51, no. 9, pp. 2381–2401, September 2003.

[50] R. Hunger, M. Joham, and W. Utschick, "On the mse-duality of the broadcast channel and the multiple access channel," *Signal Processing, IEEE Transactions on*, vol. 57, no. 2, pp. 698–713, February 2009.

[51] Z. He and M. K. Gurcan, "Optimizing radio resource allocation in hsdpa using 2 group allocation," in *Proceedings of the 2009 International Conference on Wireless Communications and Mobile Computing: Connecting the World Wirelessly*, ser. IWCMC '09. New York, NY, USA: ACM, 2009, pp. 1107–1111.

[52] M. Gurcan, I. Ma, H. Ghani, and Z. He, "Complexity reduction for multi-hop network end-to-end delay minimization," in *Computer and Information Sciences II*. Springer London, 2012, pp. 231–237.

[53] M. Jiang and L. Hanzo, "Multiuser mimo-ofdm for next-generation wireless systems," *Proceedings of the IEEE*, vol. 95, no. 7, pp. 1430–1469, July 2007.

[54] S. P. Weber, J. Andrews, X. Yang, and G. De Veciana, "Transmission capacity of wireless ad hoc networks with successive interference cancellation," *Information Theory, IEEE Transactions on*, vol. 53, no. 8, pp. 2799–2814, Aug 2007.

[55] D. Divsalar, M. K. Simon, and D. Raphaeli, "Improved parallel interference cancellation for cdma," *Communications, IEEE Transactions on*, vol. 46, no. 2, pp. 258–268, February 1998.

[56] W. Hamouda and P. J. Mclane, "A fast adaptive algorithm for mmse receivers in ds-cdma systems," *Signal Processing Letters, IEEE*, vol. 11, no. 2, pp. 86–89, Feb 2004.

[57] Y. Yoon, R. Kohno, and H. Imai, "A spread-spectrum multiaccess system with cochannel interference cancellation for multipath fading channels," *Selected Areas in Communications, IEEE Journal on*, vol. 11, no. 7, pp. 1067–1075, Sep 1993.

[58] S. Shenoy, I. Ghauri, and D. Slock, "Receiver designs and multi-user extensions to mimo hsdpa," in *HSDPA/HSUPA Handbook*, S. A. B. Furht, Ed. Boca Raton, FL, USA: CRC Press, 2010, pp. 89–109.

[59] J. Andrews, "Interference cancellation for cellular systems: a contemporary overview," *Wireless Communications, IEEE*, vol. 12, no. 2, pp. 19–29, April 2005.

[60] C. S. Park and K. B. Lee, "Transmit power allocation for successive interference cancellation in multicode mimo systems," *Communications, IEEE Transactions on*, vol. 56, no. 12, pp. 2200 –2213, December 2008.

[61] M. Golanbari, G. E. Ford, and M. J. Ready, "Simulation study of a successive interference cancellation receiver for signal monitoring on a cdma downlink," *European Transactions on Telecommunications*, vol. 20, no. 1, pp. 65–79, 2009.

[62] J. He, G. Gu, and Z. Wu, "Mmse interference suppression in mimo frequency selective and time-varying fading channels," *Signal Processing, IEEE Transactions on*, vol. 56, no. 8, pp. 3638 –3651, August 2008.

[63] A. Bastug and D. T. M. Slock, "Downlink wcdma receivers based on combined chip and symbol level equalization," *Telecommunications, European Transactions on*, vol. 16, January 2005.

[64] C. Mehlfuhrer and S. Caban, "Measurement based evaluation of low complexity receivers for d-txaa hsdpa," in *in Proc. of the 16th European Signal Processing Conference (EUSIPCO 2008)*, 2008.

[65] S. Kurkowski, T. Camp, and M. Colagrosso, "Manet simulation studies: the incredibles," *SIGMOBILE Mob. Comput. Commun. Rev.*, vol. 9, no. 4, pp. 50–61, October 2005.

[66] M. Rupp, A. Burg, and E. Beck, "Rapid prototyping for wireless designs: the five-ones approach," *Signal Processing*, vol. 83, no. 7, pp. 1427–1444, 2003.

[67] M. Gurcan, I. Ma, H. Joudeh, and Q. Liu. (2013) Building a next-generation test system for next-generation wireless communication with pxi express and labview. http://sine.ni.com/cs/app/doc/p/id/cs-15646.

[68] S. Caban, G. Mehlführer, C.and Lechner, and M. Rupp, "Testbedding MIMO HSDPA and wiMAX," in *Proc. 70th IEEE Vehicular Technology Conference (VTC2009-Fall)*, Anchorage, AK, USA, September 2009.

[69] K. Chowdhury and T. Melodia, "Platforms and testbeds for experimental evaluation of cognitive ad hoc networks," *Communications Magazine, IEEE*, vol. 48, no. 9, pp. 96–104, 2010.

[70] G. Judd and P. Steenkiste, "Design and implementation of an rf front end for physical layer wireless network emulation," in *Vehicular Technology Conference, 2007. VTC2007-Spring. IEEE 65th*, 2007, pp. 974–979.

[71] N. Instruments, "NI 5791: RF transceiver adapter module for NI FlexRIO," http://sine.ni.com/nips/cds/view/p/lang/en/nid/211063.

[72] ——, "NI PXIe-7966R: NI FlexRIO FPGA module for PXI Express," http://sine.ni.com/nips/cds/view/p/lang/en/nid/210272.

[73] ——, "Real-time MIMO channel emulation on the NI PXIe-5644R," http://www.ni.com/example/31556/en/, May 2013.

[74] J. Concha and S. Ulukus, "Optimization of cdma signature sequences in multipath channels," in *Vehicular Technology Conference, 2001. VTC 2001 Spring. IEEE VTS 53rd*, vol. 3, 2001, pp. 1978 –1982 vol.3.

[75] G. Rajappan and M. Honig, "Signature sequence adaptation for ds-cdma with multipath," *Selected Areas in Communications, IEEE Journal on*, vol. 20, no. 2, pp. 384 –395, February 2002.

[76] S. Ulukus and R. Yates, "Iterative construction of optimum signature sequence sets in synchronous cdma systems," *Information Theory, IEEE Transactions on*, vol. 47, no. 5, pp. 1989 –1998, July 2001.

[77] G. Li and T. Wong, "Sequence optimization in cdma point-to-point transmission with multipath," in *Vehicular Technology Conference, 2002. Proceedings. VTC 2002-Fall. 2002 IEEE 56th*, vol. 4, 2002, pp. 2303 – 2307 vol.4.

[78] H. Sampath, P. Stoica, and A. Paulraj, "Generalized linear precoder and decoder design for mimo channels using the weighted mmse criterion," *Communications, IEEE Transactions on*, vol. 49, no. 12, pp. 2198–2206, December 2001.

[79] A. Scaglione, P. Stoica, S. Barbarossa, G. Giannakis, and H. Sampath, "Optimal designs for space-time linear precoders and decoders," *Signal Processing, IEEE Transactions on*, vol. 50, no. 5, pp. 1051–1064, May 2002.

[80] D. Love, R. Heath, V. Lau, D. Gesbert, B. Rao, and M. Andrews, "An overview of limited feedback in wireless communication systems," *Selected Areas in Communications, IEEE Journal on*, vol. 26, no. 8, pp. 1341 –1365, October 2008.

[81] A. Ekpenyong and Y.-F. Huang, "Feedback constraints for adaptive transmission," *Signal Processing Magazine, IEEE*, vol. 24, no. 3, pp. 69 –78, May 2007.

[82] H. Shirani-Mehr and G. Caire, "Channel state feedback schemes for multiuser mimo-ofdm downlink," *Communications, IEEE Transactions on*, vol. 57, no. 9, pp. 2713 –2723, September 2009.

[83] T. Marzetta and B. Hochwald, "Fast transfer of channel state information in wireless systems," *Signal Processing, IEEE Transactions on*, vol. 54, no. 4, pp. 1268 – 1278, April 2006.

[84] M. Kobayashi and G. Caire, "Joint beamforming and scheduling for a multi-antenna downlink with imperfect transmitter channel knowledge," *Selected Areas in Communications, IEEE Journal on*, vol. 25, no. 7, pp. 1468 –1477, September 2007.

[85] G. Caire, N. Jindal, M. Kobayashi, and N. Ravindran, "Multiuser mimo achievable rates with downlink training and channel state feedback," *Information Theory, IEEE Transactions on*, vol. 56, no. 6, pp. 2845 –2866, June 2010.

[86] B. Khoshnevis and W. Yu, "Bit allocation laws for multiantenna channel feedback quantization: Multiuser case," *Signal Processing, IEEE Transactions on*, vol. 60, no. 1, pp. 367 –382, January 2012.

[87] N. Papandreou and T. Antonakopoulos, "Bit and power allocation in constrained multicarrier systems: The single-user case," *EURASIP Journal on Advances in Signal Processing*, vol. 2008, no. 1, p. 643081, 2008.

[88] S. Shi, M. Schubert, and H. Boche, "Downlink mmse transceiver optimization for multiuser mimo systems: Duality and sum-mse minimization," *Signal Processing, IEEE Transactions on*, vol. 55, no. 11, pp. 5436 –5446, November 2007.

[89] S. Bergman, D. Palomar, and B. Ottersten, "Joint bit allocation and precoding for mimo systems with decision feedback detection," *Signal Processing, IEEE Transactions on*, vol. 57, no. 11, pp. 4509–4521, 2009.

[90] T. Kim and M. Skoglund, "On the expected rate of slowly fading channels with quantized side information," *Communications, IEEE Transactions on*, vol. 55, no. 4, pp. 820 –829, April 2007.

[91] J. Lee, J.-K. Han, and J. Zhang, "Mimo technologies in 3gpp lte and lte-advanced," *EURASIP J. Wirel. Commun. Netw.*, vol. 2009, pp. 3:1–3:10, March 2009.

[92] C. Au-Yeung and D. Love, "On the performance of random vector quantization limited feedback beamforming in a miso system," *Wireless Communications, IEEE Transactions on*, vol. 6, no. 2, pp. 458 –462, February 2007.

[93] W. Santipach and M. Honig, "Capacity of a multiple-antenna fading channel with a quantized precoding matrix," *Information Theory, IEEE Transactions on*, vol. 55, no. 3, pp. 1218 –1234, March 2009.

[94] A. Ghosh, J. Zhang, J. G. Andrews, and R. Muhamed, *Fundamentals of LTE*, 1st ed. Upper Saddle River, NJ, USA: Prentice Hall Press, 2010.

[95] S. Alamouti, "A simple transmit diversity technique for wireless communications," *Selected Areas in Communications, IEEE Journal on*, vol. 16, no. 8, pp. 1451–1458, October 1998.

[96] V. Tarokh, H. Jafarkhani, and A. Calderbank, "Space-time block codes from orthogonal designs," *Information Theory, IEEE Transactions on*, vol. 45, no. 5, pp. 1456–1467, July 1999.

[97] V. Tarokh, N. Seshadri, and A. Calderbank, "Space-time codes for high data rate wireless communication: performance criterion and code construction," *Information Theory, IEEE Transactions on*, vol. 44, no. 2, pp. 744–765, March 1998.

[98] J. Mietzner, R. Schober, L. Lampe, W. Gerstacker, and P. Hoeher, "Multiple-antenna techniques for wireless communications - a comprehensive literature survey," *Communications Surveys Tutorials, IEEE*, vol. 11, no. 2, pp. 87–105, 2009.

[99] D. G. Brennan, "Linear diversity combining techniques," *Proceedings of the IEEE*, vol. 91, no. 2, pp. 331–356, February 2003.

[100] L. Zheng and D. Tse, "Diversity and multiplexing: a fundamental tradeoff in multiple-antenna channels," *Information Theory, IEEE Transactions on*, vol. 49, no. 5, pp. 1073–1096, 2003.

[101] T. Kim and M. Skoglund, "Diversity - multiplexing tradeoff in mimo channels with partial csit," *Information Theory, IEEE Transactions on*, vol. 8, no. 8, pp. 2743–2759, 2007.

[102] B. Clerckx and C. Oestges, *MIMO Wireless Networks: Channels, Techniques and Standards for Multi-Antenna, Multi-User and Multi-Cell Systems*, 2nd ed. Academic Press, 2013.

[103] Z. Wang and W. Chen, "Regularized zero-forcing for multiantenna broadcast channels with user selection," *Wireless Communications Letters, IEEE*, vol. 1, no. 2, pp. 129–132, April 2012.

[104] R. Schmidt, "Multiple emitter location and signal parameter estimation," *Antennas and Propagation, IEEE Transactions on*, vol. 34, no. 3, pp. 276–280, 1986.

[105] P. Wu and N. Jindal, "Coding versus arq in fading channels: How reliable should the phy be?" *Communications, IEEE Transactions on*, vol. 59, no. 12, pp. 3363–3374, 2011.

[106] A. Lozano and N. Jindal, "Transmit diversity vs. spatial multiplexing in modern mimo systems," *Wireless Communications, IEEE Transactions on*, vol. 9, no. 1, pp. 186–197, 2010.

[107] H. Huang, M. Trivellato, A. Hottinen, M. Shafi, P. Smith, and R. Valenzuela, "Increasing downlink cellular throughput with limited network mimo coordination," *Wireless Communications, IEEE Transactions on*, vol. 8, no. 6, pp. 2983–2989, 2009.

[108] M. Rupp, C. Mehlführer, S. Caban, R. Langwieser, M. L. W., and A. L. Scholtz, "Testbeds and rapid prototyping in wireless system design," *EURASIP Newsletter*, vol. 17, no. 3, pp. 32–50, 2006.

[109] J. Garcia-Naya, M. Gonzalez-Lopez, and L. Castedo, "An overview of mimo testbed technology," in *Proc. 4th International Symposium on Image/Video Communications over Fixed and Mobile Networks (ISIVC2008), 2008*, Bilbao,Spain, July 2008.

[110] E. Casseau, B. L. Gal, P. Bomel, C. Jego, S. Huet, and E. Martin, "C-based rapid prototyping for digital signal processing," in *Proc. of the 13th European Signal Processing Conference (EUSIPCO)*, September 2005.

[111] K. Kintali and Y. Gu, "Model-based design with simulink, hdl coder, and xilinx system generator for dsp," http://www.mathworks.com/tagteam/74244_92077v00_Xilinx_WhitePaper_final.pdf, December 2012.

[112] IEEE, "Ieee standard for local and metropolitan area networks part 16: Air interface for fixed and mobile broadband wireless access systems amendment 2: Physical and medium access control layers for combined fixed and mobile operation in licensed bands and corrigendum 1," *IEEE Std 802.16e-2005 and IEEE Std 802.16-2004/Cor 1-2005 (Amendment and Corrigendum to IEEE Std 802.16-2004)*, 2006.